Vibrational Properties of Fibre Reinforced Hoses

James Southern
MSc in Mathematical Modelling and Scientific Computing

September 2002

Acknowledgements

I would like to thank my supervisor Dr David Allwright for all his help and encouragement during the course of this project. I am also grateful to Dr Jeremy Engineer and Thales Underwater Systems for suggesting the problem, supplying me with a physical description of their sonar arrays together with their mechanical properties and for providing a bursary for the duration of my research.

Contents

1 Introduction **1**
1.1 Background and Motivation . . . 1
1.2 Formulation and Notation . . . 2

2 Linear Elastic Theory **4**
2.1 Calculating the Lagrangian . . . 4
2.1.1 Kinetic Energy . . . 4
2.1.2 Potential Energy . . . 5
2.1.3 The Lagrangian . . . 6
2.2 Equations of Motion . . . 7
2.2.1 The Euler-Lagrange Equations . . . 7
2.2.2 Motion of a Fibre-Reinforced Hose . . . 8
2.2.3 Insertion of a Fourier Mode . . . 9
2.2.4 Exact Solutions in the Transversely Isotropic Case . . . 10
2.2.4.1 Exact Solution for Non-Zero n . . . 10
2.2.4.2 Exact Solution When $n = 0$, $k \neq 0$ . . . 12
2.2.4.3 Exact Solution When $n = k = 0$ . . . 13
2.2.5 Exact Solutions in the Orthotropic Case . . . 13
2.3 Determination of the Constants . . . 14
2.3.1 Green, Troth & Nicol's Models for Rubber Hosepipes . . . 14
2.3.1.1 Bursting Pressure for an Incompressible Hose . . . 14
2.3.1.2 Effects of Compressibility . . . 15
2.3.2 Uniform Distribution Model . . . 15
2.3.2.1 Contribution From the Substrate . . . 15
2.3.2.2 Contribution From the Fibres . . . 15
2.3.2.3 Total Potential Energy . . . 16
2.3.3 The Composite Cylinders Model . . . 16
2.3.3.1 Longitudinal Young's Modulus . . . 16
2.3.3.2 Major Poisson's Ratio . . . 19
2.3.3.3 Transverse Young's Modulus . . . 19
2.3.3.4 Minor Poisson's Ratio . . . 20
2.3.3.5 Longitudinal Shear Modulus . . . 20
2.3.3.6 Transverse Shear Modulus . . . 20
2.3.4 Three Phase Cylinder Model . . . 20
2.3.4.1 Transverse Shear Modulus . . . 20
2.3.4.2 Transverse Poisson's Ratio . . . 22
2.3.5 Constants for a Material Reinforced With Uni-Directional Fibres . . . 22
2.3.5.1 Frame Aligned With the Fibres . . . 22
2.3.5.2 Frame Aligned with the Hose . . . 23
2.3.6 Effects of Bi-Directional Fibres . . . 24

3 Linear Acoustic Waves **26**
3.1 Equations Of Motion . . . 26
3.1.1 Insertion of a Fourier Mode . . . 26
3.1.2 Continuity of Radial Displacement . . . 27
3.1.3 Fluid in the Interior of the Hose . . . 27
3.1.4 Fluid Outside the Hose . . . 27
3.1.4.1 Real-Valued κ_2 . . . 28
3.1.4.2 Imaginary-Valued κ_2 . . . 28
3.2 Waves on the Interfaces . . . 29
3.2.1 Snell's Law . . . 29
3.2.2 Rayleigh and Stoneley Waves . . . 32
3.2.2.1 Rayleigh Waves . . . 32
3.2.2.2 Stoneley Waves . . . 33
3.2.2.3 Effect of Interface Waves Away From the Interfaces . . . 33

4 Numerical Analysis **34**
4.1 Dimensional Analysis . . . 34
4.1.1 Non-Dimensionalization . . . 34
4.1.2 Parameter Analysis . . . 35
4.1.2.1 Mechanical Properties of the System . . . 35
4.1.2.2 Typical Size of the Dimensionless Parameters . . . 37
4.2 Computing Solutions . . . 37
4.2.1 Uniform Density Throughout the Hose . . . 37
4.2.1.1 Conversion to a First-Order System . . . 38
4.2.1.2 Numerical Solution by Shooting . . . 39
4.2.1.3 Plotting the Transfer Function . . . 40
4.2.2 Variable Density Using Layers . . . 42
4.2.2.1 Governing Equations and Boundary Conditions . . . 42
4.2.2.2 Numerical Solution for the Layered System . . . 42

5 Conclusion and Extensions **44**
5.1 Conclusion . . . 44
5.1.1 Explanation of Results . . . 44
5.1.2 Summary . . . 45
5.2 Possible Extensions . . . 46
5.2.1 Comparison With Experimental Results . . . 46
5.2.2 Effects of Viscoelasticity . . . 46

A Notation **48**

B Plots of the Transfer Function **49**

C MATLAB Routine **65**
C.1 Main Solver . . . 65
C.2 Determination of the Exact Solution . . . 70
C.3 Calculating the Solution for a Layered Hose . . . 75
C.4 Plotting the Hose Transfer Function . . . 83

List of Figures

1.1 Fibre reinforced hose. 2

2.1 Composite cylinders model. 17
2.2 Typical composite cylinder. 17
2.3 Three phase cylinder model. 21
2.4 Axes aligned with the hose and with the fibres. 23

3.1 Reflected and refracted waves due to a compressional wave. 30
3.2 Reflected and refracted waves due to a shear wave. 31

4.1 Numeric and exact solutions for $\omega = 10^3$, $n = 2$, $k = 1$, $N = 40$, $\phi = 0$, $P_f = 1$. . . 41

B.1 Hose transfer function at $r = 0.2$ for $n = 0$, $k = 1$, $N = 900$, $\phi = 0$, $P_f = 1$. 49
B.2 Hose transfer function at $r = 0.2$ for $n = 1$, $k = 1$, $N = 900$, $\phi = 0$, $P_f = 1$. 50
B.3 Hose transfer function at $r = 0.2$ for $n = 2$, $k = 1$, $N = 900$, $\phi = 0$, $P_f = 1$. 51
B.4 Hose transfer function at $r = 0.2$ for $n = 3$, $k = 1$, $N = 900$, $\phi = 0$, $P_f = 1$. 52
B.5 Hose transfer function at $r = 0.2$ for $n = 4$, $k = 1$, $N = 900$, $\phi = 0$, $P_f = 1$. 53
B.6 Hose transfer function at $r = 0$ for $n = 0$, $k = 10$, $N = 900$, $\phi = 0$, $P_f = 1$. 54
B.7 Hose transfer function at $r = 0$ for $n = 0$, $k = 50$, $N = 900$, $\phi = 0$, $P_f = 1$. 55
B.8 Hose transfer function at $r = 0$ for $n = 0$, $k = 100$, $N = 900$, $\phi = 0$, $P_f = 1$. 56
B.9 Hose transfer function at $r = 0$ for $n = 0$, $k = 150$, $N = 900$, $\phi = 0$, $P_f = 1$. 57
B.10 Hose transfer function at $r = 0$ for $n = 0$, $k = 1$, $N = 500$, $\phi = 0$, $P_f = 1$. 58
B.11 Hose transfer function at $r = 0$ for $n = 0$, $k = 1$, $N = 100$, $\phi = 0$, $P_f = 1$. 59
B.12 Hose transfer function at $r = 0$ for $n = 0$, $k = 1$, $N = 40$, $\phi = 0$, $P_f = 1$. 60
B.13 Hose transfer function at $r = 0$ for $n = 0$, $k = 1$, $N = 900$, $\phi = \pi/12$, $P_f = 1$. . . . 61
B.14 Hose transfer function at $r = 0$ for $n = 0$, $k = 1$, $N = 900$, $\phi = \pi/6$, $P_f = 1$. 62
B.15 Hose transfer function at $r = 0$ for $n = 0$, $k = 1$, $N = 900$, $\phi = \pi/4$, $P_f = 1$. 63
B.16 Hose transfer function at $r = 0$ for $n = 0$, $k = 1$, $N = 900$, $\phi = \pi/3$, $P_f = 1$. 64

Chapter 1

Introduction

1.1 Background and Motivation

This project was originally presented as a possible MSc dissertation topic by Dr Jeremy Engineer of Thales Underwater Systems on 13 March 2002. It is an extension of work currently being carried out by Dr Engineer at Thales to optimise the performance of towed sonar arrays.

A towed sonar array is made up of a large number of hydrophones strung out in a flexible line up to 10km long behind a ship. Since the hydrophones are relatively delicate they are encased in a plastic hose for protection. The interior of the hose may be filled with fluid or left empty except for the hydrophones. Thales aim to produce a model for the performance of such an array. As the ship drags the array through the water a turbulent boundary layer is generated. The noise from this boundary layer, known as *self noise*, is then picked up by the hydrophones, possibly obscuring the noise generated by targets and hence reducing the effectiveness of the array. It is intended that the model will suggest ways of reducing the self noise produced by the array, thus increasing its ability to locate targets. In this project we aim to model the vibrations of the towed array in response to pressure fluctuations in the turbulent boundary layer. We will not model the turbulent pressure fluctuations themselves, but will consider the transfer function between them and the hydrophones.

In general the PVC hose encasing the hydrophones is reinforced using nylon or kevlar fibres. The fibres are bound in two spirals that wind around in opposite directions and share a central axis with the hose. Existing models for the towed array use classical thin shell theory (see, e.g., Junger and Feit [21]) modified to allow for the effects of fibre reinforcing. These models seem to work well in most cases, but tend to break down as the hose walls get thick in comparison to the outer radius of the hose. In order to overcome this difficulty attempts have been made to model the hose using exact elastic theory, but Dr Engineer believes that such models have so far been produced only for an isotropic material. In general fibre reinforced hoses are not isotropic so there is still work to be done to produce a model for the vibrations of a towed array.

Two possible approaches to the problem were suggested by Dr Engineer during his presentation. Firstly, modifying the known elastic theory for an isotropic hose to include the contribution from the fibres. This was the method that he had used unsuccessfully to try to find a solution (see Engineer [8]). His second suggestion was to attempt to match together different plate theory solutions in different regions of interest to us in the hose. This could be done by building on his existing work on using thick shell theory to model the hose [7].

1.2 Formulation and Notation

Since the length of the hose is very much longer than its outer radius a it seems reasonable to model it as being infinitely long. The hose thickness is denoted by h and we are interested in the situation where h/a is not negligible — in the case we will look at we have $h/a = 1/3$. The hose is modelled as an isotropic substrate of density ρ with Lamé constants λ and μ reinforced with N isotropic fibres of radius a_0 and density ρ^f with Lamé constants λ^f and μ^f. The fibres are wound spirally in two layers, generally close to one another, with fibres being wound at the same angle but in opposite directions around the hose in each layer. This means that the magnitude of the winding angle of the fibres can be taken to be the same for all fibres. Half of them have winding angle ϕ relative to the z-axis, which is taken to run along the centre line of the tube, and the other half having winding angle $-\phi$.

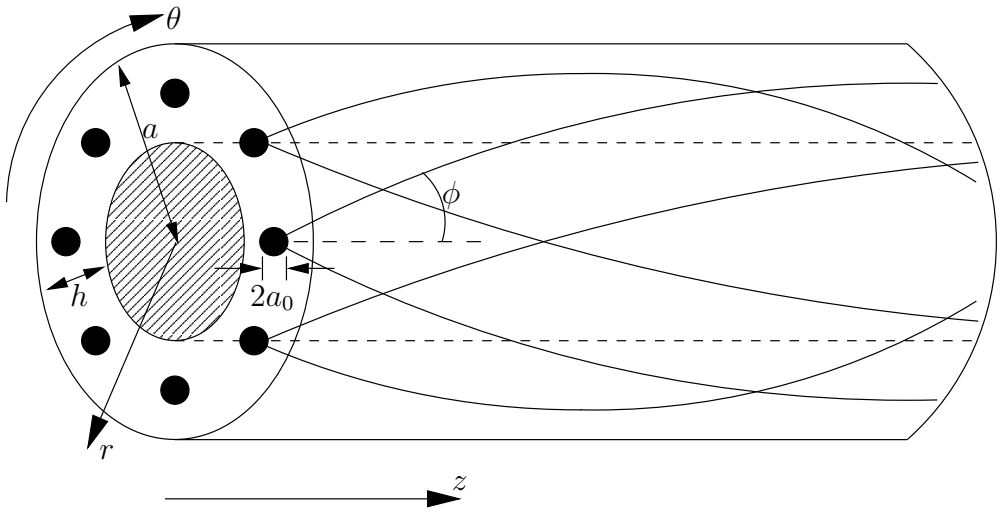


Figure 1.1: Fibre reinforced hose.

Suppose we define the fractional cross-sectional area of the hose occupied by the fibres to be

$$\delta = \frac{N a_0^2 \sec\phi}{2ah - h^2}. \tag{1.1}$$

We will consider hoses with $0 \leqslant \delta \leqslant 0.2$ performing small amplitude vibrations (so that we have a linear vibration problem) in the frequency range 0 Hz to 2 kHz and forced by a single Fourier component acting on the surface of the hose. This is an artificial method of forcing the system. In reality the forcing pressure and the vibration in response to it are a coupled system — we can measure typical forcing pressure spectra on a rigid cylinder, but when an elastic cylinder is present its deformation affects the whole acoustic field. The problem is modelled using the following assumptions:

(i) The fibres do not slip relative to the substrate.

(ii) The fibres are small compared to the wavelengths of the vibrations. We can justify this assumption by loking at typical mechanical properties for a PVC hose. This has shear modulus $G_{12} = O(10^8)$ and density $\rho = O(10^3)$, so the shear wave speed (which is always greater than the compressive wave speed) is

$$c_s = \sqrt{\frac{G_{12}}{\rho}} \sim 300 \text{ ms}^{-1}. \tag{1.2}$$

The maximum frequency that is of interest to us is 2 kHz, so our shortest possible wavelength is given by

$$\lambda = c_s/f = 0.15 \text{ m}. \tag{1.3}$$

Our fibres will generally have radius $a_0 = O(10^{-3})$, so $a_0 \ll \lambda$ in accordance with our assumption.

We will exploit the geometry of the hose by working in cylindrical polars (r, θ, z) and denote the displacement of the hose by $\mathbf{u} = (u, v, w)$. In general properties of the substrate will be denoted just by letters (e.g. ρ), properties of the fibres by superscripts f (e.g. ρ^f) and properties of the composite by overbars (e.g. $\bar{\rho}$).

Chapter 2

Linear Elastic Theory

In this chapter we seek to adapt the analysis of Engineer [8] by modelling the motion of the hose using Lagrangian mechanics. This assumes the hose material is perfectly elastic. Having obtained the equations of motion in this way it is then possible to modify them to allow for non-elastic behaviour. We will calculate its kinetic and potential energies in terms of the displacements in the r-, θ- and z-directions and then use the Euler-Lagrange equations of the Calculus of Variations to derive the equations of motion. Since the vibration wavelengths are large compared to the fibres and their spacing, we shall treat the fibre-reinforced material as a homogeneous anisotropic material in Section 2.1 – 2.2 (Skelton & James [35] goes directly to a numerical model of a similar situation without writing down the equations of motion). Different approaches to determining the effective elastic constants of the homogenized material will be presented in Section 2.3.

2.1 Calculating the Lagrangian

We know (see, e.g., Lunn [25]), that the Lagrangian of our system is given by

$$L = T - V \tag{2.1}$$

where T is the kinetic energy (per unit volume) of the system and V is the potential energy (per unit volume) of the system.

2.1.1 Kinetic Energy

Recall (again from Lunn [25]) that the kinetic energy of a body of unit volume and density ρ is given by

$$T = \frac{1}{2}\rho \mathbf{u}^2. \tag{2.2}$$

So on adding the contributions from the substrate and the fibres we see that the kinetic energy per unit volume is

$$T = \frac{1}{2}\bar{\rho}\left[\left(\frac{\partial u}{\partial t}\right)^2 + \left(\frac{\partial v}{\partial t}\right)^2 + \left(\frac{\partial w}{\partial t}\right)^2\right], \tag{2.3}$$

where

$$\bar{\rho} = (1-\delta)\rho + \delta\rho^f. \tag{2.4}$$

2.1.2 Potential Energy

We calculate the potential (strain) energy of a system by considering the work done on an arbitrary cuboidal element with sides of length δx, δy, δz when we deform it (see Timoshenko & Goodier [41]). Suppose our element is subjected to a normal stress τ_{xx} resulting in a strain e_{xx}. Then the work done on this element is given by

$$\begin{aligned}\delta V &= \frac{1}{2} \times \text{force} \times \text{extension} \\ &= \frac{1}{2}(\tau_{xx}\delta y\delta z)(e_{xx}\delta x) \\ \delta V &= \frac{1}{2}\tau_{xx}e_{xx}\delta x\delta y\delta z. \end{aligned} \tag{2.5}$$

We assume that all of this energy is stored as strain energy (i.e. none is lost as heat or sound or is converted to kinetic energy). We can apply the same argument to each of the other five components of stress and conservation of energy tells us that the work done cannot depend on the order in which the forces are applied (otherwise we could get a net change in energy from loading and then unloading the element). Hence we see that the total work done on the element of volume $\delta x\delta y\delta z$ is

$$\delta V = V\delta x\delta y\delta z, \tag{2.6}$$

where

$$V = \frac{1}{2}(\tau_{xx}e_{xx} + \tau_{yy}e_{yy} + \tau_{zz}e_{zz} + 2\tau_{xy}e_{xy} + 2\tau_{xz}e_{xz} + 2\tau_{yz}e_{yz}) = \frac{1}{2}\tau_{ij}e_{ij}. \tag{2.7}$$

So, V is the potential energy per unit volume of the system.

Now, Hooke's Law tells us (again see Timoshenko & Goodier [41]) that for an isotropic material

$$e_{xx} = \frac{1}{E_1}(\tau_{xx} - \nu_{12}(\tau_{yy} + \tau_{zz})), \tag{2.8}$$

$$e_{yy} = \frac{1}{E_1}(\tau_{yy} - \nu_{12}(\tau_{xx} + \tau_{zz})), \tag{2.9}$$

$$e_{zz} = \frac{1}{E_1}(\tau_{zz} - \nu_{12}(\tau_{xx} + \tau_{yy})), \tag{2.10}$$

$$e_{xy} = \frac{1}{2G_{12}}\tau_{xy}, \quad e_{xy} = \frac{1}{2G_{12}}\tau_{xy}, \quad e_{xy} = \frac{1}{2G_{12}}\tau_{xy}, \tag{2.11}$$

where E_1 is the Young's modulus of the material, ν_{12} is the Poisson's ratio and $G_{12} = E_1/2(1+\nu_{12})$ is the shear modulus. Then on introducing the Lamé constants,

$$\lambda = \frac{E_1\nu_{12}}{(1+\nu_{12})(1-2\nu_{12})}, \tag{2.12}$$

$$\mu = G_{12}, \tag{2.13}$$

and switching to cylindrical polar coordinates we see that our potential energy per unit volume is given by

$$V = \frac{1}{2}\left[\lambda\left(e_{rr}+e_{\theta\theta}+e_{zz}\right)^2+2\mu\left(e_{rr}^2+e_{\theta\theta}^2+e_{zz}^2\right)+4\mu\left(e_{r\theta}^2+e_{rz}^2+e_{\theta z}^2\right)\right] = \frac{1}{2}\left(\lambda(e_{kk})^2+2\mu e_{ij}e_{ij}\right). \tag{2.14}$$

Although the fibre-reinforced hose is made up of two different isotropic materials it is not itself isotropic. However, at each point in the material it has three planes of symmetry at right angles to one another (the r-, θ- and z-planes). This means that the material is *orthotropic*. For an orthotropic material it is convenient to take the planes of symmetry to be our coordinate planes. On doing this the stress-strain relations (2.8) – (2.11) generalise to

$$\begin{bmatrix} e_{rr} \\ e_{\theta\theta} \\ e_{zz} \\ e_{r\theta} \\ e_{rz} \\ e_{\theta z} \end{bmatrix} = \begin{bmatrix} 1/E_r & -\nu_{\theta r}/E_\theta & -\nu_{zr}/E_z & 0 & 0 & 0 \\ -\nu_{r\theta}/E_r & 1/E_\theta & -\nu_{z\theta}/E_z & 0 & 0 & 0 \\ -\nu_{rz}/E_r & -\nu_{\theta z}/E_\theta & 1/E_z & 0 & 0 & 0 \\ 0 & 0 & 0 & 1/2G_{r\theta} & 0 & 0 \\ 0 & 0 & 0 & 0 & 1/2G_{rz} & 0 \\ 0 & 0 & 0 & 0 & 0 & 1/2G_{\theta z} \end{bmatrix} \begin{bmatrix} \tau_{rr} \\ \tau_{\theta\theta} \\ \tau_{zz} \\ \tau_{r\theta} \\ \tau_{rz} \\ \tau_{\theta z} \end{bmatrix}, \tag{2.15}$$

where E_r, E_θ, E_z are the Young's moduli in the r-, θ- and z-directions respectively, $G_{r\theta}$, G_{rz}, $G_{\theta z}$ the shear moduli in the planes indicated by the subscripts and $\nu_{r\theta}$, ν_{rz}, ... are the Poisson's ratios in the directions indicated by the subscripts (note that in general $\nu_{r\theta} \neq \nu_{\theta r}$). Love [24] tells us that the above matrix must be symmetric, so we see that

$$\frac{\nu_{r\theta}}{E_r} = \frac{\nu_{\theta r}}{E_\theta}, \quad \frac{\nu_{rz}}{E_r} = \frac{\nu_{zr}}{E_z}, \quad \frac{\nu_{\theta z}}{E_\theta} = \frac{\nu_{z\theta}}{E_z}. \tag{2.16}$$

Then (2.7) tells us that for an orthotropic material the potential energy per unit volume is given by

$$V = \frac{1}{2}\begin{bmatrix} e_{rr} & e_{\theta\theta} & e_{zz} \end{bmatrix} \begin{bmatrix} A & D & E \\ D & B & F \\ E & F & C \end{bmatrix} \begin{bmatrix} e_{rr} \\ e_{\theta\theta} \\ e_{zz} \end{bmatrix} + \frac{1}{2}\big(G(2e_{r\theta})^2 + H(2e_{rz})^2 + I(2e_{\theta z})^2\big), \tag{2.17}$$

where

$$\begin{bmatrix} A & D & E \\ D & B & F \\ E & F & C \end{bmatrix} = \begin{bmatrix} 1/E_r & -\nu_{\theta r}/E_\theta & -\nu_{zr}/E_z \\ -\nu_{\theta r}/E_\theta & 1/E_\theta & -\nu_{z\theta}/E_z \\ -\nu_{zr}/E_z & -\nu_{z\theta}/E_z & 1/E_z \end{bmatrix}^{-1}, \tag{2.18}$$

$$G = G_{r\theta}, \tag{2.19}$$

$$H = G_{rz}, \tag{2.20}$$

$$I = G_{\theta z}. \tag{2.21}$$

2.1.3 The Lagrangian

Using (2.1), (2.3) and (2.17) we have

$$L = \frac{1}{2}\bar{\rho}\left[\left(\frac{\partial u}{\partial t}\right)^2 + \left(\frac{\partial v}{\partial t}\right)^2 + \left(\frac{\partial w}{\partial t}\right)^2\right] - \frac{1}{2}\big[Ae_{rr}^2 + Be_{\theta\theta}^2 + Ce_{zz}^2 + 2De_{rr}e_{\theta\theta} + 2Ee_{rr}e_{zz} + 2Fe_{\theta\theta}e_{zz} + G(2e_{r\theta})^2 + H(2e_{rz})^2 + I(2e_{\theta z})^2\big]. \tag{2.22}$$

where we recall that (u, v, w) are the (r, θ, z) components of displacement. The components of strain are given by (see, e.g., Acheson [1])

$$e_{rr} = \frac{\partial u}{\partial r}, \tag{2.23}$$

$$e_{\theta\theta} = \frac{1}{r}\frac{\partial v}{\partial \theta} + \frac{u}{r}, \tag{2.24}$$

$$e_{zz} = \frac{\partial w}{\partial z}, \tag{2.25}$$

$$2e_{r\theta} = \frac{\partial v}{\partial r} - \frac{v}{r} + \frac{1}{r}\frac{\partial u}{\partial \theta}, \tag{2.26}$$

$$2e_{rz} = \frac{\partial u}{\partial z} + \frac{\partial w}{\partial r}, \tag{2.27}$$

$$2e_{\theta z} = \frac{1}{r}\frac{\partial w}{\partial \theta} + \frac{\partial v}{\partial z}. \tag{2.28}$$

On substituting these into (2.22) we obtain our final expression for the Lagrangian:

$$\begin{aligned} L = \frac{1}{2}\bar{\rho}\Bigg[\left(\frac{\partial u}{\partial t}\right)^2 + \left(\frac{\partial v}{\partial t}\right)^2 + \left(\frac{\partial w}{\partial t}\right)^2\Bigg] \\ - \frac{1}{2}\Bigg[A\left(\frac{\partial u}{\partial r}\right)^2 + B\left(\frac{1}{r}\frac{\partial v}{\partial \theta} + \frac{u}{r}\right)^2 + C\left(\frac{\partial w}{\partial z}\right)^2 + 2D\frac{\partial u}{\partial r}\left(\frac{1}{r}\frac{\partial v}{\partial \theta} + \frac{u}{r}\right) + 2E\frac{\partial u}{\partial r}\frac{\partial w}{\partial z} \\ + 2F\left(\frac{1}{r}\frac{\partial v}{\partial \theta} + \frac{u}{r}\right)\frac{\partial w}{\partial z} + G\left(\frac{\partial v}{\partial r} - \frac{v}{r} + \frac{1}{r}\frac{\partial u}{\partial \theta}\right)^2 + H\left(\frac{\partial u}{\partial z} + \frac{\partial w}{\partial r}\right)^2 \\ + I\left(\frac{1}{r}\frac{\partial w}{\partial \theta} + \frac{\partial v}{\partial z}\right)^2\Bigg]. \end{aligned} \tag{2.29}$$

2.2 Equations of Motion

2.2.1 The Euler-Lagrange Equations

Hamilton's principle (see, e.g., Riley, Hobson & Bence [31]) tells us that in moving from one configuration to another the motion of a system will leave

$$\mathcal{L} = \int L dx dy dz dt \tag{2.30}$$

stationary. In cylindrical polar coordinates

$$\mathcal{L} = \int L_1 dr d\theta dz dt, \tag{2.31}$$

where

$$L_1 = rL. \tag{2.32}$$

So, the Euler-Lagrange equations (again see Riley, Hobson & Bence [31]) of our system are

$$\frac{\partial}{\partial t}\left(\frac{\partial L_1}{\partial t}\right) = \frac{\partial L_1}{\partial u} - \frac{\partial}{\partial r}\left(\frac{\partial L_1}{\partial u_r}\right) - \frac{\partial}{\partial \theta}\left(\frac{\partial L_1}{\partial u_\theta}\right) - \frac{\partial}{\partial z}\left(\frac{\partial L_1}{\partial u_z}\right), \tag{2.33}$$

$$\frac{\partial}{\partial t}\left(\frac{\partial L_1}{\partial t}\right) = \frac{\partial L_1}{\partial v} - \frac{\partial}{\partial r}\left(\frac{\partial L_1}{\partial v_r}\right) - \frac{\partial}{\partial \theta}\left(\frac{\partial L_1}{\partial v_\theta}\right) - \frac{\partial}{\partial z}\left(\frac{\partial L_1}{\partial v_z}\right), \tag{2.34}$$

$$\frac{\partial}{\partial t}\left(\frac{\partial L_1}{\partial t}\right) = \frac{\partial L_1}{\partial w} - \frac{\partial}{\partial r}\left(\frac{\partial L_1}{\partial w_r}\right) - \frac{\partial}{\partial \theta}\left(\frac{\partial L_1}{\partial w_\theta}\right) - \frac{\partial}{\partial z}\left(\frac{\partial L_1}{\partial w_z}\right). \tag{2.35}$$

where subscripts denote partial derivatives.

2.2.2 Motion of a Fibre-Reinforced Hose

On substituting for our Lagrangian from (2.29) into the three Euler-Lagrange equations (2.33) – (2.35) we obtain the three equations of motion

$$\begin{aligned}\bar{\rho}\frac{\partial^2 u}{\partial t^2} &= A\left(\frac{\partial^2 u}{\partial r^2}+\frac{1}{r}\frac{\partial u}{\partial r}\right)-\frac{B}{r^2}\left(\frac{\partial v}{\partial \theta}+u\right)+\frac{D}{r}\frac{\partial^2 v}{\partial r\partial\theta}+E\left(\frac{1}{r}\frac{\partial w}{\partial z}+\frac{\partial^2 w}{\partial r\partial z}\right)-\frac{F}{r}\frac{\partial w}{\partial z}\\ &\quad+G\left(\frac{1}{r}\frac{\partial^2 v}{\partial r\partial\theta}-\frac{1}{r^2}\frac{\partial v}{\partial\theta}+\frac{1}{r^2}\frac{\partial^2 u}{\partial\theta^2}\right)+H\left(\frac{\partial^2 u}{\partial z^2}+\frac{\partial^2 w}{\partial r\partial z}\right),\end{aligned} \tag{2.36}$$

$$\begin{aligned}\bar{\rho}\frac{\partial^2 v}{\partial t^2} &= \frac{B}{r^2}\left(\frac{\partial^2 v}{\partial\theta^2}+\frac{\partial u}{\partial\theta}\right)+\frac{D}{r}\frac{\partial^2 u}{\partial r\partial\theta}+\frac{F}{r}\frac{\partial^2 w}{\partial\theta\partial z}\\ &\quad+G\left(\frac{1}{r}\frac{\partial v}{\partial r}-\frac{v}{r^2}+\frac{1}{r^2}\frac{\partial u}{\partial\theta}+\frac{\partial^2 v}{\partial r^2}+\frac{1}{r}\frac{\partial^2 u}{\partial r\partial\theta}\right)+I\left(\frac{1}{r}\frac{\partial^2 w}{\partial\theta\partial z}+\frac{\partial^2 v}{\partial z^2}\right),\end{aligned} \tag{2.37}$$

$$\begin{aligned}\bar{\rho}\frac{\partial^2 w}{\partial t^2} &= C\frac{\partial^2 w}{\partial z^2}+E\frac{\partial^2 u}{\partial r\partial z}+\frac{F}{r}\left(\frac{\partial^2 v}{\partial\theta\partial z}+\frac{\partial u}{\partial z}\right)+H\left(\frac{1}{r}\frac{\partial u}{\partial z}+\frac{1}{r}\frac{\partial w}{\partial r}+\frac{\partial^2 u}{\partial r\partial z}+\frac{\partial^2 w}{\partial r^2}\right)\\ &\quad+\frac{I}{r}\left(\frac{1}{r}\frac{\partial^2 w}{\partial\theta^2}+\frac{\partial^2 v}{\partial\theta\partial z}\right).\end{aligned} \tag{2.38}$$

for the fibre-reinforced hose. And, looking ahead to one model for the constants A, B, ... from (2.131) – (2.139) we see that in vector form (2.36) – (2.38) become

$$\begin{aligned}\bar{\rho}\frac{\partial^2 \mathbf{u}}{\partial t^2} &= (1-\delta)\big[(\lambda+\mu)\nabla(\nabla.\mathbf{u})+\mu\nabla^2\mathbf{u}\big]\\ &\quad+\delta\big(\lambda^f+2\mu^f\big)\Bigg\{-\frac{\sin^2\phi}{r}\left[\left(\frac{\partial v}{\partial\theta}+u\right)\frac{\sin^2\phi}{r}+\frac{\partial w}{\partial z}\cos^2\phi\right]\mathbf{e_r}\\ &\qquad+\sin^2\phi\left[\left(\frac{\partial^2 v}{\partial\theta^2}+\frac{\partial u}{\partial\theta}\right)\frac{\sin^2\phi}{r^2}+\left(\frac{2}{r}\frac{\partial^2 w}{\partial\theta\partial z}+\frac{\partial^2 v}{\partial z^2}\right)\cos^2\phi\right]\mathbf{e}_\theta\\ &\qquad+\cos^2\phi\left[\frac{\partial^2 w}{\partial z^2}\cos^2\phi+\left(2\frac{\partial^2 v}{\partial\theta\partial z}+\frac{\partial u}{\partial z}+\frac{1}{r}\frac{\partial^2 w}{\partial\theta^2}\right)\frac{\sin^2\phi}{r}\right]\mathbf{e_z}\Bigg\}.\end{aligned} \tag{2.39}$$

If $\delta = 0$ we see that (2.39) reduces to the Navier equation for an isotropic solid and if $\phi = 0$ (the transversely isotropic case) we have

$$\bar{\rho}\frac{\partial^2 \mathbf{u}}{\partial t^2} = (1-\delta)\big[(\lambda+\mu)\nabla(\nabla.\mathbf{u})+\mu\nabla^2\mathbf{u}\big]+\delta\big(\lambda^f+2\mu^f\big)\frac{\partial^2 w}{\partial z^2}\mathbf{e_z}. \tag{2.40}$$

Two of our boundary conditions are due to continuity of radial displacement across the fluid-hose interfaces, which we will derive later in our work on the fluids. We also have boundary conditions to ensure that the components of the stress tensor at the fluid-hose interfaces match with the pressure in the fluid surrounding the hose. So,

$$\tau_{rr} = -p_1 \quad \text{at } r = a-h, \tag{2.41}$$

$$\tau_{rr} = -p_f - p_2 \quad \text{at } r = a, \tag{2.42}$$

where p_f is the forcing pressure (recall from Chapter 1 that this is considered to be a single Fourier mode acting on the surface of the hose), p_1 is the (perturbation) pressure in the fluid inside the hose and p_2 the (perturbation) pressure in the outer fluid, and

$$\tau_{r\theta} = 0, \tag{2.43}$$

$$\tau_{rz} = 0 \tag{2.44}$$

at both $r = a$ and $r = a - h$. On using (2.15) and (2.23) – (2.28) we see that in terms of the displacements our boundary conditions become

$$A\frac{\partial u}{\partial r} + D\left(\frac{1}{r}\frac{\partial v}{\partial \theta} + \frac{u}{r}\right) + E\frac{\partial w}{\partial z} = -p_1 \quad \text{ar } r = a - h, \tag{2.45}$$

$$A\frac{\partial u}{\partial r} + D\left(\frac{1}{r}\frac{\partial v}{\partial \theta} + \frac{u}{r}\right) + E\frac{\partial w}{\partial z} = -p_f - p_2 \quad \text{at } r = a, \tag{2.46}$$

$$\frac{\partial v}{\partial r} - \frac{v}{r} + \frac{1}{r}\frac{\partial u}{\partial \theta} = 0 \quad \text{at } r = a - h,\ r = a, \tag{2.47}$$

$$\frac{\partial u}{\partial z} + \frac{\partial w}{\partial r} = 0 \quad \text{at } r = a - h,\ r = a, \tag{2.48}$$

together with continuity of radial displacement at $r = a - h$ and $r = a$.

2.2.3 Insertion of a Fourier Mode

Suppose we look for solutions in the form of a single Fourier mode, i.e.

$$u(r, \theta, z, t) = \mathfrak{R}\big[U(r)e^{i(\omega t - kz - n\theta)}\big], \tag{2.49}$$

$$v(r, \theta, z, t) = \mathfrak{R}\big[iV(r)e^{i(\omega t - kz - n\theta)}\big], \tag{2.50}$$

$$w(r, \theta, z, t) = \mathfrak{R}\big[iW(r)e^{i(\omega t - kz - n\theta)}\big], \tag{2.51}$$

where $\mathfrak{R}$ tells us to take the real part only. Seeking a solution of this form can be justified since we have assumed that we are looking at the response to a single frequency ω, the hose is infinitely long (z-dependence) and has rotational symmetry (θ-dependence) so our forcing pressure is of the form

$$p_f(z, \theta, t) = \mathfrak{R}\big[P_f e^{i(\omega t - kz - n\theta)}\big]. \tag{2.52}$$

Then on substituting into (2.36) – (2.38) we obtain a system of second-order ordinary differential equations for U, V and W:

$$\begin{aligned} -\bar{\rho}\omega^2 U = A\left(U'' + \frac{U'}{r}\right) - \frac{BU}{r^2} - \frac{Gn^2U}{r^2} - Hk^2U + \frac{n}{r}(G + D)V' - \frac{n}{r^2}(G + B)V \\ + k(E + H)W' + \frac{k}{r}(E - F)W, \end{aligned} \tag{2.53}$$

$$\bar{\rho}\omega^2 V = \frac{n}{r}(G + D)U' + \frac{n}{r^2}(G + B)U - G\left(V'' + \frac{V'}{r} - \frac{V}{r^2}\right) + \frac{Bn^2V}{r^2} + Ik^2V + \frac{nk}{r}(I + F)W, \tag{2.54}$$

$$\bar{\rho}\omega^2 W = k(H + E)U' + \frac{k}{r}(H + F)U + \frac{nk}{r}(I + F)V - H\left(W'' + \frac{W'}{r}\right) + \frac{In^2W}{r^2} + Ck^2W. \tag{2.55}$$

And, our matching boundary conditions (2.45) – (2.48) become

$$AU' + \frac{D}{r}(nV + U) + EkW = -p_1 e^{-i(\omega t - kz - n\theta)} \quad \text{at } r = a - h, \tag{2.56}$$

$$AU' + \frac{D}{r}(nV + U) + EkW = -P_f - p_2 e^{-i(\omega t - kz - n\theta)} \quad \text{at } r = a, \tag{2.57}$$

and

$$V' - \frac{V}{r} - \frac{nU}{r} = 0, \tag{2.58}$$

$$W' - kU = 0 \tag{2.59}$$

and continuity of radial displacement at both $r = a$ and $r = a - h$.

2.2.4 Exact Solutions in the Transversely Isotropic Case

Analytic solutions to equations (2.53) – (2.55) are known in the isotropic and transversely isotropic cases. If our hose is transversely isotropic in the (r, θ)-plane then

$$A = B, \tag{2.60}$$
$$E = F, \tag{2.61}$$
$$H = I, \tag{2.62}$$
$$D = A - 2G, \tag{2.63}$$

so our equations for U, V and W simplify to

$$\begin{aligned} -\bar{\rho}\omega^2 U = A\left(U'' + \frac{U'}{r} - \frac{U}{r^2}\right) - \frac{Gn^2U}{r^2} - Hk^2U + \frac{n}{r}(A-G)V' - \frac{n}{r^2}(G+A)V \\ + k(H+E)W', \end{aligned} \tag{2.64}$$

$$\bar{\rho}\omega^2 V = \frac{n}{r}(A-G)U' + \frac{n}{r^2}(G+A)U - G\left(V'' + \frac{V'}{r} - \frac{V}{r^2}\right) + \frac{An^2V}{r^2} + Hk^2V + \frac{nk}{r}(H+E)W, \tag{2.65}$$

$$\bar{\rho}\omega^2 W = k(H+E)U' + \frac{k}{r}(H+E)U + \frac{nk}{r}(H+E)V - H\left(W'' + \frac{W'}{r} - \frac{n^2W}{r^2}\right) + Ck^2W. \tag{2.66}$$

2.2.4.1 Exact Solution for Non-Zero n

We know from Love [24] that the general solution for non-zero n in the isotropic case is

$$U = p\big(A_1J_n'(pr) + B_1Y_n'(pr)\big) + q\big(A_2J_n'(qr) + B_2Y_n'(qr)\big) + \frac{n}{r}\big(A_3J_n(qr) + B_3Y_n(qr)\big), \tag{2.67}$$

$$V = -\frac{n}{r}\big(A_1J_n(pr) + B_1Y_n(pr) + A_2J_n(qr) + B_2Y_n(qr)\big) - q\big(A_3J_n'(qr) + B_3Y_n'(qr)\big), \tag{2.68}$$

$$W = -k\big(A_1J_n(pr) + B_1Y_n(pr)\big) + \frac{q^2}{k}\big(A_2J_n(qr) + B_2Y_n(qr)\big), \tag{2.69}$$

where,

$$p^2 = \frac{\bar{\rho}\omega^2}{A} - k^2, \quad q^2 = \frac{\bar{\rho}\omega^2}{G} - k^2. \tag{2.70}$$

The terms involving pr are like P-waves (irrotational compressive waves) and those involving qr ar like S-waves (solenoidal shear waves).

Mirsky [26] suggests that for the transversely isotropic case we seek a solution to these equations that is also of the form

$$U = \frac{nf(r)}{r} + g'(r), \tag{2.71}$$

$$V = -f'(r) - \frac{ng(r)}{r}, \tag{2.72}$$

$$W = \lambda g(r), \tag{2.73}$$

where we note that here λ is an adjustable parameter and not a Lamé modulus. Trying solutions of this form in (2.64) – (2.66) gives

$$\frac{d}{dr}\left[A\left(g''+\frac{g'}{r}-\frac{n^2g}{r^2}\right)+\big(\bar\rho\omega^2-Hk^2+\lambda k(H+E)\big)g\right] +\frac{n}{r}\left[G\left(f''+\frac{f'}{r}-\frac{n^2f}{r^2}\right)+\big(\bar\rho\omega^2-Hk^2\big)f\right]=0, \tag{2.74}$$

$$\frac{n}{r}\left[A\left(g''+\frac{g'}{r}-\frac{n^2g}{r^2}\right)+\big(\bar\rho\omega^2-Hk^2+\lambda k(H+E)\big)g\right] +\frac{d}{dr}\left[G\left(f''+\frac{f'}{r}-\frac{n^2f}{r^2}\right)+\big(\bar\rho\omega^2-Hk^2\big)f\right]=0, \tag{2.75}$$

$$\big[\lambda H-k(H+E)\big]\left(g''+\frac{g'}{r}-\frac{n^2g}{r^2}\right)+\big(\bar\rho\omega^2-Ck^2\big)\lambda g=0. \tag{2.76}$$

So, (2.74), (2.75) are satisfied if

$$A\left(g''+\frac{g'}{r}-\frac{n^2g}{r^2}\right)+\big(\bar\rho\omega^2-Hk^2+\lambda k(H+E)\big)g=0, \tag{2.77}$$

$$G\left(f''+\frac{f'}{r}-\frac{n^2f}{r^2}\right)+\big(\bar\rho\omega^2-Hk^2\big)f=0. \tag{2.78}$$

(2.76) and (2.77) are consistent with one another if and only if

$$\frac{\lambda\big(\bar\rho\omega^2-Ck^2\big)}{\lambda H-k(H+E)}=\frac{\bar\rho\omega^2-Hk^2+\lambda k(H+E)}{A}\equiv p^2. \tag{2.79}$$

Eliminating λ from this gives a quadratic equation from which we can determine p^2:

$$AH\big(p^2\big)^2-p^2\big[(A+H)\bar\rho\omega^2+k^2\big(E^2+2HE-AC\big)\big]+\big(\bar\rho\omega^2-Hk^2\big)\big(\bar\rho\omega^2-Ck^2\big)=0. \tag{2.80}$$

Let p_1^2, p_2^2 be the roots of (2.80). Then we have two possible values for λ and two functions g_1, g_2 that satisfy (2.76), (2.77). Our equations for f, g_1, g_2 become

$$r^2f''+rf'+\big(r^2q^2-n^2\big)f=0, \tag{2.81}$$

$$r^2g_1''+rg_1'+\big(r^2p_1^2-n^2\big)g=0, \tag{2.82}$$

$$r^2g_2''+rg_2'+\big(r^2p_2^2-n^2\big)g=0, \tag{2.83}$$

where

$$q^2=\frac{\bar\rho\omega^2-Hk^2}{G}. \tag{2.84}$$

(2.81)–(2.83) are all Bessel's equations of order n in qr, p_1r and p_2r respectively and so have solutions

$$f(r)=A_3J_n(qr)+B_3Y_n(qr), \tag{2.85}$$

$$g_1(r)=A_1J_n(p_1r)+B_1Y_n(p_1r), \tag{2.86}$$

$$g_2(r)=A_2J_n(p_2r)+B_2Y_n(p_2r). \tag{2.87}$$

And so,

$$U=p_1\big(A_1J_n'(p_1r)+B_1Y_n'(p_1r)\big)+p_2\big(A_2J_n'(p_2r)+B_2Y_n'(p_2r)\big)+\frac{n}{r}\big(A_3J_n(qr)+B_3Y_n(qr)\big), \tag{2.88}$$

$$V=-\frac{n}{r}\big(A_1J_n(p_1r)+B_1Y_n(p_1r)+A_2J_n(p_2r)+B_2Y_n(p_2r)\big)-q\big(A_3J_n'(qr)+B_3Y_n'(qr)\big), \tag{2.89}$$

$$W=\lambda_1\big(A_1J_n(p_1r)+B_1Y_n(p_1r)\big)+\lambda_2\big(A_2J_n(p_2r)+B_2Y_n(p_2r)\big). \tag{2.90}$$

To check that this solution is consistent with the isotropic case we set $C = A$, $E = A - 2G$, $H = G$. Then our equation for q^2 becomes

$$q^2 = \frac{\bar{\rho}\omega^2}{G} - k^2, \tag{2.91}$$

which agrees with what we had for an isotropic hose. And, (2.80) reduces to

$$AG\big(p^2\big)^2 - p^2\big[(A+G)\bar{\rho}\omega^2 - 2k^2AG\big] + \big(\bar{\rho}\omega^2 - Gk^2\big)\big(\bar{\rho}\omega^2 - Ak^2\big) = 0, \tag{2.92}$$

which is symmetric in A and G and can be shown to have solutions

$$p_1^2 = \frac{\bar{\rho}\omega^2}{A} - k^2 = p, \quad p_2^2 = \frac{\bar{\rho}\omega^2}{G} - k^2 = q. \tag{2.93}$$

Using these values of p_1, p_2 we see that our transversely isotropic solution (2.88) – (2.90) does indeed reduce to the isotropic solution (2.67) – (2.69) as we would expect.

2.2.4.2 Exact Solution When $n = 0$, $k \neq 0$

If $n = 0$ then equations (2.64)–(2.66) simplify to

$$-\bar{\rho}\omega^2 U = A\left(U'' + \frac{U'}{r} - \frac{U}{r^2}\right) - Gk^2U + k(A-G)W', \tag{2.94}$$

$$-\bar{\rho}\omega^2 V = G\left(V'' + \frac{V'}{r} - \frac{V}{r^2}\right) - Hk^2V, \tag{2.95}$$

$$-\bar{\rho}\omega^2 W = H\left(W'' + \frac{W'}{r}\right) - Ck^2W - k(H+E)U' - \frac{k}{r}(H+E)U. \tag{2.96}$$

The equation for V is not coupled to the those for U and W and can be solved (since it is Bessel's equation of order 1 in qr) to give

$$V = A_2J_1(qr) + B_2Y_1(qr). \tag{2.97}$$

Love [24] tells us that for an isotropic material the U and W components of the general radially symmetric ($n = 0$) solution when $k \neq 0$ are

$$U = k\big(A_1J_1(qr) + B_1Y_1(qr)\big) + p\big(A_3J_0'(pr) + B_3Y_0'(pr)\big), \tag{2.98}$$

$$W = -\frac{1}{r}\frac{d}{dr}\big(r\big(A_1J_1(qr) + B_1Y_1(qr)\big)\big) - k\big(A_3J_0(pr) + B_3Y_0(pr)\big). \tag{2.99}$$

As this is a special case of the transversely isotropic solution we look for a solution where V is given by (2.97) and U and W are of the form

$$U = kf(r) + g'(r), \tag{2.100}$$

$$W = -\frac{1}{r}\frac{d}{dr}\big(rf(r)\big) - kg(r). \tag{2.101}$$

Trying solutions of this form in (2.94) and (2.96) gives

$$\frac{d}{dr}\left[A\left(g'' + \frac{g'}{r}\right) - (2H+E)k^2g + \bar{\rho}\omega^2 g\right] + k\left[(A-H-E)\left(f'' + \frac{f'}{r} - \frac{f}{r^2}\right) - Hk^2f + \bar{\rho}\omega^2 f\right] = 0, \tag{2.102}$$

$$k\left[(2H+E)\left(g'' + \frac{g'}{r}\right) - Ck^2g + \bar{\rho}\omega^2 g\right] + \frac{1}{r}\frac{d}{dr}\left[r\left(H\left(f'' + \frac{f'}{r} - \frac{f}{r^2}\right) - (C-H-E)k^2f + \bar{\rho}\omega^2 f\right)\right] = 0. \tag{2.103}$$

For arbitrary constants these equations do not have a closed form solution in terms of standard functions. In the isotropic case (when $C = A$, $E = A - 2G$, $H = G$), however, they reduce to

$$\frac{d}{dr}\left[A\left(g'' + \frac{g'}{r} - k^2 g\right) + \bar{\rho}\omega^2 g\right] + k\left[G\left(f'' + \frac{f'}{r} - \frac{f}{r^2} - k^2 f\right) + \bar{\rho}\omega^2 f\right] = 0, \tag{2.104}$$

$$k\left[A\left(g'' + \frac{g'}{r} - k^2 g\right) + \bar{\rho}\omega^2 g\right] + \frac{1}{r}\frac{d}{dr}\left[r\left(G\left(f'' + \frac{f'}{r} - \frac{f}{r^2} - k^2 f\right) + \bar{\rho}\omega^2 f\right)\right] = 0. \tag{2.105}$$

It is simple to verify that as we would expect these equations are satisfied by the known isotropic solutions for U and W, (2.98) and (2.99), so any solution we managed to obtain from (2.102), (2.103) would be consistent with the isotropic solution.

2.2.4.3 Exact Solution When $n = k = 0$

If $n = 0$ and $k = 0$ then (2.64) – (2.66) become

$$r^2U'' + rU' + \left(r^2p_1^2 - 1\right)U = 0, \tag{2.106}$$

$$r^2V'' + rV' + \left(r^2q^2 - 1\right)V = 0, \tag{2.107}$$

$$r^2W'' + rW' + r^2p_2^2U = 0, \tag{2.108}$$

with

$$p_1^2 = \frac{\bar{\rho}\omega^2}{A} \tag{2.109}$$

$$p_2^2 = \frac{\bar{\rho}\omega^2}{H} \tag{2.110}$$

$$q^2 = \frac{\bar{\rho}\omega^2}{G}. \tag{2.111}$$

These equations are not coupled and are all Bessel's equations. So, our general solution is

$$U = A_1J_1(p_1r) + B_1Y_1(p_1r), \tag{2.112}$$

$$V = A_2J_1(qr) + B_2Y_1(qr), \tag{2.113}$$

$$W = A_3J_0(p_2r) + C_3Y_0(p_2r). \tag{2.114}$$

2.2.5 Exact Solutions in the Orthotropic Case

At least one analytic solution does exist in the orthotropic case. As we have seen above the equations of motion decouple if $n = k = 0$. In the orthotropic case, similarly to in the transversely isotropic case, (2.53) – (2.55) reduce to

$$r^2U'' + rU' + \left(r^2p_1^2 - \frac{B}{A}\right)U = 0, \tag{2.115}$$

$$r^2V'' + rV' + \left(r^2q^2 - 1\right)V = 0, \tag{2.116}$$

$$r^2W'' + rW' + r^2p_2^2U = 0, \tag{2.117}$$

where p_1, p_2, q are given as in the transversely isotropic case by (2.109) – (2.111). Again we solve the decoupled Bessel's equations to give the solution

$$U = A_1J_{\sqrt{B/A}}(p_1r) + B_1Y_{\sqrt{B/A}}(p_1r), \tag{2.118}$$

$$V = A_2J_1(qr) + B_2Y_1(qr), \tag{2.119}$$

$$W = A_3J_0(p_2r) + C_3Y_0(p_2r). \tag{2.120}$$

We note that if $A = B$ this reduces to the transversely isotropic solution with $n = k = 0$ as we would expect.

2.3 Determination of the Constants

The above solutions depend on the constants A, B, ..., I that appear in our expression (2.17) for the potential energy of the system. In this section we present a review of various models to calculate these constants for a fibre-reinforced material.

2.3.1 Green, Troth & Nicol's Models for Rubber Hosepipes

In Green & Troth [11] and Green & Nicol [10] thin shell theory is used to calculate the bursting pressure of rubber hosepipes reinforced by a number of spirally wound layers of metal wires deformed symmetrically by inflation, extension and torsion so that the displacement field is of the form

$$u = u(r), \quad v = \psi r z, \quad w = Kz, \tag{2.121}$$

where ψ is a constant representing twist per unit length and K is the axial strain. Each layer of wire reinforcing consists, as in our case, of equal numbers of wires winding in opposite directions around the hose with winding angle $\pm\phi$. This is a static equilibrium problem, unlike the present situation were we are looking at a dynamic system, but the structure of the hose is the same in both cases. Also both papers made simplifying assumptions similar to those we made in Chapter 1 — the system is modelled using linear elasticity and the wires are assumed to adhere to the rubber so that they do not slip relative to it. In the case of the hosepipe, however, one additional assumption is made that we cannot make: the wires are modelled as ideally thin and perfectly flexible so that their properties only appear in the matching boundary conditions between the layers of rubber either side of the wires. Since this assumption affects the dynamical behaviour of the system (as the moduli of elasticity of the wires influence the moduli of elasticity of the composite) this model will not prove useful in the case of a vibrating hose. Nevertheless we include a brief description of the results produced by this model.

2.3.1.1 Bursting Pressure for an Incompressible Hose

Suppose the hose (still with outer radius a and thickness h) is composed of $n+1$ concentric cylinders. Each cylinder is made up of incompressible rubber-like material, although each section may have a different Young's modulus. At each interface between each two adjacent cylinders there is a layer of wires as described above. Define r_i, $i = 1, \ldots, n$ where $r_i < r_{i+1}$ for all i to be radius at which the ith wire layer is situated. Let the distance between two adjacent wires with winding angle $\pm\phi$ be denoted by Δ (assumed to be the same in each layer). Each layer of wires is regarded as a thin flexible shell in equilibrium under the tensions of the membrane and the normal pressures on it from the adjacent sections of the rubber hose. On solving the static equilibrium problem in each region for a hose assumed to be acted on by pressures p_1 and p_2 at $r = a - h$ and $r = a$ respectively and not twisted or stretched parallel to its axis (so that the problem reduces to the plane strain 'gun-barrel' problem) it is found that for one layer of wires rupture occurs when the pressure difference is given by

$$p_1 - p_2 = \frac{\tau^* \tan\phi}{r_1 \Delta}, \tag{2.122}$$

where τ^* is the tensile strength of the wires. When the number of layers of wires is increased it is found that the inner layer of wires will always be the first to fail and, in the case of two layers of wire, this occurs when

$$p_1 - p_2 = \frac{\tau^* \left(r_1^3 + r_2^3\right) \tan\phi}{r_1 r_2^3 \Delta}. \tag{2.123}$$

Both of the above values for the bursting pressure agree well with experimental values (for comparison see Green & Troth [11]) and it turns out that adding a second layer of wires increases the bursting pressure — in fact according to Green & Troth's [11] data it nearly doubles it. However, for $n > 2$ the theory predicts that adding extra layers of wire reinforcing will continue to increase the bursting pressure. This behaviour is not observed expreimentally.

2.3.1.2 Effects of Compressibility

Green & Nicol [10] extended the model proposed by Green & Troth [11] to include the effects of compressibility in the rubber tube. The only difference between this model and that of Green & Troth [11] above is that the Poisson's ratio ν_{12} is not assumed to be $1/2$ — all the governing equations and boundary conditions remain the same apart from this. This modified model succeeded in replicating experimental results for $n > 2$. No additional benefit is seen from including more than two layers of wire. It turns out that if the Poisson ratio of the rubber-like material making up the hose differs from $1/2$ by as little as 0.5% then a very different bursting pressure is produced for the wires. Green & Nicol [10] include numerical solutions of the equations resulting from their compressible model and show that if $\nu_{12} = 1/2$ then these solutions reduce to those given by the incompressible model. They found that increasing the number of wire layers past two does not significantly increase the bursting pressure of the wires, agreeing with experimental data. The actual numerical values of the bursting pressure obtained by using this model are also significantly closer to the actual values than those obtained using the incompressible model of Green & Troth [11].

2.3.2 Uniform Distribution Model

The model used by Engineer [8] assumes that the fibres are uniformly distributed throughout the substrate, so that the density $\bar{\rho}$ of the composite is constant, and that longitudinal stress dominates in the fibres. In this case we can calculate the potential energy of the substrate and the fibres separately in terms of the components of strain. The total potential energy is then given by

$$V = (1-\delta)V^s + \delta V^f. \tag{2.124}$$

Comparing the expression we obtain in this way with (2.17) allows us to read off the values of A, B, ..., I.

2.3.2.1 Contribution From the Substrate

Recall that the substrate has Lamé constants λ and μ. So, using (2.14), we see that the potential energy per unit volume of the substrate is

$$V^s = \frac{1}{2}\big[(\lambda+2\mu)\big(e_{rr}^2 + e_{\theta\theta}^2 + e_{zz}^2\big) + 2\lambda\big(e_{rr}e_{\theta\theta} + e_{rr}e_{zz} + e_{\theta\theta}e_{zz}\big) + 4\mu\big(e_{r\theta}^2 + e_{rz}^2 + e_{\theta z}^2\big)\big]. \tag{2.125}$$

2.3.2.2 Contribution From the Fibres

We have assumed that the longitudinal stress e_L is dominant in the fibres, which have Lamé constants λ^f and μ^f. So (2.14) tells us that the potential energy per unit volume of the fibres is

$$V^f = \frac{1}{2}(\lambda^f + 2\mu^f)e_L^2. \tag{2.126}$$

The direction of a fibre with winding angle ϕ is $(0, \sin\phi, \cos\phi)^T$, so

$$e_L = e_{\theta\theta}\sin^2\phi + 2e_{\theta z}\sin\phi\cos\phi + e_{zz}\cos^2\phi. \tag{2.127}$$

Hence,

$$\begin{aligned} V^f = \frac{1}{2}\big(\lambda^f + 2\mu^f\big)\big(&e_{\theta\theta}^2\sin^4\phi + 4e_{\theta z}^2\sin^2\phi\cos^2\phi + e_{zz}^2\cos^4\phi + 4e_{\theta\theta}e_{\theta z}\sin^3\phi\cos\phi \\ &+ 2e_{\theta\theta}e_{zz}\sin^2\phi\cos^2\phi + 4e_{\theta z}e_{zz}\sin\phi\cos^3\phi\big). \end{aligned} \tag{2.128}$$

If we now include the assumption that half of the fibres have winding angle ϕ and the other half winding angle $-\phi$ then the terms with odd powers of $\sin\phi$ will cancel, so

$$V^f = \frac{1}{2}\big(\lambda^f + 2\mu^f\big)\big(e_{\theta\theta}^2\sin^4\phi + 4e_{\theta z}^2\sin^2\phi\cos^2\phi + e_{zz}^2\cos^4\phi + 2e_{\theta\theta}e_{zz}\sin^2\phi\cos^2\phi\big). \tag{2.129}$$

2.3.2.3 Total Potential Energy

Since the volume fraction of our hose occupied by the fibres is δ with the substrate filling up the rest of the available space we have total potential energy

$$\begin{aligned} V &= (1-\delta)V^s + \delta V^f \\ &= \frac{1}{2}\begin{bmatrix} e_{rr} & e_{\theta\theta} & e_{zz} \end{bmatrix} \begin{bmatrix} A & D & E \\ D & B & F \\ E & F & C \end{bmatrix} \begin{bmatrix} e_{rr} \\ e_{\theta\theta} \\ e_{zz} \end{bmatrix} + \frac{1}{2}\big(G(2e_{r\theta})^2 + H(2e_{rz})^2 + I(2e_{\theta z})^2\big), \end{aligned} \tag{2.130}$$

where

$$A = (1-\delta)(\lambda + 2\mu), \tag{2.131}$$

$$B = (1-\delta)(\lambda + 2\mu) + \delta(\lambda^f + 2\mu^f)\sin^4\phi, \tag{2.132}$$

$$C = (1-\delta)(\lambda + 2\mu) + \delta(\lambda^f + 2\mu^f)\cos^4\phi, \tag{2.133}$$

$$D = (1-\delta)\lambda, \tag{2.134}$$

$$E = (1-\delta)\lambda, \tag{2.135}$$

$$F = (1-\delta)\lambda + \delta(\lambda^f + 2\mu^f)\sin^2\phi\cos^2\phi, \tag{2.136}$$

$$G = (1-\delta)\mu, \tag{2.137}$$

$$H = (1-\delta)\mu, \tag{2.138}$$

$$I = (1-\delta)\mu + \delta(\lambda^f + 2\mu^f)\sin^2\phi\cos^2\phi. \tag{2.139}$$

Notice that if $\delta = 0$ we have $A = B = C$, $D = E = F = A - 2G$, $G = H = I$ so the material is isotropic. And, if $\phi = 0$ we have $A = B$, $E = F$, $D = A - 2G$, $H = I$ so the material is transversely isotropic in the (r, θ)-plane.

2.3.3 The Composite Cylinders Model

The most common model for a material reinforced by *unidirectional* fibres is the composite cylinders model, first introduced by Hill [16] and subsequently developed by Whitney & Riley [44], Halpin & Kordos [13] and others to produce the Halpin-Tsai equations for properties of the composite, generally acknowledged to be the best model for materials reinforced with unidirectional continuous fibres (see, e.g. Fu, Hu & Yue [9]). Reviews of this theory in varying amounts of detail can be found in Halpin & Kordos [13], Christensen [5], Whitney [43] and Smith [37]. Christensen's account is perhaps the most complete. We model the composite material as if it was made up of cylindrical fibres of radius a_0 surrounded by a cylindrical substrate of radius b_0 (as shown in Figures 2.1 and 2.2). It is assumed that the gaps that are left when we attempt to tesellate such structures are not significant. Such a model seems reasonable at least in the case of small volume fraction δ, here given by

$$\delta = \frac{a_0^2}{b_0^2}. \tag{2.140}$$

Since a material reinforced by unidirectional fibres will be transversely isotropic we need to calculate 5 independent elastic constants in order to determine the 5 constants we have in our equations for the transversely isotropic case.

2.3.3.1 Longitudinal Young's Modulus

Suppose we follow Whitney & Riley [44] and apply an axial force to our composite cylinders so that the only non-zero component of strain is

$$e_{zz} = \epsilon. \tag{2.141}$$

This is then an axisymmetric plane strain problem with stresses, strains and displacements dependent on r alone. We solve plane strain problems using the Airy stress function $A(r)$ (see Love [24]

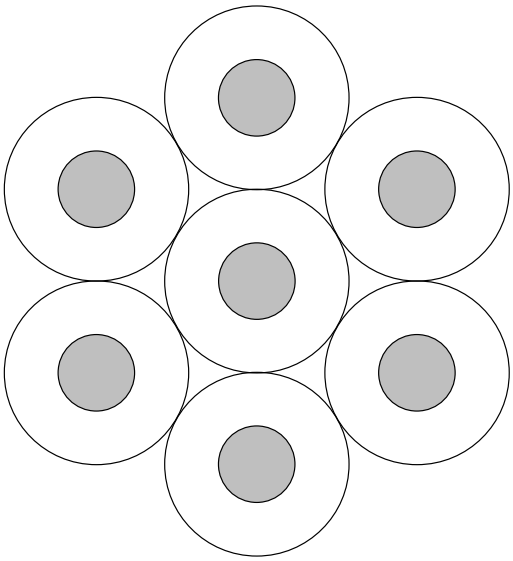


Figure 2.1: Composite cylinders model.

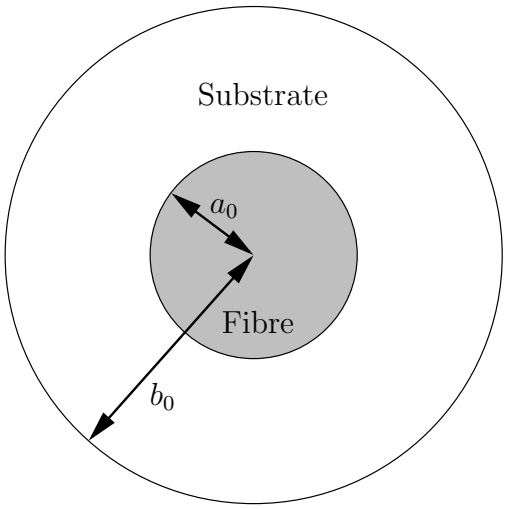


Figure 2.2: Typical composite cylinder.

or Ockendon [28]). It is shown in Love that our compatibility conditions demand that A satisfies the *biharmonic equation*

$$\nabla^4 A = \frac{d^4A}{dr^4} + \frac{2}{r}\frac{d^3A}{dr^3} - \frac{1}{r^2}\frac{d^2A}{dr^2} + \frac{1}{r^3}\frac{dA}{dr} = 0. \tag{2.142}$$

This has solutions of the form

$$A = c_1 \log r + c_2 r^2 \log r + c_3 r^2 + c_4. \tag{2.143}$$

We use separate stress functions A^f for the fibre and A for the substrate. Then, in the fibre our stresses are given by

$$\tau_{rr} = \frac{1}{r}\frac{dA^f}{dr} = \frac{c_1^f}{r^2} + c_2^f(1 + 2\log r) + 2c_3^f, \tag{2.144}$$

$$\tau_{\theta\theta} = \frac{d^2A^f}{dr^2} = -\frac{c_1^f}{r^2} + c_2^f(3 + 2\log r) + 2c_3^f. \tag{2.145}$$

in order to avoid infinite stress at $r = 0$ we see that $c_1^f = c_2^f = 0$, so that

$$\tau_{rr} = \tau_{\theta\theta} = 2c_3^f \tag{2.146}$$

in the fibres. Similarly, in the substrate our stresses are

$$\tau_{rr} = \frac{1}{r}\frac{dA}{dr} = \frac{c_1}{r^2} + c_2(1 + 2\log r) + 2c_3, \tag{2.147}$$

$$\tau_{\theta\theta} = \frac{d^2A}{dr^2} = -\frac{c_1}{r^2} + c_2(3 + 2\log r) + 2c_3. \tag{2.148}$$

It can be shown (see, e.g. Sechler [33]) that in the substrate our strain conditions require $c_2 = 0$, giving

$$\tau_{rr} = \frac{c_1}{r^2} + 2c_3, \tag{2.149}$$

$$\tau_{\theta\theta} = -\frac{c_1}{r^2} + 2c_3. \tag{2.150}$$

The longitudinal stresses in the z-direction are determined from the stress-strain relationship for an isotropic material (2.10)

$$e_{zz} = \epsilon = \frac{1}{E_1}\big[\tau_{zz} - \nu_{12}\big(\tau_{rr} - \tau_{\theta\theta}\big)\big]. \tag{2.151}$$

This relationship applies in both fibres and substrate, so on substituting from (2.146), (2.149) and (2.150) we see that

$$\tau_{zz} = \begin{cases} \epsilon E_1^f + 4\nu_{12}^f c_3^f & \text{if } r < a_0, \\ \epsilon E_1 + 4\nu_{12} c_3 & \text{if } a_0 < r < b_0. \end{cases} \tag{2.152}$$

Then the radial displacement is given by

$$u = re_{\theta\theta} = \begin{cases} r\big[2c_3^f - \nu_{12}^f\big(2c_3^f + 4\nu_{12}^f c_3^f + \epsilon E_1^f\big)\big]/E_1^f & \text{if } r < a_0, \\ r\big[2c_3 - c_1/r^2 - \nu_{12}\big(c_1/r^2 + 2c^3 + 4\nu_{12}c_3 + \epsilon E_1\big)\big]/E_1 & \text{if } a_0 < r < b_0, \end{cases} \tag{2.153}$$

since (2.9) tells us that

$$e_{\theta\theta} = \frac{1}{E_1}\big[\tau_{\theta\theta} - \nu_{12}\big(\tau_{rr} - \tau_{zz}\big)\big] \tag{2.154}$$

for an isotropic material.

The constants c_1, c_3 and c_1^f are determined from our boundary conditions at $r = a_0$ and $r = b_0$. At the fibre-substrate interface $r = a_0$ continuity of τ_{rr} in (2.146) and (2.149) requires

$$2c_3^f = \frac{c_1}{a_0^2} + 2c_3. \tag{2.155}$$

And, continuity of displacement at $r = a_0$ in (2.153) gives the condition

$$E_1\big[2c_3^f\big(1 - \nu_{12}^f - 2\big(\nu_{12}^f\big)^2\big) - \nu_{12}^f \epsilon E_1^f\big] = E_1^f\left[2c_3\big(1 - \nu_{12} - 2\nu_{12}^2\big) - \frac{c_1}{a_0^2}\big(1 + \nu_{12}\big) - \nu_{12}\epsilon E\right]. \tag{2.156}$$

Since we assume that all the composite cylinders behave in the same way we must have zero stress across any possible interface between two cylinders, i.e. $\tau_{rr} = 0$ at $r = b_0$. In (2.153) this tells us that

$$2c_3 = -\frac{c_1}{b_0^2}. \tag{2.157}$$

On solving for c_1, c_3, c_3^f from (2.155) – (2.157) and substituting into our expressions (2.146), (2.149), (2.150), (2.152) for the stresses we see that in the fibres ($r < a_0$)

$$\tau_{rr} = \tau_{\theta\theta} = \frac{\big(\nu_{12} - \nu_{12}^f\big)E_1 E_1^f(1-\delta)\epsilon}{E_1(1-\delta)L^f + \big(L\delta + \big(1+\nu_{12}\big)\big)E_1^f} \tag{2.158}$$

$$\tau_{zz} = \epsilon E_1^f + \frac{2\nu_{12}^f\big(\nu_{12} - \nu_{12}^f\big)E_1 E_1^f(1-\delta)\epsilon}{E_1(1-\delta)L^f + \big(L\delta + \big(1+\nu_{12}\big)\big)E_1^f}, \tag{2.159}$$

where

$$L = 1 - \nu_{12} - 2\nu_{12}^2, \tag{2.160}$$

$$L^f = 1 - \nu_{12}^f - 2\big(\nu_{12}^f\big)^2. \tag{2.161}$$

And in the substrate ($a_0 < r < b_0$)) we have

$$\tau_{rr} = \frac{\big(\nu_{12}^f - \nu_{12}\big)E_1 E_1^f\big(b_0^2 - r^2\big)\delta\epsilon}{r^2\big[E_1(1-\delta)L^f + \big(L\delta + \big(1+\nu_{12}\big)\big)E_1^f\big]} \tag{2.162}$$

$$\tau_{\theta\theta} = \frac{\big(\nu_{12} - \nu_{12}^f\big)E_1 E_1^f\big(b_0^2 + r^2\big)\delta\epsilon}{r^2\big[E_1(1-\delta)L^f + \big(L\delta + \big(1+\nu_{12}\big)\big)E_1^f\big]} \tag{2.163}$$

$$\tau_{zz} = \epsilon E_1 + \frac{2\nu_{12}\big(\nu_{12} - \nu_{12}^f\big)E_1 E_1^f\delta\epsilon}{E_1(1-\delta)L^f + \big(L\delta + \big(1+\nu_{12}\big)\big)E_1^f}. \tag{2.164}$$

The effective Young's modulus in the longitudinal direction is now calculated using an energy balance — the strain energy applied to the composite cylinder must equal the sum of the strain energies in the fibre and the substrate. Since we have zero stresses outside the composite cylinders we have, using (2.7)

$$\frac{1}{2}\int_{\bar{V}} \tau_{zz}\epsilon dV = \frac{1}{2}\int_{V^f} \big(\tau_{zz}\epsilon + \tau_{\theta\theta}e_{\theta\theta} + \tau_{rr}e_{rr}\big)dV^f + \frac{1}{2}\int_{V} \big(\tau_{zz}\epsilon + \tau_{\theta\theta}e_{\theta\theta} + \tau_{rr}e_{rr}\big)dV, \quad (2.165)$$

where V, V^f, $\bar{V}$ are the regions occupied by the substrate, fibre and composite respectively. We can use our stress-strain relationships to obtain (2.165) in terms of ϵ, the longitudinal Young's modulus $\bar{E}_1$ and the stresses in the fibre and substrate. Then using (2.158) – (2.164) and integrating we see that

$$\bar{E}_1 = (1-\delta)E_1 + \delta E_1^f + \frac{2\big(\nu_{12}^f - \nu_{12}\big)^2 E_1 E_1^f (1-\delta)\delta}{E_1(1-\delta)L^f + \big(L\delta + \big(1+\nu_{12}\big)\big)E_1^f}. \quad (2.166)$$

In general, the last term in this expression will not be significant because the Poisson's ratios of substrate and fibre do not differ widely and the last term is quadratic in the difference. So $\bar{E}_1$ can be approximated by a simple 'law of mixtures' approximation

$$\bar{E}_1 = (1-\delta)E_1 + \delta E_1^f, \quad (2.167)$$

which is our first Halpin-Tsai equation.

2.3.3.2 Major Poisson's Ratio

Using the above plane strain model the major Poisson's ratio $\bar{\nu}_{12}(\neq \bar{\nu}_{21})$ of the composite (where axis 1 is in the fibre direction) is defined to be minus the ratio of the lateral strain response to the imposed axial strain, i.e.

$$\bar{\nu}_{12} = -\frac{u|_{r=b_0}}{\epsilon b_0}. \quad (2.168)$$

Then, on substituting for u from (2.153) we see that

$$\bar{\nu}_{12} = \nu_{12} - \frac{2\big(\nu_{12} - \nu_{12}^f\big)\big(1-\nu_{12}^2\big)E_1^f\delta}{E_1(1-\delta)L^f + \big(L\delta + \big(1+\nu_{12}\big)\big)E_1^f}. \quad (2.169)$$

It is shown in Christensen [5] that as for the longitudinal Young's modulus this expression for $\bar{\nu}_{12}$ can be approximated by the 'law of mixtures' for most typical composites, so that

$$\bar{\nu}_{12} = (1-\delta)\nu_{12} + \delta\nu_{12}^f. \quad (2.170)$$

Christensen [5] also shows that this is generally not as good an approximation as (2.167). This is the second Halpin-Tsai equation.

2.3.3.3 Transverse Young's Modulus

If we apply a uniform radial pressure at $r = \infty$ whilst maintaining zero axial strain it can be shown (see, e.g. Whitney [43] or Smith [37]) that the transverse Young's modulus is approximated by

$$\bar{E}_2 = \frac{E_1\big[2E_1 + E_1^f + 2\big(E_1^f - E_1\big)\delta\big]}{2E_1 + E_1^f - \big(E_1^f - E_1\big)\delta}. \quad (2.171)$$

This is our third Halpin-Tsai equation.

2.3.3.4 Minor Poisson's Ratio

We now have enough information to be able to calculate the minor Poisson's ratio $\bar{\nu}_{21}$ which although not one of our five independent elastic constants will prove useful later in simplifying our expressions for A, B, ..., I. We see from (2.16) that $\bar{\nu}_{21}$ is determined by the expression

$$\bar{\nu}_{21} = \frac{\bar{\nu}_{12}\bar{E}_2}{\bar{E}_1}. \tag{2.172}$$

2.3.3.5 Longitudinal Shear Modulus

By applying a uniform longitudinal shear at $r = \infty$ and proceeding in a similar way as for the longitudinal Young's modulus above it can be shown (see, e.g. Hill [16], Halpin & Kordos [13] or Christensen [5]) that the longitudinal shear modulus of the composite is given by our fourth Halpin-Tsai equation:

$$\bar{G}_{12} = \frac{G_{12}\big[G_{12} + G_{12}^f + \big(G_{12}^f - G_{12}\big)\delta\big]}{G_{12} + G_{12}^f - \big(G_{12}^f - G_{12}\big)\delta}. \tag{2.173}$$

2.3.3.6 Transverse Shear Modulus

The fifth and final elastic constant that we require to complete our model for a uni-directional fibre reinforced material is the transverse shear modulus $\bar{G}_{23}$. There is a fifth Halpin-Tsai equation derived by applying a uniform transverse shear at $r = \infty$ to our composite cylinder. Unfortunately this does not, according to Christensen [5] and Whitney [43], produce good agreement with experimental results. This problem arises since, unlike for our other properties, the presence of more than one cylinder affects the stress field for large values of r. For uniform transverse shear we require the stresses to decrease with increasing distance from the centre of *every* fibre. Clearly this is impossible. So, we need a different model to determine the transverse shear modulus.

2.3.4 Three Phase Cylinder Model

To calculate the transverse shear modulus and Poisson's ratio we consider the composite cylinders model as above, but with all but a single composite cylinder replaced by an equivalent homogeneous medium, i.e. a material with the same bulk properties as the composite (in particular shear modulus $\bar{G}_{23}$) but without the fibre-substrate structure (see Figure 2.3).

2.3.4.1 Transverse Shear Modulus

On applying a uniform transverse shear at $r = \infty$ to the three phase cylinder model it can be shown (see Christensen [5]) that the transverse shear modulus is given by

$$\bar{G}_{23} = \frac{G_{12}}{P}\big(Q \pm \sqrt{Q^2 - PR}\big), \tag{2.174}$$

where

$$P = P_1 + \left[\frac{G_{12}^f}{G_{12}}\eta + \eta\eta^f - \left(\frac{G_{12}^f}{G_{12}}\eta - \eta^f\right)\delta^3\right]\left[\left(\frac{G_{12}^f}{G_{12}} - 1\right)\eta\delta - \left(\frac{G_{12}^f}{G_{12}}\eta + 1\right)\right], \tag{2.175}$$

$$Q = P_1 - \frac{P_2}{2}\left[(\eta - 1)\left(\frac{G_{12}^f}{G_{12}} + \eta^f\right) - 2\left(\frac{G_{12}^f}{G_{12}}\eta - \eta^f\right)\delta^3\right] - \frac{P_3}{2}(\eta + 1)\left(\frac{G_{12}^f}{G_{12}} - 1\right)\delta, \tag{2.176}$$

$$R = P_1 + P_2P_3, \tag{2.177}$$

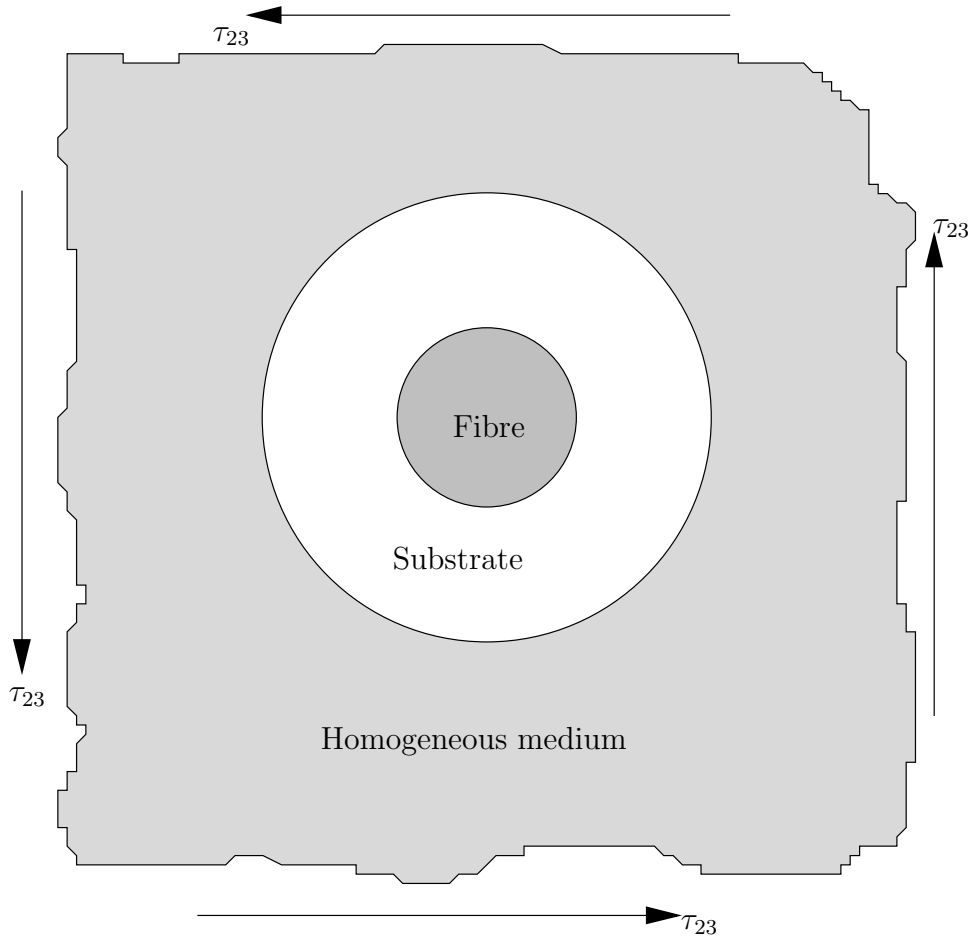


Figure 2.3: Three phase cylinder model.

and

$$P_1 = 3\delta(1-\delta)^2\left(\frac{G_{12}^f}{G_{12}} - 1\right)\left(\frac{G_{12}^f}{G_{12}} + \eta^f\right), \tag{2.178}$$

$$P_2 = \frac{G_{12}^f}{G_{12}}\eta + \left(\frac{G_{12}^f}{G_{12}} - 1\right)\delta + 1, \tag{2.179}$$

$$P_3 = \frac{G_{12}^f}{G_{12}} + \eta + \left(\frac{G_{12}^f}{G_{12}}\eta - \eta^f\right)\delta^3, \tag{2.180}$$

$$\eta = 3 - 4\nu_{12}, \tag{2.181}$$

$$\eta^f = 3 - 4\nu_{12}^f \tag{2.182}$$

Christensen [5] claims that under dilute (but unspecified) conditions the result (2.174) reduces to

$$\bar{G}_{23} = G_{12} + \frac{G_{12}\big(G_{12}^f - G_{12}\big)\big(6K + 8G_{12}\big)\delta}{G_{12}\big(6K + 8G_{12}\big) + \big(3K + 7G_{12}\big)\big(G_{12}^f - G_{12}\big)}, \tag{2.183}$$

where

$$K = \frac{E_1}{2L} \tag{2.184}$$

is the plane strain bulk modulus of the substrate. We will use (2.183) together with the four Halpin-Tsai equations to determine the five required elastic constants of a material reinforced with uni-directional fibres.

2.3.4.2 Transverse Poisson's Ratio

Recall that for a general elastic material

$$\bar{G}_{23} = \frac{\bar{E}_2}{2\big(1+\bar{\nu}_{23}\big)}, \tag{2.185}$$

where $\bar{\nu}_{23}$ is the transverse Poisson's ratio. So, on rearranging this we see that

$$\bar{\nu}_{23} = \frac{\bar{E}_2 - 2\bar{G}_{23}}{2\bar{G}_{23}}. \tag{2.186}$$

As with the minor Poisson's ratio this is not one of our independent elastic constants, but it helps to simplify our expressions for A, B, ..., I below.

2.3.5 Constants for a Material Reinforced With Uni-Directional Fibres

2.3.5.1 Frame Aligned With the Fibres

All of our above results for the elastic constants are for uni-directional fibres and axes aligned with the fibres. Suppose we assume that all of our fibres have winding angle ϕ (i.e. we have uni-directional reinforcing) and define (x_1, x_2, x_3) to be Cartesian coordinates fixed in the fibres, x_1 representing distance along the fibres and the (x_2, x_3)-plane perpendicular to them with the line of intersection of this plane and the (r, θ)-plane being a diameter of the hose. We choose the the x_2-axis to be this line of intersection so that the x_2- and r-directions are the same and our frame is right-handed (see Figure 2.4). In our expressions for the various elastic constants the subscript 1 represents the x_1-direction, etc. Then, since this material is orthotropic with planes of symmetry $x_i = 0$, $i = 1, 2, 3$, there exist constants A', B', ..., I' such that

$$V = \frac{1}{2}\begin{bmatrix} e_{11} & e_{22} & e_{33} \end{bmatrix}\begin{bmatrix} A' & D' & E' \\ D' & B' & F' \\ E' & F' & C' \end{bmatrix}\begin{bmatrix} e_{11} \\ e_{22} \\ e_{33} \end{bmatrix} + \frac{1}{2}\big(G'(2e_{12})^2 + H'(2e_{13})^2 + I'(2e_{23})^2\big) \tag{2.187}$$

where e_{11}, e_{12}, ..., e_{33} are the components of the strain tensor with respect to our (x_1, x_2, x_3) axes (c.f. (2.17)). Since our material is transversely isotropic in the (x_2, x_3)-plane (2.18) reduces to

$$\begin{bmatrix} A' & D' & E' \\ D' & B' & F' \\ E' & F' & C' \end{bmatrix} = \begin{bmatrix} 1/\bar{E}_1 & -\bar{\nu}_{12}/\bar{E}_1 & -\bar{\nu}_{12}/\bar{E}_1 \\ -\bar{\nu}_{12}/\bar{E}_1 & 1/\bar{E}_2 & -\bar{\nu}_{23}/\bar{E}_2 \\ -\bar{\nu}_{12}/\bar{E}_1 & -\bar{\nu}_{23}/\bar{E}_2 & 1/\bar{E}_2 \end{bmatrix}^{-1}. \tag{2.188}$$

On solving (2.188) and using (2.19) – (2.21) we see that

$$A' = \frac{\big(1-\bar{\nu}_{23}\big)\bar{E}_1}{1-\bar{\nu}_{23}-2\bar{\nu}_{12}\bar{\nu}_{21}}, \tag{2.189}$$

$$B' = C' = \frac{\big(1-\bar{\nu}_{12}\bar{\nu}_{21}\big)\bar{E}_2}{\big(1+\bar{\nu}_{23}\big)\big(1-\bar{\nu}_{23}-2\bar{\nu}_{12}\bar{\nu}_{21}\big)}, \tag{2.190}$$

$$D' = E' = \frac{\bar{\nu}_{12}\bar{E}_2}{1-\bar{\nu}_{23}-2\bar{\nu}_{12}\bar{\nu}_{21}}, \tag{2.191}$$

$$F' = \frac{\big(\bar{\nu}_{23}+\bar{\nu}_{12}\bar{\nu}_{21}\big)\bar{E}_2}{\big(1+\bar{\nu}_{23}\big)\big(1-\bar{\nu}_{23}-2\bar{\nu}_{12}\bar{\nu}_{21}\big)}, \tag{2.192}$$

$$G' = H' = \bar{G}_{12}. \tag{2.193}$$

$$I' = \bar{G}_{23}, \tag{2.194}$$

Although it appears that we have six independent elastic constants we observe that

$$B' - F' = \frac{\bar{E}_2}{1 + \bar{\nu}_{23}} = 2\bar{G}_{23} = 2I', \tag{2.195}$$

as we would expect for a transversely isotropic material, reducing the number of independent constants to five.

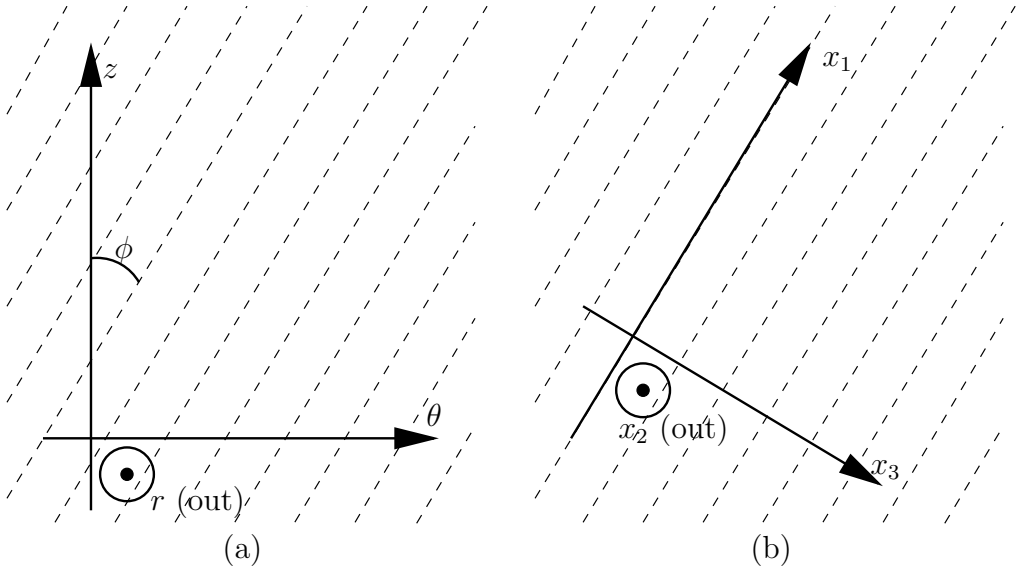


Figure 2.4: (a) Axes (r, θ, z) aligned with the hose and (b) axes (x_1, x_2, x_3) aligned with the fibres (represented by dashed lines).

2.3.5.2 Frame Aligned with the Hose

We now need to transform the constants $A', B', \ldots, I'$ calculated above into the relevant quantities $A, B, \ldots, I$ necessary for use in the frame fixed in the hose. Since we have not chosen the planes of symmetry to be our axes (since the fibres are slanted and uni-directional) we expect to get an expression for V in terms of our stress components in cylindrical polars and a symmetric 6-by-6 matrix, i.e.

$$V = \frac{1}{2}\begin{bmatrix} e_{rr} & e_{\theta\theta} & e_{zz} & 2e_{r\theta} & 2e_{rz} & 2e_{\theta z} \end{bmatrix} \begin{bmatrix} A & D & E & V_{14} & V_{15} & V_{16} \\ D & B & F & V_{24} & V_{25} & V_{26} \\ E & F & C & V_{34} & V_{35} & V_{36} \\ V_{14} & V_{24} & V_{34} & G & V_{45} & V_{46} \\ V_{15} & V_{25} & V_{35} & V_{45} & H & V_{56} \\ V_{16} & V_{26} & V_{36} & V_{46} & V_{56} & I \end{bmatrix} \begin{bmatrix} e_{rr} \\ e_{\theta\theta} \\ e_{zz} \\ 2e_{r\theta} \\ 2e_{rz} \\ 2e_{\theta z} \end{bmatrix}. \tag{2.196}$$

Note from (2.17) that this is what we get in the orthotropic case, but with the 6-by-6 matrix reducing to a block matrix with four 3-by-3 blocks, the two off diagonal blocks being made up completely of zeros and the lower right block being diagonal.

We observe that at any point in the hose our unit vectors fixed in the fibre are related to those fixed in the hose by

$$\begin{bmatrix} \mathbf{e}_1 \\ \mathbf{e}_2 \\ \mathbf{e}_3 \end{bmatrix} = \begin{bmatrix} 0 & \sin\phi & \cos\phi \\ 1 & 0 & 0 \\ 0 & \cos\phi & -\sin\phi \end{bmatrix} \begin{bmatrix} \mathbf{e}_r \\ \mathbf{e}_\theta \\ \mathbf{e}_z \end{bmatrix}, \tag{2.197}$$

where $\mathbf{e}_r$ $\mathbf{e}_\theta$, ..., $\mathbf{e}_3$ are unit vectors in the r, θ, ..., x_3 directions respectively. Since e is a tensor its components transform as

$$e_{rs} = l_{ri} l_{sj} e'_{ij} \tag{2.198}$$

where l_{ij} is the (i,j)-th entry of the orthogonal transformation matrix L satisfying $(\mathbf{e}_1, \mathbf{e}_2, \mathbf{e}_3)^T = L(\mathbf{e}'_1, \mathbf{e}'_2, \mathbf{e}'_3)^T$. Here

$$L = \begin{bmatrix} 0 & \sin\phi & \cos\phi \\ 1 & 0 & 0 \\ 0 & \cos\phi & -\sin\phi \end{bmatrix}, \tag{2.199}$$

where we note that $\det L = 1$ as expected since both the (r, θ, z) and (x_1, x_2, x_3) axes are right-handed, and hence our strains are given by

$$e_{11} = \sin^2\phi e_{\theta\theta} + 2\sin\phi\cos\phi e_{\theta z} + \cos^2\phi e_{zz}, \tag{2.200}$$
$$e_{22} = e_{rr}, \tag{2.201}$$
$$e_{33} = \cos^2\phi e_{\theta\theta} - 2\sin\phi\cos\phi e_{\theta z} + \sin^2\phi e_{zz}, \tag{2.202}$$
$$e_{12} = \sin\phi e_{r\theta} + \cos\phi e_{rz}, \tag{2.203}$$
$$e_{13} = \sin\phi\cos\phi e_{\theta\theta} + \big(\cos^2\phi - \sin^2\phi\big) e_{\theta z} - \sin\phi\cos\phi e_{zz}, \tag{2.204}$$
$$e_{23} = \cos\phi e_{r\theta} - \sin\phi e_{rz}. \tag{2.205}$$

Then on substituting these expressions into (2.187) we find that the potential energy does indeed take the form of (2.197) with

$$A = B', \tag{2.206}$$
$$B = A'\sin^4\phi + B'\cos^4\phi + 2(D' + 2G')\sin^2\phi\cos^2\phi, \tag{2.207}$$
$$C = A'\cos^4\phi + B'\sin^4\phi + 2(D' + 2G')\sin^2\phi\cos^2\phi, \tag{2.208}$$
$$D = D'\sin^2\phi + F'\cos^2\phi, \tag{2.209}$$
$$E = D'\cos^2\phi + F'\sin^2\phi, \tag{2.210}$$
$$F = D'\big(\sin^4\phi + \cos^4\phi\big) + (A' + B' - 4G')\sin^2\phi\cos^2\phi, \tag{2.211}$$
$$G = G'\sin^2\phi + H'\cos^2\phi, \tag{2.212}$$
$$H = G'\cos^2\phi + H'\sin^2\phi, \tag{2.213}$$
$$I = (A' + B' - 2D')\sin^2\phi\cos^2\phi + G'\big(\cos^2\phi - \sin^2\phi\big)^2, \tag{2.214}$$
$$V_{16} = (D' - F')\sin\phi\cos\phi, \tag{2.215}$$
$$V_{26} = A'\sin^3\phi\cos\phi - B'\sin\phi\cos^3\phi + (D' + G')\sin\phi\cos\phi\big(\cos^2\phi - \sin^2\phi\big), \tag{2.216}$$
$$V_{36} = A'\sin\phi\cos^3\phi - C'\sin^3\phi\cos\phi + (D' + G')\sin\phi\cos\phi\big(\sin^2\phi - \cos^2\phi\big), \tag{2.217}$$
$$V_{45} = G'\sin\phi\cos\phi - I'\sin\phi\cos\phi \tag{2.218}$$

and all the other entries in the 6-by-6 matrix being zero. We observe that if $\phi = 0$ then $V_{26} = V_{36} = V_{45} = 0$, $A = B$, $E = F$, $H = I$ and, on using (2.195), $D = F' = B' - 2I' = A - 2G$. So, the material is transversely isotropic when $\phi = 0$ as expected.

2.3.6 Effects of Bi-Directional Fibres

Our above theory for uni-directional reinforcing fibres does not apply to our case (except in the simple case $\phi = 0$) since the hose we are interested in has bi-directional fibres. We can, however, adapt the above theory to deal with bi-directional fibres. Smith [36, 37] tells us that we can deal with multi-directional fibre reinforcing by taking a weighted average of the solutions in each of the uni-directional cases (weighted in accordance with the number of fibres in each direction). So, in our case where half the fibres have lay angle ϕ and the other half lay angle $-\phi$ this amounts to averaging each of (2.206) – (2.218) with the equivalent expression but with ϕ replaced by $-\phi$.

Since including an equal number of fibres winding in each direction means that our axes once again lie in the planes of symmetry we expect that our potential energy will once again take the orthotropic form (2.17), i.e. the only non-zero constants in (2.197) will be A, B, $\ldots$, I. This is indeed what happens, since the V_{ij} terms involve only odd powers of $\sin\phi$, and

$$A = B', \tag{2.219}$$

$$B = A' \sin^4\phi + B' \cos^4\phi + 2(D' + 2G') \sin^2\phi \cos^2\phi, \tag{2.220}$$

$$C = A' \cos^4\phi + B' \sin^4\phi + 2(D' + 2G') \sin^2\phi \cos^2\phi, \tag{2.221}$$

$$D = D' \sin^2\phi + F' \cos^2\phi, \tag{2.222}$$

$$E = D' \cos^2\phi + F' \sin^2\phi, \tag{2.223}$$

$$F = D'\big(\sin^4\phi + \cos^4\phi\big) + (A' + B' - 4G') \sin^2\phi \cos^2\phi, \tag{2.224}$$

$$G = G' \sin^2\phi + I' \cos^2\phi, \tag{2.225}$$

$$H = G' \cos^2\phi + H' \sin^2\phi, \tag{2.226}$$

$$I = (A' + B' - 2D') \sin^2\phi \cos^2\phi + G'\big(\cos^2\phi - \sin^2\phi\big)^2. \tag{2.227}$$

Chapter 3

Linear Acoustic Waves

In this chapter we consider the motion of the fluids inside and outside the hose. We do this by assuming that the fluid is undergoing small perturbations about an undisturbed state and considering linearized acoustic waves (see, e.g., Acheson [1] or Batchelor [2]). Solutions for such wave in cylindrical polars are well known and are presented here.

3.1 Equations Of Motion

Recall (from Acheson [1]) that the pressure perturbations of linearized acoustic in inviscid fluid waves obey

$$\frac{\partial^2 p}{\partial t^2} = c^2 \nabla^2 p, \tag{3.1}$$

where p is the acoustic (perturbation) pressure and c the speed of sound in the fluid. Our boundary conditions will be continuity of p at $r = 0$, continuity of radial displacement at $r = a - h$ and $r = a$, matching conditions between the fluid pressure and the stress in the hose at the fluid-hose interfaces, i.e.

$$p = -\tau_{rr},\ \tau_{r\theta} = \tau_{rz} = 0 \text{ at } r = a - h \text{ and } r = a, \tag{3.2}$$

and a suitable *decay* or *radiation condition* as $r \to \infty$ to ensure that no waves propagate inwards from infinity in order to ensure that we see only the waves that are produced as a response to the forcing on the hose. We have two options in how we impose this condition. We can either apply boundary conditions on the partial differential equation (3.1) as $r \to \infty$ (see Jones [20]) or we can pick the correct linear combination of the available solutions to ensure that no energy propagates inwards from infinity. We will use the latter approach.

3.1.1 Insertion of a Fourier Mode

In order to match with the solution in the hose we look for solutions in the form of a single Fourier mode, i.e.

$$p_i(r, \theta, z, t) = \Re\big[P_i(r) e^{i(\omega t - kz - n\theta)}\big], \quad i = 1, 2, \tag{3.3}$$

where p_1 is the pressure of the fluid in the interior of the hose, $0 \leqslant r < a - h$, p_2 that of the fluid outside the hose, $r > a$, and $\Re$ again tells us to take the real part. Then on substituting into (3.1), recalling that in cylindrical polars

$$\nabla^2 = \frac{1}{r}\frac{\partial}{\partial r}\left(r\frac{\partial}{\partial r}\right) + \frac{1}{r^2}\frac{\partial^2}{\partial \theta^2} + \frac{\partial^2}{\partial z^2} \tag{3.4}$$

(see, e.g. Bourne & Kendall [3]), we obtain an ordinary differential equation for P_i:

$$r^2 P_i'' + r P_i' + \big(r^2 \kappa_i^2 - n^2\big) P_i = 0, \quad i = 1, 2, \tag{3.5}$$

where

$$\kappa_i^2 = \frac{\omega^2}{c_i^2} - k^2, \quad i = 1, 2, \tag{3.6}$$

and c_1 is the speed of sound in the fluid inside the hose and c_2 the sound speed in the fluid outside the hose. This is Bessel's equation of order n and (as it did in the hose) it has solutions

$$P_i = C_i J_n(\kappa_i r) + D_i Y_n(\kappa_i r), \quad i = 1, 2. \tag{3.7}$$

3.1.2 Continuity of Radial Displacement

Recall that in our description of the motion of the hose we did not derive the boundary conditions that are due to continuity of radial displacement across the fluid-hose interface. This was because whilst it is straightforward to see that the radial displacement of the hose is u we need to do some work to calculate the displacement of the fluid in terms of its pressure. Recall (from, e.g., Acheson [1]) that for a fluid linearization of our conservation of momentum equation gives

$$\rho \frac{\partial^2 \mathbf{u}}{\partial t^2} = -\nabla p, \tag{3.8}$$

where ρ is the fluid density, p its pressure and $\mathbf{u} = (u, v, w)$ its *displacement* field. Then in the radial direction we have

$$\rho \frac{\partial^2 u}{\partial t^2} = -\frac{\partial p}{\partial r}. \tag{3.9}$$

If we can ensure that accelerations at the fluid-hose interface match at all times then the displacements will also match. So, we use (3.9) together with our expressions (2.49), for the radial displacement of the hose, and (3.3), for the pressure in the fluid, to see that our final boundary conditions are

$$\rho_1 \omega^2 U = P_1' \quad \text{at } r = a - h, \tag{3.10}$$

$$\rho_2 \omega^2 U = P_2' \quad \text{at } r = a, \tag{3.11}$$

where ρ_1 and ρ_2 are the densities of the interior and exterior fluids respectively.

3.1.3 Fluid in the Interior of the Hose

The point $r = 0$ lies in the interior of the hose, so we need to ensure that our solution does not blow up here. Since $Y_n(\kappa_1 r) \to \infty$ as $r \to 0$ we must choose $D_1 = 0$, so that

$$P_1 = C_1 J_n(\kappa_1 r). \tag{3.12}$$

The remaining constant C_1 is to be determined by the matching condition at $r = a - h$. If $\kappa_1^2 < 0$ then we can write $\kappa_1 = ik_1$ for real k_1, and then

$$P_1 = C_1 I_n(k_1 r), \tag{3.13}$$

where I_n is a *modified Bessel function of the first kind*, defined for real $z > 0$ by (see, e.g., Temme [39])

$$I_n(z) = e^{\frac{1}{2} n \pi i} J_n(iz). \tag{3.14}$$

3.1.4 Fluid Outside the Hose

For the fluid outside the hose we can reduce the number of arbitrary constants to one from the decay or radiation condition as $r \to \infty$. This constant is then determined from the matching condition at $r = a$. The exact form of the radiation condition depends on whether κ_2 is real or imaginary.

3.1.4.1 Real-Valued κ_2

Suppose first that

$$\kappa_2^2 = \frac{\omega^2}{c_2^2} - k^2 > 0 \tag{3.15}$$

so that $\kappa_2 \in \mathbb{R}$ and we choose $\kappa_2 > 0$. In this case we re-write our solution as

$$P_2 = \tilde{C}_2 H_n^{(1)}(\kappa_2 r) + \tilde{D}_2 H_n^{(2)}(\kappa_2 r), \tag{3.16}$$

where $H_n^{(1)}$, $H_n^{(2)}$ are the *Hankel functions*, defined by (see, e.g. Temme [39])

$$H_n^{(1)} = J_n + iY_n, \tag{3.17}$$

$$H_n^{(2)} = J_n - iY_n. \tag{3.18}$$

We now observe that as $\kappa_2 r \to \infty$ the Hankel functions exhibit the following asymptotic behaviour (see Jones [20]):

$$H_n^{(1)}(\kappa_2 r) \sim \sqrt{\frac{2}{\pi \kappa_2 r}} e^{i(\kappa_2 r - n\pi/2 - \pi/4)}, \tag{3.19}$$

$$H_n^{(2)}(\kappa_2 r) \sim \sqrt{\frac{2}{\pi \kappa_2 r}} e^{-i(\kappa_2 r - n\pi/2 - \pi/4)}. \tag{3.20}$$

When we include our time dependence $e^{i\omega t}$ we see that as $\kappa_2 r \to \infty$,

$$H_n^{(1)}(\kappa_2 r) e^{i\omega t} \sim \sqrt{\frac{2}{\pi \kappa_2 r}} e^{i(\omega t + \kappa_2 r - n\pi/2 - \pi/4)}, \tag{3.21}$$

$$H_n^{(2)}(\kappa_2 r) e^{i\omega t} \sim \sqrt{\frac{2}{\pi \kappa_2 r}} e^{i(\omega t - \kappa_2 r + n\pi/2 + \pi/4)}. \tag{3.22}$$

So, in (3.21) a point of constant phase ($\omega t + kr =$ constant) is moving *inwards* at speed ω/k: $H_n^{(1)}$ represents an incoming wave. Similarly, in (3.22) $\omega t - kr =$ constant represents a point moving outwards at speed ω/k. Hence we need to choose $\tilde{C}_2 = 0$ so that

$$P_2 = \tilde{D}_2 H_n^{(2)}(\kappa_2 r) \tag{3.23}$$

and we only have outgoing waves, as required. The remaining constant $\tilde{D}_2$ is to be determined by the matching condition at $r = a$.

3.1.4.2 Imaginary-Valued κ_2

Now suppose that

$$\kappa_2^2 = \frac{\omega^2}{c_2^2} - k^2 < 0. \tag{3.24}$$

In this case κ_2 is purely imaginary and we write

$$P_2 = \hat{C}_2 I_n(k_0 r) + \hat{D}_2 K_n(k_0 r), \tag{3.25}$$

where K_n is a *modified Bessel function of the second kind*, defined for real $z > 0$ by (see, e.g., Temme [39])

$$K_n(z) = \frac{1}{2}\pi i e^{\frac{1}{2}n\pi i} H_n^{(1)}(iz), \tag{3.26}$$

and

$$k_0 = i\kappa_2 = \sqrt{k^2 - \frac{\omega^2}{c_2^2}}. \tag{3.27}$$

Now, we know from Jones [20] that as $k_0 r \to \infty$,

$$J_n(k_0 r) \sim \sqrt{\frac{2}{\pi k_0 r}}\left[d_1 \cos\left(k_0 r - \frac{1}{2}n\pi - \frac{1}{4}\pi\right) + d_2 \sin\left(k_0 r - \frac{1}{2}n\pi - \frac{1}{4}\pi\right)\right], \tag{3.28}$$

where d_1, d_2 are real constants. So, recalling that $\cos(iz) \sim e^z/2$ and $\sin(iz) \sim ie^z/2$ as $z(\in \mathbb{R}) \to \infty$, we observe from (3.14) that

$$I_n(k_0 r) = e^{\frac{1}{2}n\pi i} J_n(ik_0 r) \sim \sqrt{\frac{\pi}{2k_0 r}} e^{k_0 r} \to \infty \tag{3.29}$$

as $k_0 r \to \infty$. And, (3.21) and (3.26) tell us that as $k_0 r \to \infty$,

$$K_n(k_0 r) = \frac{1}{2}\pi i e^{\frac{1}{2}n\pi i} H_n^{(1)}(ik_0 r) \sim \sqrt{\frac{\pi}{2k_0 r}} e^{-k_0 r} \to 0. \tag{3.30}$$

The physically relevant solution for forcing on the hose is, therefore, the K_n solution, so we must choose $\hat{C}_2 = 0$ giving

$$P_2 = \hat{D}_2 K_n(k_0 r) \tag{3.31}$$

and $p \to 0$ as $k_0 r \to \infty$ and energy is not radiated to or from infinity. Again the final constant $\hat{D}_2$ is determined from matching with the radial stress in the hose at $r = a$.

3.2 Waves on the Interfaces

We now include a description of the excitation of waves on the interface between a fluid and an elastic solid. Since interface waves are solutions of our equations of motion and boundary conditions their effects are included in our existing model for the vibrating hose, so our discussion is relatively brief. We also restrict our discussion to plane waves incident on a plane interface (although our fluid-hose interfaces are not planes). The theory set out below would need to be modified to fully explain the behaviour of a cylindrical interface, but it is sufficient to describe the effects due to waves in the radial direction (normal to the interface). A more complete description can be found in Hudson [19], Tew [40] or Überall [42]. A description of waves on a thin cylindrical shell is given in Scott [32].

3.2.1 Snell's Law

Snell's law (see, e.g. Hudson [19]) provides a relationship between the angle of incidence of a wave on an interface and the angles of emergence of the reflected and refracted waves in terms of the wave speeds either side of the interface. Suppose initially that we have a compressional (P) wave

$$\mathbf{u} = \mathbf{n}u\left(t - \frac{\mathbf{n}.\mathbf{x}}{\alpha}\right), \quad |\mathbf{n}| = 1, \quad \mathbf{x} \equiv (x, y, z), \tag{3.32}$$

obliquely incident on the interface between two homogeneous elastic solids. For simplicity we choose the (x, y)-plane to be the plane of incidence and the line $y = 0$ to be the interface. Let α, β be the wave speeds of compressional and shear (S) waves respectively in the region in which the wave originates ($y < 0$) and α', β' the wave speeds in $y > 0$. Then $\mathbf{n}$ becomes the 2-vector

$$\mathbf{n} = (n_x, n_y), \quad n_y > 0. \tag{3.33}$$

We define the *angle of incidence* of the incoming wave to be the acute angle

$$\theta_\alpha = \sin^{-1} n_\alpha. \tag{3.34}$$

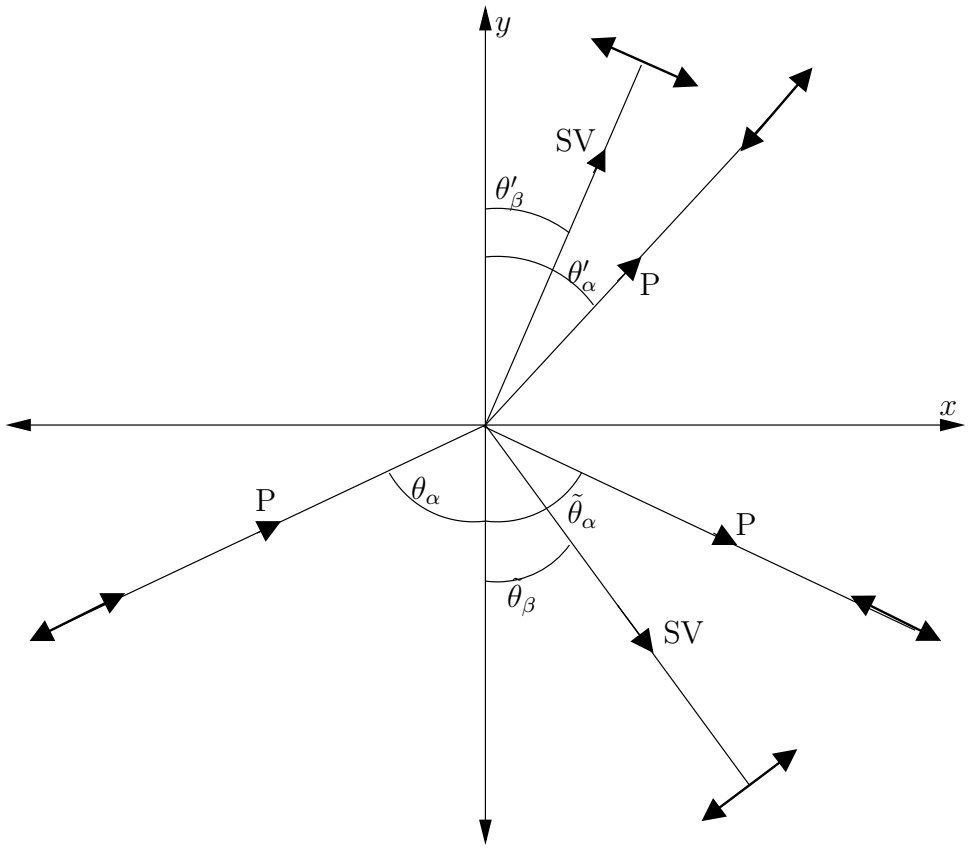


Figure 3.1: Reflected and refracted waves due to a compressional wave incident on $y = 0$.

The disturbance resulting from the incident plane wave consists of plane waves travelling outwards into both materials. We introduce reflected and refracted P and S waves. Since this is a plane strain problem (all of the incoming displacements lie in the (x, y)-plane) the displacements of the outgoing waves and the polarisation of the shear waves must, by symmetry, lie in the plane of incidence. Shear waves polarised in this plane are known as SV waves. Those with polarisation normal to the plane of incidence are known as SH waves. So, in $y < 0$ we have a reflected P wave

$$A\tilde{\mathbf{n}}u\big(t - \tilde{\mathbf{n}}.\mathbf{x}/\alpha\big), \quad |\tilde{\mathbf{n}}| = 1, \tag{3.35}$$

and a reflected SV wave

$$B\tilde{\mathbf{p}}u\big(t - \tilde{\mathbf{m}}.\mathbf{x}/\beta\big), \quad |\tilde{\mathbf{p}}| = |\tilde{\mathbf{n}}| = 1, \quad \tilde{\mathbf{p}}.\tilde{\mathbf{m}} = 0, \tag{3.36}$$

where A, B are real constants and we have the same time function u as before to ensure matching of displacements on the interface. In $y > 0$ we have refracted P and SV waves given by

$$C\mathbf{n}'u\big(t - \mathbf{n}'.\mathbf{x}/\alpha'\big), \quad |\mathbf{n}'| = 1, \tag{3.37}$$

$$D\mathbf{p}'u\big(t - \mathbf{m}'.\mathbf{x}/\beta'\big), \quad |\mathbf{p}'| = |\mathbf{n}'| = 1, \quad \mathbf{p}'.\mathbf{m}' = 0, \tag{3.38}$$

where C, D are constants (see Figure 3.1). Then the requirement that the incident, refracted and reflected waves must coincide as functions of x and t on the interface tells us that

$$\frac{n_x}{\alpha} = \frac{\tilde{n}_x}{\alpha} = \frac{\tilde{m}_x}{\beta} = \frac{n'_x}{\alpha'} = \frac{m'_x}{\beta'}. \tag{3.39}$$

Defining *angles of emergence* $\tilde{\theta}_\alpha$, $\tilde{\theta}_\beta$ for the reflected P and SV waves respectively, θ'_α, θ'_β for the refracted waves in the same way we did in (3.34) for the incident wave we can rewrite (3.38) as

$$\frac{\sin\theta_\alpha}{\alpha} = \frac{\sin\tilde{\theta}_\alpha}{\alpha} = \frac{\sin\tilde{\theta}_\beta}{\beta} = \frac{\sin\theta'_\alpha}{\alpha'} = \frac{\sin\theta'_\beta}{\beta'}, \tag{3.40}$$

which is *Snell's law*. We see that for the reflected P wave $\tilde{\theta}_\alpha = \theta_\alpha$ and, since $\beta < \alpha$, we have $\theta_\beta \in \mathbb{R}$. However, if $\alpha' > \alpha$ then θ'_α may not be real and we need a different representation for the refracted P wave. Similarly if $\beta' > \alpha$ then θ'_β may be complex. There are at most two critical angles of incidence above which one of the emerging waves ceases to be an outgoing plane wave:

$$\sin\theta^*_\alpha = \frac{\alpha}{\alpha'},\ \frac{\alpha}{\beta'}. \tag{3.41}$$

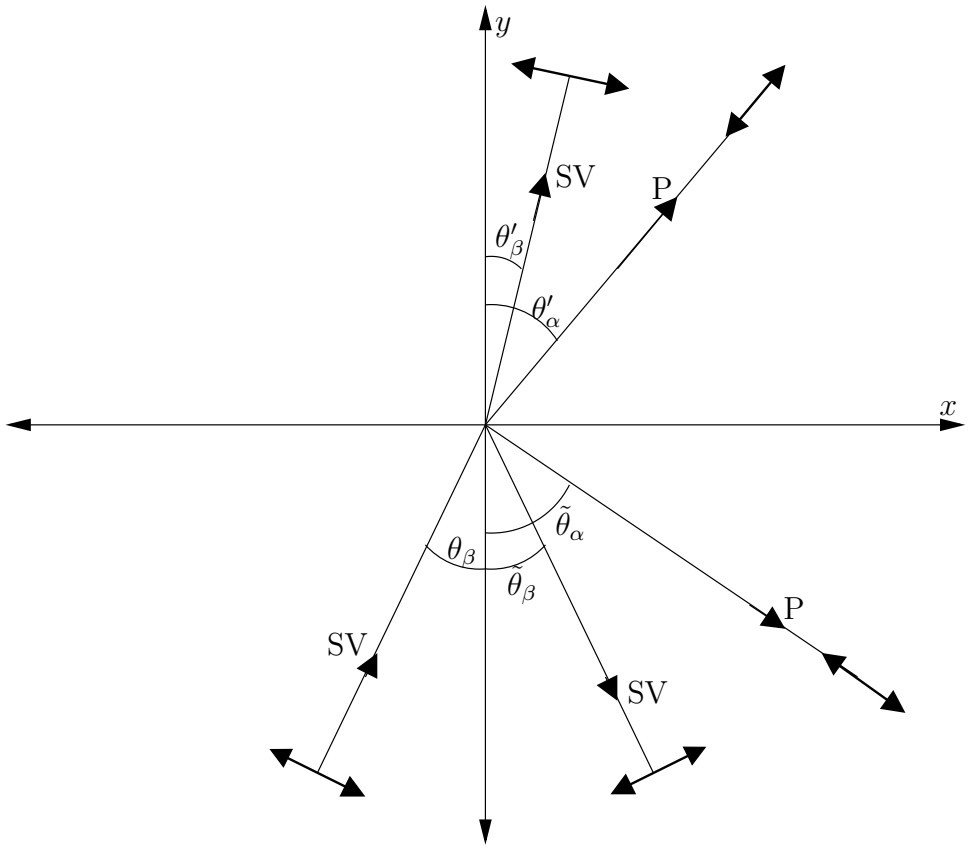


Figure 3.2: Reflected and refracted waves due to a shear wave polarised in the direction of the plane of incidence incident on $y = 0$.

If the incident wave is instead an SV

$$\mathbf{u} = \mathbf{p}u\left(t - \frac{\mathbf{m}.\mathbf{u}}{\beta}\right), \quad |\mathbf{p}| = |\mathbf{m}| = 1, \quad \mathbf{p}.\mathbf{m} = 0, \tag{3.42}$$

wave with angle of incidence θ_β then we see the same pattern of reflected and refracted waves (see Figure 3.2), except that the amplitudes A, B, C, D are changed. Again Snell's law applies but in

this case there may be up to three critical angles of incidence (since in this case the reflected P wave may also cease to be an outgoing plane wave as $\beta < \alpha$) given by

$$\sin\theta^*_\beta = \frac{\beta}{\alpha},\ \frac{\beta}{\alpha'},\ \frac{\beta}{\beta'}. \tag{3.43}$$

Finally, the incident wave may be an SH wave with angle of incidence θ_β. In this case the problem becomes one of antiplane strain (since all our incoming displacements are in the direction normal to the (x, y)-plane) and so only reflected and refracted SH waves are produced. An incident wave with amplitude

$$u(t - \mathbf{m}.\mathbf{x}/\beta), \quad |\mathbf{m}| = 1, \tag{3.44}$$

will excite a reflected wave of amplitude

$$Au(t - \tilde{\mathbf{m}}.\mathbf{x}/\beta), \quad |\tilde{\mathbf{m}}| = 1, \tag{3.45}$$

and a refracted wave with amplitude

$$Cu(t - \mathbf{m}'.\mathbf{x}/\beta), \quad |\mathbf{m}'| = 1. \tag{3.46}$$

Snell's law (3.40) becomes

$$\frac{\sin\theta_\beta}{\beta} = \frac{\sin\tilde{\theta}_\beta}{\beta} = \frac{\sin\theta'_\beta}{\beta'} \tag{3.47}$$

and there is just one critical angle of incidence:

$$\sin\theta^*_\beta = \frac{\beta}{\beta'}. \tag{3.48}$$

Hudson [19] shows that in all of the above cases we get waves propagating along the interface for any angle of incidence above the smallest critical angle. Each time the angle of incidence increases beyond a critical angle the outgoing plane wave corresponding to that critical angle (the wave whose speed appears in the expression for the critical angle) is replaced by a wave travelling along the interface with an amplitude that decreases towards zero as the distance from the interface increases. In the case of P and SV waves the interface waves generated are elliptically polarised in the plane of incidence. In all three cases (degeneration of P, SV and SH waves) the interface wave carries energy parallel to the interface at the phase velocity.

3.2.2 Rayleigh and Stoneley Waves

3.2.2.1 Rayleigh Waves

The existence of waves on the interface excited by an incident plane wave suggests that such waves may exist freely on the interface as guided waves under certain circumstances, i.e. they may be present even when there is no incident wave to generate them. Lord Rayleigh showed (see Hudson [19]) that free interface waves of this kind do exist on the interface between a solid and a vacuum under all circumstances. These *Rayleigh waves* are, according to Überall [42] and Hudson [19], non-dispersive plane inhomogeneous waves that travel along the interface at speed $c_R < \beta < \alpha$ given by

$$c_R^2 = \beta^2\xi, \tag{3.49}$$

where ξ is a root of

$$\xi^3 - 8\xi^2 + 8(1 + 2q)\xi - 16q = 0, \tag{3.50}$$

with

$$q = 1 - \frac{\beta^2}{\alpha^2}. \tag{3.51}$$

Clearly ξ can take either one or three positive roots but for a material with a Poisson's ratio in the interval $[-1, 1/2]$ it turns out (see Hudson [19]) that (3.50) has only one root. So, all Rayleigh waves propagate along the interface with the same wave speed c_R.

3.2.2.2 Stoneley Waves

If we have elastic solids on both sides of the interface (rather than a vacuum on one side as for Rayleigh waves) then the situation becomes more complex. The Rayleigh waves described above still exist, but we may also have *Stoneley waves* on the interface. Stoneley waves exist only if the determinant of a certain matrix (M_4) (see Hudson [19]) is zero. This matrix is a function of the Stoneley wave speed c_S so where possible we choose $c_S > 0$ to ensure that $\det M_4 = 0$. Where we can do this we have a Stoneley wave propagating along the interface at speed $c_S < \min\{\beta, \beta'\} < \min\{\alpha, \alpha'\}$. If we cannot choose such a c_S then the Stoneley wave degenerates to a leaky Rayleigh wave (these are surface waves that decay with distance along the interface and with time and are described in Hudson [19]). When we replace one of the solids with a fluid (as in our case) it turns out (again, see Hudson [19]) that it is always possible to construct a Stoneley wave at the interface.

3.2.2.3 Effect of Interface Waves Away From the Interfaces

Since Rayleigh and Stoneley waves travel only along the interface and decay rapidly with distance away from it they cannot be easily observed away from the interface. The same is true for the interface waves generated by an incident plane wave. However, their effect may be felt indirectly away from the interface as they can give rise to a *head wave* being radiated from the interface into the material either side of the interface. Such a wave is generated as a consequence of singularities and branch points in the Fourier representation of the interface waves. A full description of head waves can be found in Überall [42] or Tew [40].

Chapter 4

Numerical Analysis

4.1 Dimensional Analysis

Before beginning our numerical analysis we non-dimensionalize our equations of motion. This allows us to identify the important parameters in the system and possibly use perturbation methods to simplify the system further before computing solutions to the $O(1)$ part of the problem.

4.1.1 Non-Dimensionalization

Suppose we introduce the scaled variables U^*, V^* W^*, r^*, P_1^*, P_2^*, all of which are $O(1)$ in magnitude, defined by

$$(U, V, W) = \bar{U}(U^*, V^*, W^*), \tag{4.1}$$

$$r = ar^*, \tag{4.2}$$

$$P_1 = \rho_1 \omega^2 a^2 P_1^*, \tag{4.3}$$

$$P_2 = \rho_2 \omega^2 a^2 P_2^*, \tag{4.4}$$

where

$$\bar{U} = \frac{kP_f}{\bar{\rho}\omega^2}. \tag{4.5}$$

Then on substituting in (2.53) – (2.55) and dropping the * notation we see that

$$\begin{aligned} -U = A\alpha\left(U'' + \frac{U'}{r}\right) - \frac{B\alpha U}{r^2} - \frac{Gn^2\alpha U}{r^2} - H\gamma U + \frac{n\alpha}{r}(G+D)V' - \frac{n\alpha}{r^2}(G+B)V \\ + \beta(E+H)W' + \frac{\beta}{r}(E-F)W, \end{aligned} \tag{4.6}$$

$$V = \frac{n\alpha}{r}(G+D)U' + \frac{n\alpha}{r^2}(G+B)U - G\alpha\left(V'' + \frac{V'}{r} - \frac{V}{r^2}\right) + \frac{Bn^2\alpha V}{r^2} + I\gamma V + \frac{n\beta}{r}(I+F)W, \tag{4.7}$$

$$W = \beta(H+E)U' + \frac{\beta}{r}(H+F)U + \frac{n\beta}{r}(I+F)V - H\alpha\left(W'' + \frac{W'}{r}\right) + \frac{In^2\alpha W}{r^2} + C\gamma W, \tag{4.8}$$

where

$$\alpha = \frac{1}{\bar{\rho}\omega^2 a^2}, \tag{4.9}$$

$$\beta = \frac{k}{\bar{\rho}\omega^2 a}, \tag{4.10}$$

$$\gamma = \frac{k^2}{\bar{\rho}\omega^2}. \tag{4.11}$$

And, non-dimensionalizing our boundary conditions (2.56) – (2.59), (3.10), (3.11) gives

$$A\delta_1 U' + \frac{D\delta_1}{r}(nV + U) + Eak\delta_1 W = -\frac{aP_1}{\bar{U}}, \tag{4.12}$$

$$U = \frac{aP_1'}{\bar{U}}, \tag{4.13}$$

at $r = 1 - h/a$,

$$A\delta_2 U' + \frac{D\delta_2}{r}(nV + U) + Eak\delta_2 W = -\frac{a\delta_2 P_f}{\bar{U}} - \frac{\bar{\rho}\omega^2 aP_2}{kP_f}, \tag{4.14}$$

$$U = \frac{aP_2'}{\bar{U}}, \tag{4.15}$$

at $r = 1$, and

$$V' - \frac{V}{r} - \frac{nU}{r} = 0, \tag{4.16}$$

$$W' - akU = 0 \tag{4.17}$$

at both $r = 1$ and $r = 1 - h/a$, where

$$\delta_i = \frac{1}{\rho_i \omega^2 a^2}, \quad i = 1, 2. \tag{4.18}$$

4.1.2 Parameter Analysis

4.1.2.1 Mechanical Properties of the System

Thales provided us with a description of the structure of the fibre-reinforced hose and typical mechanical properties of the materials it is made of. The hose itself is usually made of some type of PVC, which has a typical density of

$$\rho = 1380 \text{ kgm}^{-3}. \tag{4.19}$$

The Young's modulus of PVC varies depending on the frequency it is oscillating at. Typical values are

$$E_1 = \begin{cases} 7.5 \times 10^7 \text{ Nm}^{-2} & \text{at 1 Hz}, \\ 4.7 \times 10^8 \text{ Nm}^{-2} & \text{at 1 kHz}, \\ 5.5 \times 10^8 \text{ Nm}^{-2} & \text{at 2 kHz}. \end{cases} \tag{4.20}$$

The Poisson's ratio of PVC is

$$\nu_{12} = 0.33 \tag{4.21}$$

and its shear modulus is given by

$$G_{12} = \frac{E_1}{2\big(1 + \nu_{12}\big)}. \tag{4.22}$$

The reinforcing fibres can be made of nylon, which has typical density

$$\rho^f = 1140 \text{ kgm}^{-3} \tag{4.23}$$

and, according to Thales, has a typical shear modulus of

$$G_{12}^f = 1.275 \times 10^9 \text{ Nm}^{-2} \tag{4.24}$$

and bulk modulus

$$K^f = 3.4 \times 10^9. \tag{4.25}$$

Then, recalling that for a general isotropic elastic solid $K = E_1/2(1+\nu_{12})(1-2\nu_{12})$ and $G = E_1/2(1+\nu_{12})$, we see that the Poisson's ratio and Young's modulus of nylon are, typically,

$$\nu_{12}^f = 0.33, \tag{4.26}$$

$$E_1^f = 3.3 \times 10^9 \text{ Nm}^{-2}. \tag{4.27}$$

Alternatively the fibres could be kevlar. The density of kevlar is typically

$$\rho^f = 1450 \text{ kgm}^{-3} \tag{4.28}$$

and its Poisson's ratio is

$$\nu_{12}^f = 0.35 \tag{4.29}$$

and Thales give typical values of the Young's modulus of kevlar as

$$E_1^f = \begin{cases} 3.8 \times 10^7 \text{ Nm}^{-2} & \text{at 1 Hz,} \\ 5.2 \times 10^7 \text{ Nm}^{-2} & \text{at 1 kHz,} \\ 5.4 \times 10^7 \text{ Nm}^{-2} & \text{at 2 kHz.} \end{cases} \tag{4.30}$$

And, hence, its shear modulus can be calculated as

$$G_{12}^f = \frac{E_1^f}{2\big(1+\nu_{12}^f\big)}. \tag{4.31}$$

The structure of the hoses can be split into two classes. In both classes the dimensions of the hose will usually be roughly

$$a = 0.0375 \text{ m}, \tag{4.32}$$

$$h = 0.0125 \text{ m}. \tag{4.33}$$

In the first class (A) the hose will be reinforced with about 40 fibres, each having a diameter of 0.0008 – 0.0012 m, grouped in one layer near $r = a - h/2$. In the second class (B) we have 6 closely grouped layers of fibre reinforcing, each containing around 150 fibres with a diameter of 0.0008 – 0.0015 m. The fibres in alternate layers wind in alternating directions. So,

$$N \approx \begin{cases} 40 & \text{in class A,} \\ 900 & \text{in class B,} \end{cases} \tag{4.34}$$

$$a_0 \approx 0.0005 \text{ m}. \tag{4.35}$$

In both cases we are interested in looking at fibres with winding angle

$$0 \leqslant \phi \leqslant \frac{\pi}{3}, \tag{4.36}$$

although in reality ϕ is unlikely to be much in excess of $\pi/4$.

Thales tell us that the hose is usually filled with kerosene. The speed of sound in kerosene and its density are dependent on temperature, but typical values are

$$c_1 = 1320 \text{ ms}^{-1}, \tag{4.37}$$

$$\rho_1 = 750 \text{ kgm}^{-3}. \tag{4.38}$$

Clearly the outer fluid is water, which has typical sound speed and density (again dependent on temperature)

$$c_2 = 1480\text{ms}^{-1}, \tag{4.39}$$

$$\rho_2 = 1000 \text{ kgm}^{-3}. \tag{4.40}$$

We are interested in looking at forcing with frequency $f(=\omega/2\pi)$ and wave number k in the range

$$f = 5 \text{ Hz} - 3 \text{ kHz}, \tag{4.41}$$

$$k = 0 - 150 \text{ m}^{-1}. \tag{4.42}$$

Finally, the maximum tow speed is 10 ms^{-1}.

4.1.2.2 Typical Size of the Dimensionless Parameters

Using the above data we see that in S.I. units typical values could be

$$\bar{\rho} \sim 10^3 \text{ kgm}^{-3}, \tag{4.43}$$

$$\omega \sim 10^4 \text{ rads}^{-1}, \tag{4.44}$$

$$a \sim 10^{-2} \text{ m} \tag{4.45}$$

$$k \sim 10^2 \text{ m}^{-1}, \tag{4.46}$$

$$\rho_1 \sim 10^3 \text{ kgm}^{-3}, \tag{4.47}$$

$$\rho_2 \sim 10^3 \text{ kgm}^{-3}. \tag{4.48}$$

So, using these values, our (dimensional) parameters have typical order of magnitude

$$\alpha \sim \beta \sim \gamma \sim \delta_1 \sim \delta_2 \sim 10^{-7}\text{Nm}^{-2}. \tag{4.49}$$

But, the non-dimensional parameters that we are interested in are all made up of one of the above parameters multiplied by one of our constants A, B, ..., I. All of these have the same order of magnitude as the moduli of elasticity, i.e.

$$A \sim B \sim \ldots \sim I \sim 10^8 \text{ Nm}^{-2}. \tag{4.50}$$

Hence, all of our non-dimensional parameters are $O(10)$ in this case. There is also the possibility that k or ω could be much smaller than the typical sizes given above, which would result in the size of the parameters being altered. However, given that for these values of k and ω the parameters are neither exceptionally large or exceptionally small we will compute using the non-dimensional equations (4.6) – (4.8) and boundary conditions (4.12) – (4.17).

4.2 Computing Solutions

Numerical solutions of (4.6) – (4.8) subject to (4.12) – (4.17) can be computed by conversion to a first-order system of equations and the use of a shooting method to convert the boundary value problem to an initial value problem.

4.2.1 Uniform Density Throughout the Hose

Initially we will model the hose as if the fibres are uniformly distributed across it. This means that the physical and mechanical properties of the hose are independent of our position within the hose and simplifies the computing that is required. We know that, in fact, the fibres are situated in layered regions within the hose and later we will compute using this type of structure for increased accuracy. Our aim is to produce a plot of the hose transfer function T, defined by

$$T(r, \omega, n, k) = \frac{P_1(r, \omega, n, k)}{P_f}. \tag{4.51}$$

4.2.1.1 Conversion to a First-Order System

In order to compute solutions more easily we convert (4.6) – (4.8) to a first-order system of 6 ordinary differential equations by setting

$$U'(r) = X(r), \tag{4.52}$$
$$V'(r) = Y(r), \tag{4.53}$$
$$W'(r) = Z(r). \tag{4.54}$$

We can then write our non-dimensional equations as the first-order matrix equation

$$\mathbf{U}' = P\mathbf{U}, \tag{4.55}$$

where $\mathbf{U} = (U, V, W, X, Y, Z)^T$ and P is the 6-by-6 matrix

$$P = \begin{bmatrix} 0 & 0 & 0 & 1 & 0 & 0 \\ 0 & 0 & 0 & 0 & 1 & 0 \\ 0 & 0 & 0 & 0 & 0 & 1 \\ \frac{(B+Gn^2)\alpha/r^2+H\gamma-1}{A\alpha} & \frac{n(G+B)}{Ar^2} & \frac{\beta(F-E)}{A\alpha r} & -\frac{1}{r} & -\frac{n(G+D)}{Ar} & -\frac{\beta(H+E)}{A\alpha} \\ \frac{n(G+B)}{Gr^2} & \frac{(G+Bn^2)\alpha/r^2+I\gamma-1}{G\alpha} & \frac{n\beta(I+F)}{G\alpha r} & \frac{n(G+D)}{Gr} & -\frac{1}{r} & 0 \\ \frac{\beta(H+F)}{H\alpha r} & \frac{n\beta(I+F)}{H\alpha r} & \frac{In^2\alpha/r^2+C\gamma-1}{H\alpha} & \frac{\beta(H+E)}{H\alpha} & 0 & -\frac{1}{r} \end{bmatrix}. \tag{4.56}$$

On making the substitutions (4.52) – (4.54) our boundary conditions (4.12) – (4.17) become

$$A\delta_1 X + \frac{D\delta_1}{r}(nV + U) + Eak\delta_1 W = -\frac{aP_1}{\bar{U}}, \tag{4.57}$$
$$U = \frac{aP_1'}{\bar{U}}, \tag{4.58}$$

at $r = 1 - h/a$,

$$A\delta_2 X + \frac{D\delta_2}{r}(nV + U) + Eak\delta_2 W = -\frac{a\delta_2 P_f}{\bar{U}} - \frac{aP_2'}{\bar{U}}, \tag{4.59}$$
$$U = \frac{aP_2'}{\bar{U}}, \tag{4.60}$$

at $r = 1$, and

$$Y - \frac{V}{r} - \frac{nU}{r} = 0, \tag{4.61}$$
$$Z - akU = 0 \tag{4.62}$$

at both $r = 1$ and $r = 1 - h/a$. Here we recall from (3.12) that P_1 is given (in physical units) by

$$P_1(r) = C_1 J_n(\kappa_1 ar). \tag{4.63}$$

Then, recalling the expressions for derivatives of Bessel functions (see, e.g., Jones [20] or Temme [39]) we see that

$$P_1'(r) = \frac{C_1\kappa_1 a}{2}\big(J_{n-1}(\kappa_1 ar) - J_{n+1}(\kappa_1 ar)\big). \tag{4.64}$$

So, we can eliminate C_1 between (4.57) and (4.58) to give

$$A\delta_1 X + \frac{D\delta_1}{r}(nV + U) + Eak\delta_1 W + \frac{2UJ_n(\kappa_1 ar)}{\kappa_1 a\big(J_{n-1}(\kappa_1 ar) - J_{n+1}(\kappa_1 ar)\big)} = 0 \tag{4.65}$$

at $r = 1 - h/a$. Similarly, using our expressions (3.23) and (3.31) we can eliminate P_2 between (4.14) and (4.60) to give

$$A\delta_1 X + \frac{D\delta_1}{r}(nV + U) + Eak\delta_1 W + \frac{U\mathcal{J}_n(\kappa_2 ar)}{\kappa_2 a\mathcal{J}_n'(\kappa_2 ar)} = -\frac{a\delta_2 P_f}{\bar{U}} \tag{4.66}$$

at $r = 1$, where

$$\mathcal{J}_n(\kappa_2 ar) = \begin{cases} H_n^{(2)}(\kappa_2 ar), & \text{if } \omega^2 > (c_2 k)^2 \\ K_n(i\kappa_2 ar), & \text{if } \omega^2 < (c_2 k)^2 \end{cases} \tag{4.67}$$

and its derivative is calculated using the relationships

$$\big(H_n^{(2)}\big)'(z) = \frac{1}{2}\big(H_{n-1}^{(2)}(z) - H_{n+1}^{(2)}(z)\big), \tag{4.68}$$

$$K_n'(z) = -\frac{1}{2}\big(K_{n-1}(z) + K_{n+1}(z)\big). \tag{4.69}$$

given in Jones [20]. Our boundary conditions can then be written in matrix form as

$$Q\mathbf{U}(1 - h/a) + R\mathbf{U}(1) = \boldsymbol{\alpha}, \tag{4.70}$$

where $\boldsymbol{\alpha} = (0, 0, 0, -a\delta_2 P_f/\bar{U}, 0, 0)^T$ and Q and R are the 6-by-6 matrices

$$Q = \begin{bmatrix} \frac{D\delta_1}{r_1} + \frac{2J_n(\kappa_1 ar_1)}{\kappa_1 a(J_{n-1}(\kappa_1 ar_1) - J_{n+1}(\kappa_1 ar_1))} & \frac{Dn\delta_1}{r_1} & Eak\delta_1 & A\delta_1 & 0 & 0 \\ \frac{n}{r_1} & \frac{1}{r_1} & 0 & 0 & -1 & 0 \\ ak & 0 & 0 & 0 & 0 & -1 \\ 0 & 0 & 0 & 0 & 0 & 0 \\ 0 & 0 & 0 & 0 & 0 & 0 \\ 0 & 0 & 0 & 0 & 0 & 0 \end{bmatrix}, \tag{4.71}$$

$$R = \begin{bmatrix} 0 & 0 & 0 & 0 & 0 & 0 \\ 0 & 0 & 0 & 0 & 0 & 0 \\ 0 & 0 & 0 & 0 & 0 & 0 \\ \frac{D\delta_2}{r_2} + \frac{\mathcal{J}_n(\kappa_2 ar_2)}{\kappa_2 a\mathcal{J}_n'(\kappa_2 ar_2)} & \frac{Dn\delta_2}{r_2} & Eak\delta_2 & A\delta_2 & 0 & 0 \\ \frac{n}{r_2} & \frac{1}{r_2} & 0 & 0 & -1 & 0 \\ ak & 0 & 0 & 0 & 0 & -1 \end{bmatrix}. \tag{4.72}$$

We will make use of MATLAB's ability to handle matrices to compute the solution of (4.55) subject to (4.70).

4.2.1.2 Numerical Solution by Shooting

In order to solve our differential equation (4.55) with boundary conditions (4.70) we use a shooting method as described in Keller [22]. Consider the six initial value problems

$$\mathbf{U}_{(\nu)}' = P\mathbf{U}_{(\nu)}, \quad \mathbf{U}_{(\nu)}(1 - h/a) = \mathbf{I}_{(\nu)}, \quad \nu = 1, \ldots, 6, \tag{4.73}$$

where $\mathbf{I}_{(\nu)}$ is the νth unit 6-vector (i.e. the νth column of I_6, the 6-by-6 identity matrix). These problems are trivial to solve numerically. Our routine uses MATLAB's built-in ordinary differential equation solver `ode45`. Having solved the initial value problems we then construct the 6-by-6 matrix

$$\hat{U}(r) = \big[\mathbf{U}_{(1)}(r), \mathbf{U}_{(2)}(r), \mathbf{U}_{(3)}(r), \mathbf{U}_{(4)}(r), \mathbf{U}_{(5)}(r), \mathbf{U}_{(6)}(r)\big] \tag{4.74}$$

and define, for arbitrary $\mathbf{s} \in \mathbb{R}^6$,

$$\mathbf{U}(r; \mathbf{s}) = \hat{U}(r)\mathbf{s}. \tag{4.75}$$

Then, $\mathbf{U}(r;\mathbf{s})$ is a solution of (4.55) since it is a linear combination of the solutions $\mathbf{U}_{(1)},\ldots,\mathbf{U}_{(6)}$. So, we seek $\mathbf{s}$ such that

$$\boldsymbol{\phi}(\mathbf{s}) \equiv Q\mathbf{U}(1-h/a;\mathbf{s}) + R\mathbf{U}(1;\mathbf{s}) - \boldsymbol{\alpha} = \mathbf{0}. \tag{4.76}$$

If we can find such an $\mathbf{s}$ then $\mathbf{U}(r;\mathbf{s})$ will satisfy (4.70) in addition to (4.55) and so be a solution of our boundary value problem. We notice that $\hat{U}(1-h/a) = I_6$, so $\mathbf{U}(1-h/a;\mathbf{s}) = \mathbf{s}$ and, hence, (4.76) becomes

$$\boldsymbol{\phi}(\mathbf{s}) \equiv Q\mathbf{s} + R\mathbf{U}(1;\mathbf{s}) - \boldsymbol{\alpha} = \mathbf{0}. \tag{4.77}$$

On substituting for $\mathbf{U}(1;\mathbf{s})$ from (4.74) we see that $\boldsymbol{\phi}(\mathbf{s})$ is linear in $\mathbf{s}$ and $\mathbf{s}$ can be determined by solving the linear system of equations

$$[Q + R\hat{U}(1)]\mathbf{s} = \boldsymbol{\alpha}. \tag{4.78}$$

This can be done trivially using MATLAB's \ command for solving square systems of linear equations. The whole solution can then be determined by evaluating $\mathbf{U}_{(\nu)}, \nu = 1,\ldots,6$ at a series of grid points between $1-h/a$ and 1 and then forming, at each grid point, $\mathbf{U}(r;\mathbf{s}) = \hat{U}(r)\mathbf{s}$. We note that $\mathbf{s}$ can always be determined (unless $Q + R\hat{U}(1)$ is singular — in which case we are at the resonant frequency and have an eigenvalue problem) since $\hat{U}(1)$ depends only on the solutions $\mathbf{U}_{(\nu)}, \nu = 1,\ldots,6$ of our initial value problems. A MATLAB routine `hose.m` to carry out these calculations and determine U, V, W and P_1 is shown in Appendix C.1. This routine assumes that the moduli of elasticity are constant at any frequency (assumed to be the value at 1 kHz given in Section 4.1.2.1) and uses the mechanical properties of nylon fibres. A discussion of how we could include the varying moduli of elasticity (due to the fact that our materials are in fact viscoelastic rather than linearly elastic) is given later.

4.2.1.3 Plotting the Transfer Function

Included in our routine `hose.m` is a command for MATLAB to output plots of the real and imaginary parts of U, V and W against r. These plots allow us to compare our computed solutions with the exact solutions we calculated in Section 2.2.4 for the transversely isotropic ($\phi = 0$) case. The constants A_1, ..., B_3 in the expressions for the exact solutions are determined by the boundary conditions and were calculated using the MATLAB routine `exact.m` shown in Appendix C.2. Figure 4.1 shows the real and imaginary parts of U, V and W in our exact and numeric solutions for $\omega = 10^3$, $n = 2$, $k = 1$, $N = 40$, $\phi = 0$, $P_f = 1$ plotted against r. We observe that there is good agreement between the two solutions. From this we conclude that our MATLAB routine is working correctly and outputting the correct numerical solution — there are no errors in our programming and the shooting method converges to the exact solution.

Having established that our MATLAB routine is working as we expected we now use it to output a plot of the hose transfer function against ω — the main aim of our work. This is done by running `hose.m` for a series of values of ω between 1 Hz and 2 kHz (recall that the maximum and minimum values of f supplied by Thales were 1 Hz and 2 kHz respectively, but it turns out that most of the interesting behaviour occurs at low frequency, so we truncate the frequency range we compute for so that we can see the low frequency behaviour more clearly). At each value of ω we calculate the internal pressure P_1 at some radius $r_0 < 1 - a/h$ by using (4.13) to determine C_1 and then recalling that

$$P_1(r) = C_1 J_n(\kappa_1 r). \tag{4.79}$$

The value of the hose transfer function $T(r_0,\omega,n,k)$ at each value of ω is then calculated using (4.51). This is done using the MATLAB routine `transfer.m` shown in Appendix C.4. This routine outputs plots of $20\log_{10}|T|$ (T in decibels) and $\arg(T)$ against ω. Plots of the transfer function for various values of n and k are shown in Appendix B.

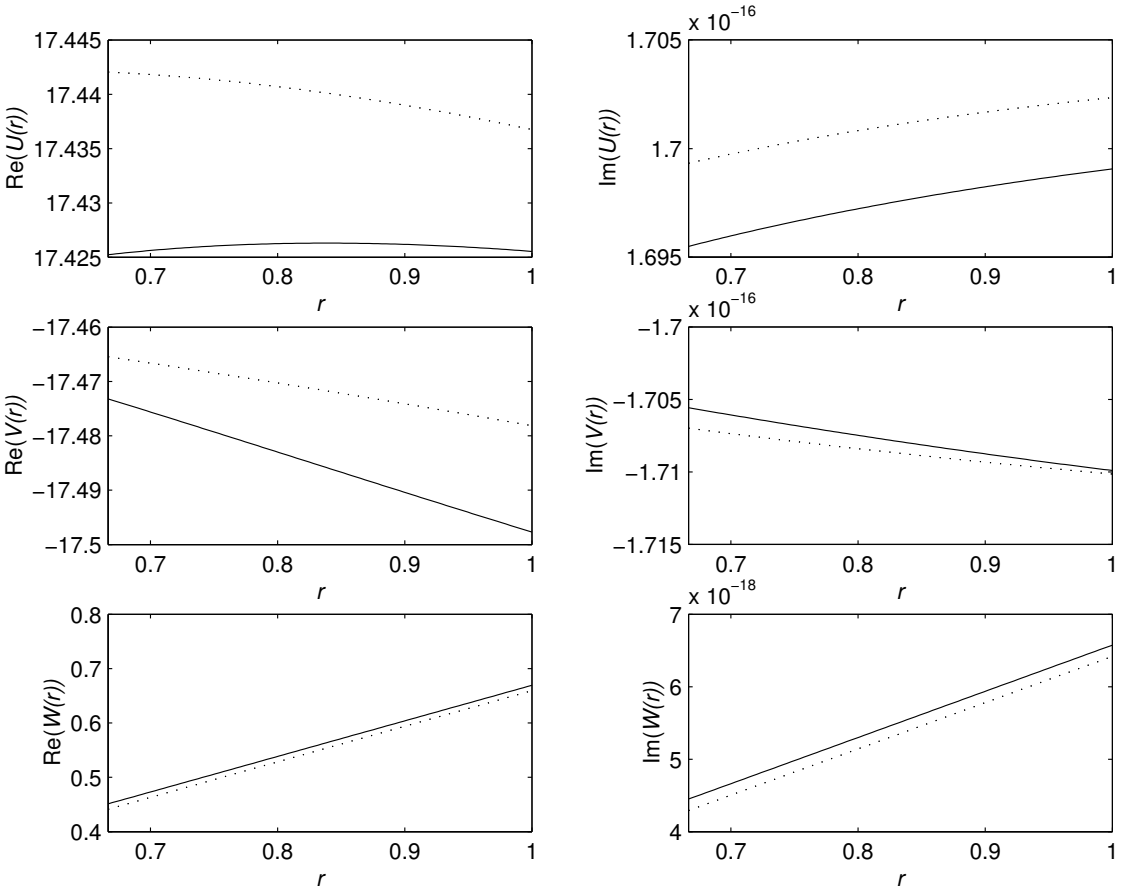


Figure 4.1: A plot of our numeric (solid line) and exact (dotted) solutions against r for $\omega = 10^3$, $n = 1$, $k = 1$, $N = 40$, $\phi = 0$, $P_f = 1$.

All of our hose transfer functions in Appendix B have the same basic shape — a steep rise for small values of ω (up to about 100 Hz) followed by a levelling off with the transfer function remaining roughly constant for larger values of ω. For $\omega < c_2 k$ (where the solution in the outer fluid does not radiate energy to ∞) the argument of T is piecewise constant and takes values 0 and $\pm\pi$ indicating that the transfer function is real-valued. When $\omega > c_2 k$ the transfer function becomes complex as energy is lost by radiation to ∞. We see that the argument of T increases very slowly from zero with increasing ω. In some of the plots we have values of ω for which the hose transfer function blows up to a singularity and there is a discontinuity in its argument. These are the resonant values of ω. There appear to be two classes of resonance: firstly a class like the singularity in Figure B.1 at $\omega \approx 400$ Hz where we have a single peak accompanied by a jump of π in the argument of T and secondly singularities like that in Figure B.11 at $\omega \approx 850$ Hz where we have a peak and a trough close together and both accompanied by a jump of π in the argument of the transfer function.

We only see resonances in our frequency range at low values of n ($\leqslant 1$) and k (we only see them at $k = 1$). The magnitude of the hose transfer function for $n = 0$ is much greater at $r = 0$ than at $r = 0.2$ (if $n \neq 0$ then the transfer function vanishes at $r = 0$ since $J_n(0) = 0$ for $n \neq 0$ so P_1 vanishes at $r = 0$). This is easily explained by recalling that $P_1 = C_1 J_n(\kappa_1 r)$ and P_f is constant — $J_0(z)$ has its maximum at $r = 0$. Changing the values of N and ϕ changes the values of the resonant frequencies — in general increasing N decreases the frequencies of each type of

resonance (although the change is small) whilst the effect of changing ϕ does not seem to follow such a simple pattern.

4.2.2 Variable Density Using Layers

We now aim to increase the accuracy of our solution by modelling the position of the fibres within the hose more accurately. This will result in the composite density and elastic properties of the hose varying with r rather than being constant.

4.2.2.1 Governing Equations and Boundary Conditions

The description of the hose structure given to us by Thales tells us that the fibres are grouped in layers midway between $r = 1 - a/h$ and $r = 1$ (non-dimensionally). We seek to include this layered structure in our numeric solution. To do this we must compute in three regions — the two unreinforced layers close to the boundaries of the hose and a central layer where the fibres are situated. We see that using this structure the composite density is, in fact, piecewise constant: in the unreinforced layers $\bar{\rho} = \rho$, whilst in the central layer $\bar{\rho}$ is calculated as before from the densities of the substrate and fibres.

In all three regions the motion of the hose is governed by (4.55), although the values of the contants $A, \ldots, I$ and parameters α, β, γ are different in the different regions since they depend on δ (which is zero in the unreinforced regions, but non-zero in the central region). Our boundary conditions at $r = 1 - a/h$ and $r = 1$ remain the same and are given by (4.61) – (4.66), but in addition we have matching boundary conditions at both of the interfaces between layers. These boundary conditions tell us that the three components of displacement, U, V and W, and the radial stresses τ_{rr}, $\tau_{r\theta}$ and τ_{rz} are continuous across the interfaces. If we continue to denote the displacements in the central layer by U, V and W and use subscripts 1 and 2 to denote those in the inner and outer layers respectively then we can write these boundary conditions as

$$U = U_i, \tag{4.80}$$

$$V = V_i, \tag{4.81}$$

$$W = W_i, \tag{4.82}$$

$$AU' + \frac{D}{r}(nV + U) + EakW = \hat{A}U_i' + \frac{\hat{D}}{r}(nV_i + U_i) + \hat{D}akW_i, \tag{4.83}$$

$$V' - \frac{V}{r} - \frac{nU}{r} = V_i' - \frac{V_i}{r} - \frac{nU_i}{r}, \tag{4.84}$$

$$W' - akU = W_i' - akU_i \tag{4.85}$$

at the interfaces, where i chose to be either 1 or 2 depending on which interface we are at and $\hat{A}$, $\hat{D}$ are the values of A, D calculated using $\bar{\rho} = \rho^f$ in the outer regions (we note that $\hat{D} = \hat{E}$ since there are no fibres in the outer regions, so they are isotropic).

4.2.2.2 Numerical Solution for the Layered System

As in the uniform case above we can solve our equations of motion subject to the matching boundary conditions at the interfaces by using a shooting method. A MATLAB routine `layered.m` to do this is shown in Appendix C.3. In programming this routine we recalled that Thales told us (Section 4.1.2.1) that one form of hose has nylon fibres situated in 6 closely grouped layers of 0.0015 m thick. Our routine uses these dimensions and groups all six layers together to form one layer of thickness 0.009 m. It could easily be altered to allow us to model the other type of hose (one layer of wires, typically of thickness 0.001 m) or to calculate the effects of using kevlar fibres. This routine is the equivalent of `hose.m` for the uniform case: it calculates the pressure in the interior of the hose and produces plots of U, V and W against r. The solution of `layered.m` can

then be used as input data in `transfer.m` to give a plot of the hose transfer function for a layered hose. Appendix B contains various plots of hose transfer functions for the layered hose.

The hose transfer functions for the layered model seem to match those for the uniform model quite closely. Since in the case we are modelling the layered region has a thickness of approximately $0.7h$ this is probably to be expected. The main difference is that the value of any resonant frequencies is different in the two models (although usually fairly close). In almost all cases we see the same types of resonance in similar frequency ranges in the transfer functions for both models. The only exceptions (that we have plotted) to this are when $n = 0$, $k = 1$, $N = 900$, $P_f = 1$ and $\phi = 0$ or $\pi/12$ when our single peak resonance in the uniform model is replaced by two peaks at a slightly higher frequency, both accompanied by a jump of π in the argument of the transfer function, in the layered model. This behaviour is not repeated at any of our other resonant frequencies of either type.

Chapter 5

Conclusion and Extensions

5.1 Conclusion

5.1.1 Explanation of Results

In this section we seek to produce a description of how the various parameters in our problem affect the solution we obtain, both in terms of its general shape and the values of the resonant frequencies. Firstly we consider the general shape of the hose transfer function. We observed in the previous chapter that all the variation in our transfer function comes at low frequency. This behaviour seems to be explained by the values of the constants α, β and γ, defined in (4.9) – (4.11) and given by

$$\alpha = \frac{1}{\bar{\rho}\omega^2 a^2}, \tag{5.1}$$

$$\beta = \frac{k}{\bar{\rho}\omega^2 a}, \tag{5.2}$$

$$\gamma = \frac{k^2}{\bar{\rho}\omega^2}. \tag{5.3}$$

Recall that $\bar{\rho} \approx 1000$ kgm^{-3}, $a = 0.0375m$ and $0 \leqslant k \leqslant 150$ m^{-1}. So, at $\omega = 1$, $\alpha \approx 0.7$, so that $A\alpha \sim 10^8$ (α multiplied by any of our constants has the same order of magnitude and $\beta, \gamma = O(\alpha)$, so β or γ multiplied by a constant also have the same size) but the $1/\omega^2$ term means that it rapidly decreases from this value. When $\omega = 100$, $\alpha \approx 0.7 \times 10^{-5}$ and when $\omega = 1000$, $\alpha \approx 0.7 \times 10^{-7}$. So, by this stage $A\alpha \sim 10$. Since most of the terms in our differential equations for U, V, W have denominators of the form $A\alpha$ (only the $-1/r$ terms, which are clearly $O(1)$ do not) but the numerators have terms both of $O(1)$ and $O(A\alpha)$. At high frequency all the terms are balanced and so affect our solutions whilst at low frequency the terms of $O(A\alpha)$ dominate and so the $O(1)$ terms have little influence on the solutions. This gives rise to two differing regimes, one for low frequency vibrations and the other for high frequency. Clearly the low frequency regime is more sensitive to pressure fluctuations than the high frequency one, accounting for the way that our solution has a rapid increase to a constant value.

Next we consider the resonant frequencies of the hose. We know from our discussion of shooting methods in Section 4.2.1.2 that we get resonance (in the uniform model) when the 6-by-6 matrix $Q + R\hat{U}(1)$ is singular (Q and R are the matrices that encode our boundary conditions, so this is what we would expect). The parameters that appear in $Q + R\hat{U}(1)$ and depend on ω are α, β and

γ, defined as above, and δ_1, δ_2, κ_1 and κ_2 defined in (4.18) and (3.6) by

$$\delta_1 = \frac{1}{\rho_1 \omega^2 a^2}, \tag{5.4}$$

$$\delta_2 = \frac{1}{\rho_2 \omega^2 a^2}, \tag{5.5}$$

$$\kappa_1^2 = \frac{\omega^2}{c_1^2} - k^2, \tag{5.6}$$

$$\kappa_2^2 = \frac{\omega^2}{c_2^2} - k^2, \tag{5.7}$$

which we conclude must determine the resonant frequencies. As with α, β and γ we note that δ_1 and δ_2 are non-dimensional when multiplied by one of $A, \ldots, I$, which is the form they always appear in. κ_1 and κ_2 are non-dimensional when multiplied by a, which is the case in our boundary conditions. It would be possible to find an expression for $\det(Q + R\hat{U}(1))$ in terms of these parameters and hence calculate the singular values, also in terms of the parameters (and hence in terms of ω). This has not, however, been attempted in this case. In the layered case the situation is further complicated by the presence of matching boundary conditions and to find the resonant frequencies we need to find the determinant of an 18-by-18 matrix (although once again the only dependence on ω is through α, β, γ, δ_1, δ_2, κ_1 and κ_2). The fact that we need to find the determinant of a much larger matrix explains why we find more resonant frequencies in the layered case than the uniform one and since $Q + R\hat{U}(1)$ does not make up a block in our 18-by-18 matrix we would not necessarily expect the uniform resonant frequencies to also be resonant frequencies in the layered model.

5.1.2 Summary

At the outset of this project our main aim was to model the response of a fibre reinforced hose to pressure fluctuations set up by a turbulent boundary layer surrounding it and generated by pulling it through a fluid. To achieve this we needed to express the elastic properties of the composite hose in terms of the properties of the fibres and substrate and the structure of the hose (e.g. the number of fibres, their winding angle and position), derive and solve (either analytically or numerically) the equations of motion in the hose and the surrounding fluid (not including the turbulent boundary layer) and use these results to produce a plot of the hose transfer function, defined in (4.51) as a function of ω for various values of the other variables in our system. We also aimed to provide some qualitative explanation of how the behaviour of the system depends on those variables.

During the course of the project all of these aims have been achieved (although the explanation of the behaviour could perhaps be more complete where resonance is concerned). In Chapter 2 we showed how the anisotropic linear elastic behaviour depended on nine constants (for a given material) $A, \ldots, I$. We outlined various models to calculate approximate values of these constants for a fibre-reinforced material. Using the Composite Cylinders Model we obtained expressions for the constants in a coordinate system fixed in the fibres that we then rotated to give them in our coordinate system fixed in the hose. We also calculated exact solutions for a transversely isotropic hose, when the numner of independent constants determining the behaviour is reduced to five. In Chapter 3 we derived and solved the (well-known) equations of motion for linearized acoustic waves in the fluids inside and outside the hose. We also derived the boundary conditions at the fluid-hose interfaces and at $r = 0$ and $r = \infty$.

We non-dimensionalized our equations of motion and boundary conditions in Chapter 4, identifying seven key parameters α, β, γ, δ_1, δ_2, κ_1 and κ_2 (which appear only as part of non-dimensional parameters). These equations could then be solved numerically, which we did by using a shooting method both for a hose with the fibres distributed uniformly throughout and a layered hose

which takes into account the variation of density with radius and allows us to include the effect of the position of the fibres more completely. We showed that our numerical solution was in good agreement with the exact solution in the special case of a transversely isotropic hose and used our numerical solutions to plot various hose transfer functions (Appendix B) and noted that they all showed the same basic behaviour away from resonant frequencies. Finally, at the start of this chapter we attempted an explanation of the basic shape of the transfer function and the values of the resonant frequencies.

5.2 Possible Extensions

5.2.1 Comparison With Experimental Results

An important criterion for judging the success of any mathematical model is how well the data it produces match with experimentally observed results in the real world. In this case Thales did not supply us with any experimental observations (either plots of actual transfer functions or the values of resonant frequencies). A valuable extension to this project would be to compare our results with any such observations. It may be that our model is sufficiently accurate for modelling the rsponse of the fibre-reinforced hose to vibration, but it could also turn out that we over-simplified the problem and our model does not account for some vital feature of the actual behaviour of such a hose. In this case we would need to go back to our original assumptions and try to modify them in such a way as to produce an improved model.

5.2.2 Effects of Viscoelasticity

As mentioned earlier the materials that our hose and fibres are manufactured from are viscoelastic. In an elastic solid that is subject to a shearing force we find that the resulting stress is proportional to the shearing strain (recall our (2.11): $\tau_{xy} = G_{12}e_{xy}$, etc.). In a viscous fluid the stress is proportional to the rate of shear. We call a material that exhibits both of these behaviours under appropriate circumstances *viscoelastic*. It can be shown (see, e.g. Pipkin [30]) that both elastic and viscous behaviour are limiting cases of viscoelastic behaviour. The effects of viscoelasticity are accounted for in elastic theory by allowing our moduli of elasticity to take complex values, i.e.

$$E_1 = E_1^{(1)} + iE_1^{(2)} = |E_1|e^{i\delta}, \tag{5.8}$$

where $E_1^{(1)}, E_1^{(2)} \in \mathbb{R}$. One possible extension of this project would be to consider how the vibrations of the hose would be different if we included viscoelastic effects. If we take the values of E_1 given in (4.20), (4.30) at various frequencies to be the absolute value of E_1 then the equivalent values of δ at those frequencies will completely determine the viscoelastic behaviour at those frequencies. Further data supplied by Thales tells us that for PVC

$$\tan\delta = \begin{cases} 0.49 & \text{at 1 Hz,} \\ 0.43 & \text{at 1 kHz,} \\ 0.41 & \text{at 2 kHz.} \end{cases} \tag{5.9}$$

And for kevlar

$$\tan\delta = \begin{cases} 0.07 & \text{at 1 Hz,} \\ 0.05 & \text{at 1 kHz,} \\ 0 & \text{at 2 kHz.} \end{cases} \tag{5.10}$$

Pipkin [30] describes how to determine the moduli of elasticity for all ω from a knowledge of their values at certain points. It turns out that for *standard linear solids* such as PVC and kevlar the values of the shear modulus $G(\omega)$ lie on a semicircle in the complex plane, so the three given values of $|E_1|$ and δ will be enough to determine the complete behaviour. The exact form of $G(\omega)$ is determined from the condition $G^{(2)}(\omega) > 0$ for $\omega > 0$ (representing the fact that the material

loses energy) and the requirement that $1/G(\omega)$ has an analytic continuation into $\mathrm{Im}(\omega) < 0$ (this is required for causality — the behaviour of the material is only affected by its history, not what may happen to it in the future). Including viscoelasticity will eliminate exact resonant frequencies (for which $Q + R\hat{U}(1)$ is singular) and will tend to smooth out the changes that occur near them.

Appendix A

Notation

N = number of fibres.
E_1 = Young's modulus of the substrate.
E_1^f = Young's modulus of the fibres.
$\bar{E}_1$ = longitudinal Young's modulus of the composite.
$\bar{E}_2$ = transverse Young's modulus of the composite.
G_{12} = shear modulus of the substrate.
G_{12}^f = shear modulus of the fibres.
$\bar{G}_{12}$ = longitudinal shear modulus of the composite.
$\bar{G}_{23}$ = transverse shear modulus of the substrate.
T = hose transfer function.
a = outer radius of the hose.
a_0 = radius of the fibres.
c_1 = sound speed in the interior fluid.
c_2 = sound speed in the exterior fluid.
e = strain tensor.
f = frequency of the vibrations.
h = hose thickness.
p_1 = pressure in the fluid inside the hose.
p_2 = pressure in the fluid outside the hose.
u = radial displacement of the hose.
v = circumferential displacement of the hose.
w = axial displacement of hose.
$\mathbf{u}$ = displacement vector of the hose.
δ = fractional cross-sectional area of the hose occupied by the fibres.
λ, μ = Lamé constants of the substrate.
λ^f, μ^f = Lamé constants of the fibres.
ν_{12} = Poisson's ratio of the substrate.
ν_{12}^f = Poisson's ratio of the fibres.
$\bar{\nu}_{12}$ = major Poisson's ratio of the composite.
$\bar{\nu}_{21}$ = minor Poisson's ratio of the composite.
$\bar{\nu}_{23}$ = transverse Poisson's ratio of the composite.
ρ = density of the substrate.
ρ^f = density of the fibres.
$\bar{\rho}$ = composite density.
ρ_1 = density of the interior fluid.
ρ_2 = density of the exterior fluid.
τ = stress tensor.
ϕ = winding angle of the fibres.

Appendix B

Plots of the Transfer Function

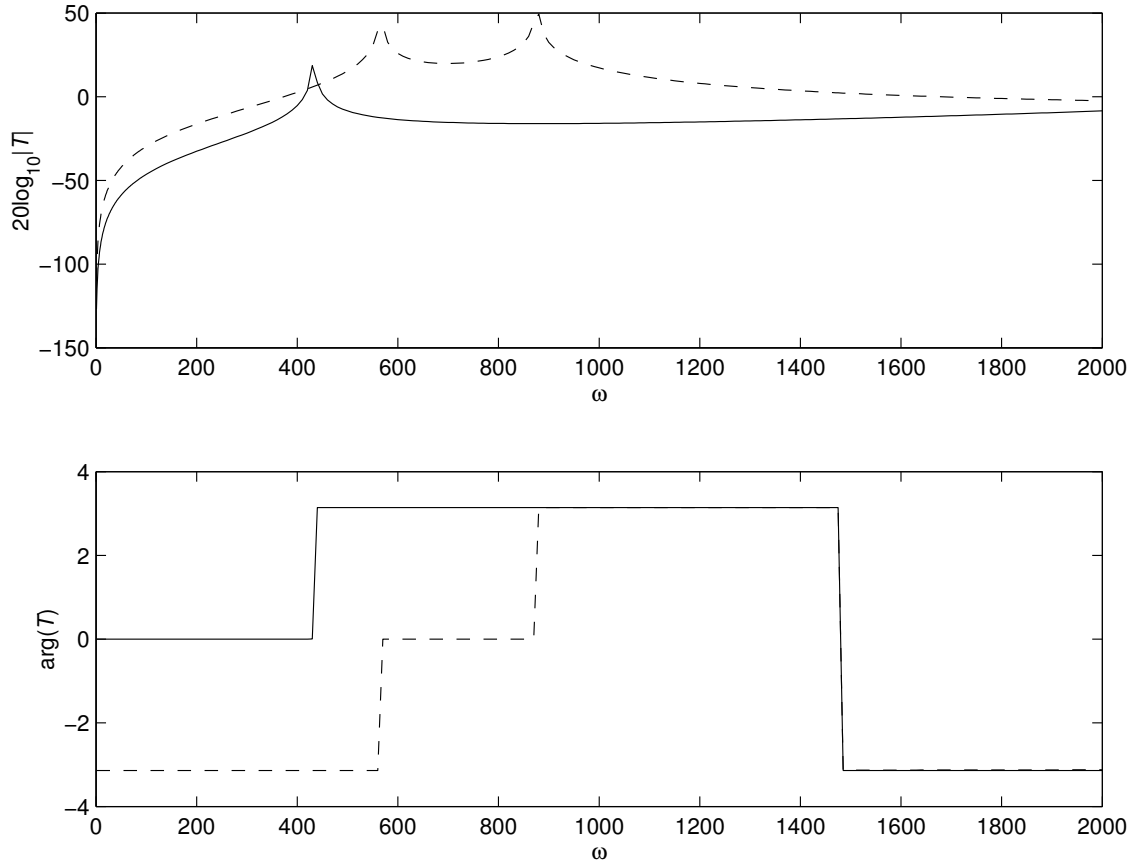


Figure B.1: Hose transfer function for the uniform (solid line) and layered (dashed) models at $r = 0.2$ for $n = 0$, $k = 1$, $N = 900$, $\phi = 0$, $P_f = 1$.

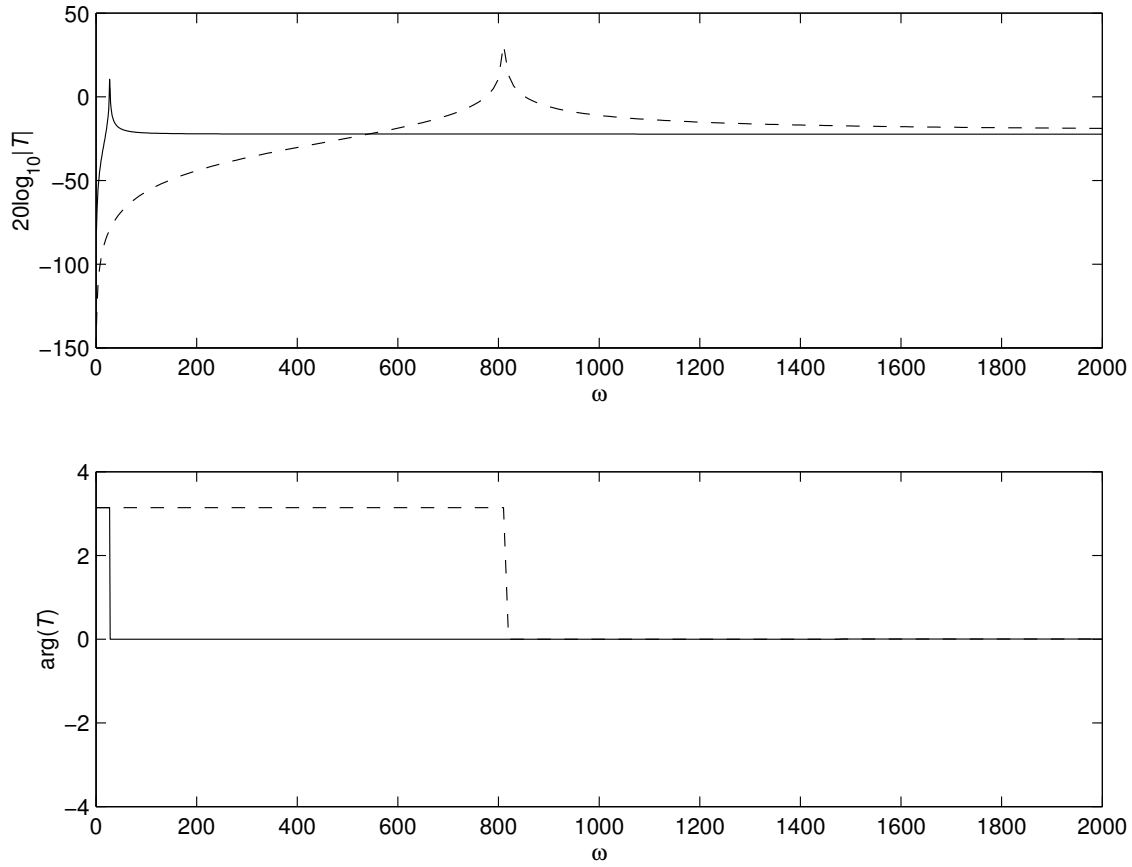


Figure B.2: Hose transfer function for the uniform (solid line) and layered (dashed) models at $r = 0.2$ for $n = 1$, $k = 1$, $N = 900$, $\phi = 0$, $P_f = 1$.

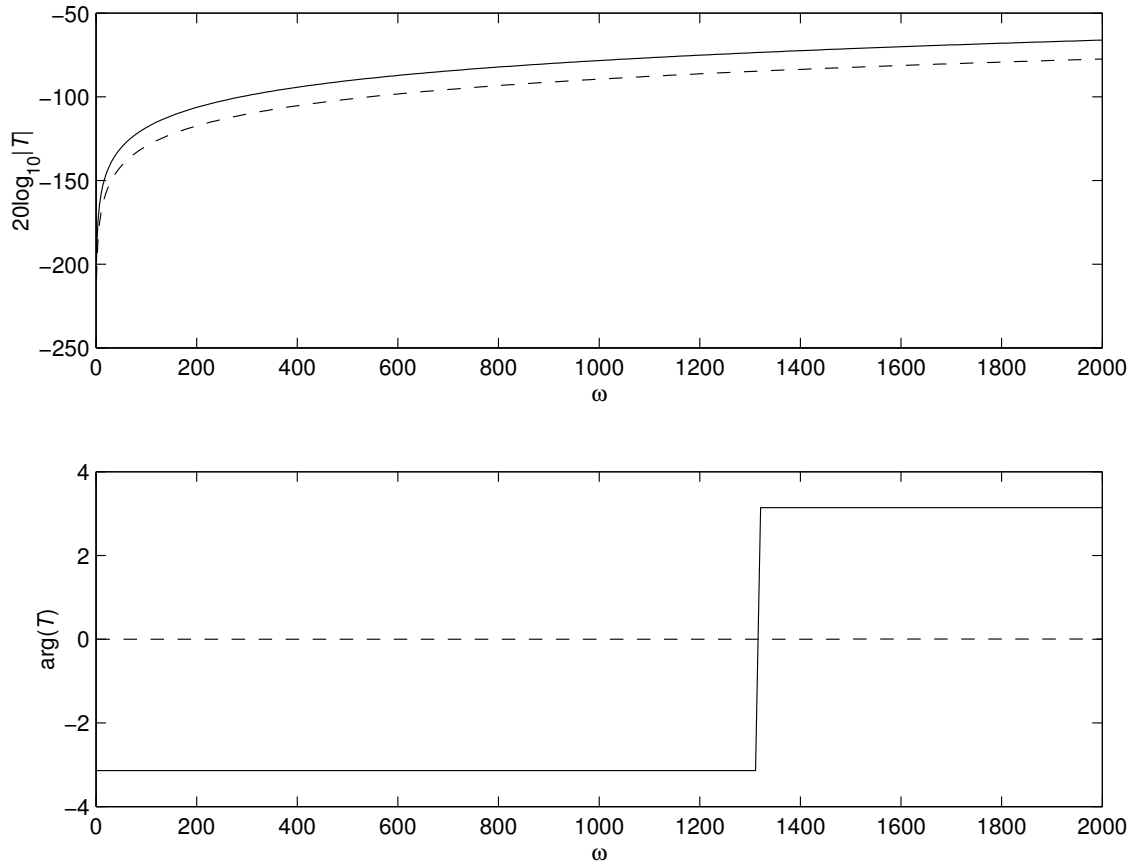


Figure B.3: Hose transfer function for the uniform (solid line) and layered (dashed) models at $r = 0.2$ for $n = 2$, $k = 1$, $N = 900$, $\phi = 0$, $P_f = 1$.

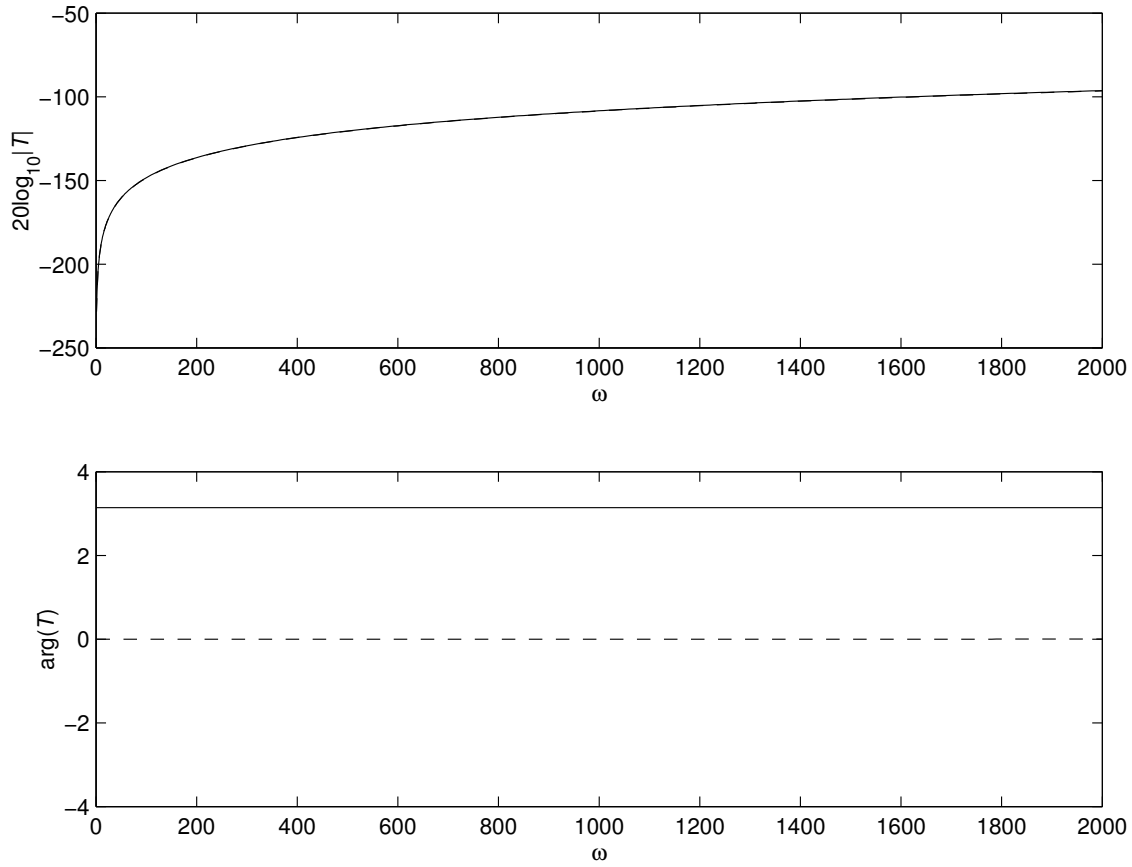


Figure B.4: Hose transfer function for the uniform (solid line) and layered (dashed) models at $r = 0.2$ for $n = 3$, $k = 1$, $N = 900$, $\phi = 0$, $P_f = 1$.

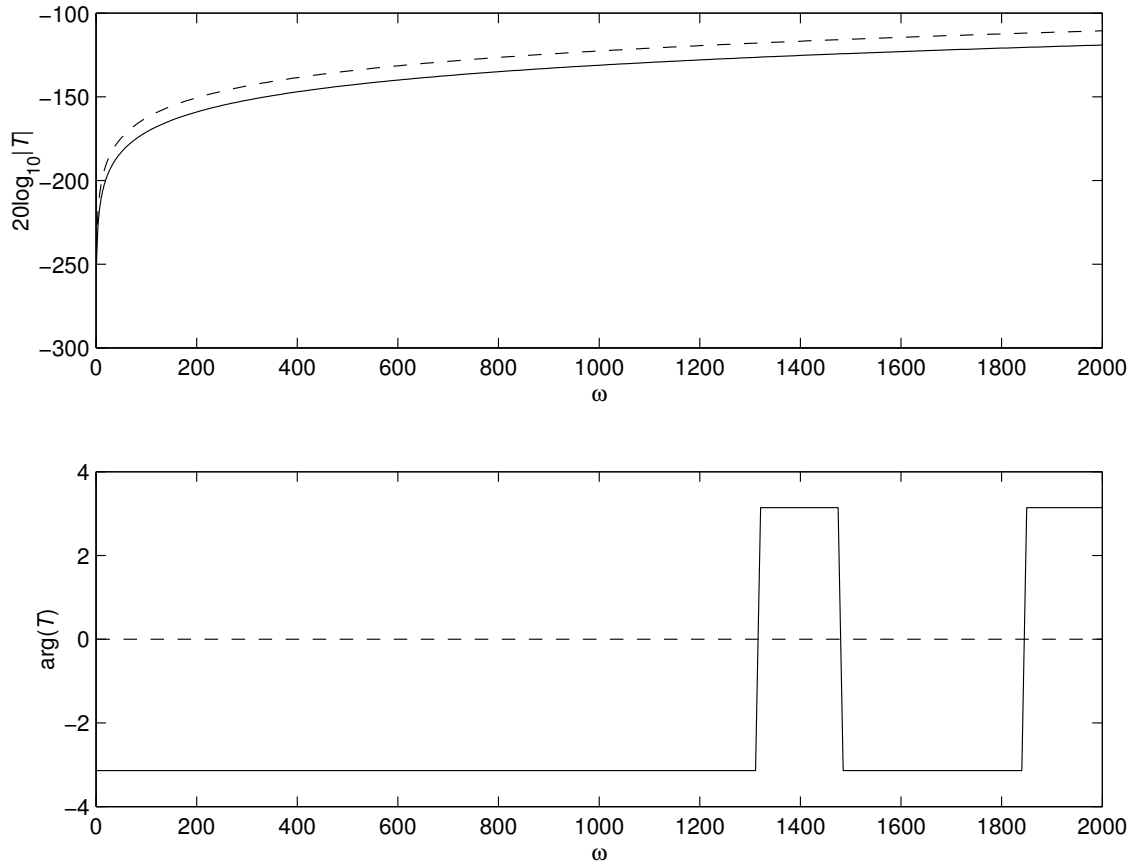


Figure B.5: Hose transfer function for the uniform (solid line) and layered (dashed) models at $r = 0.2$ for $n = 4$, $k = 1$, $N = 900$, $\phi = 0$, $P_f = 1$.

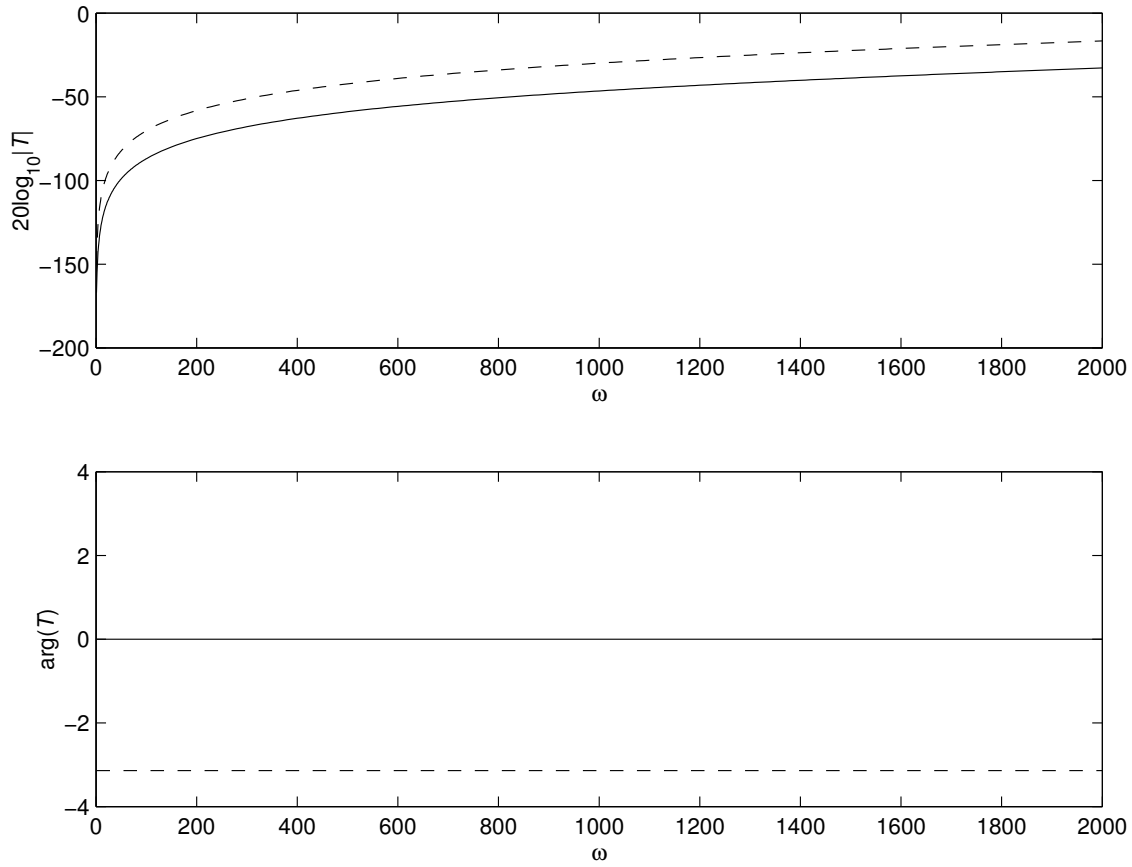


Figure B.6: Hose transfer function for the uniform (solid line) and layered (dashed) models at $r = 0$ for $n = 0$, $k = 10$, $N = 900$, $\phi = 0$, $P_f = 1$.

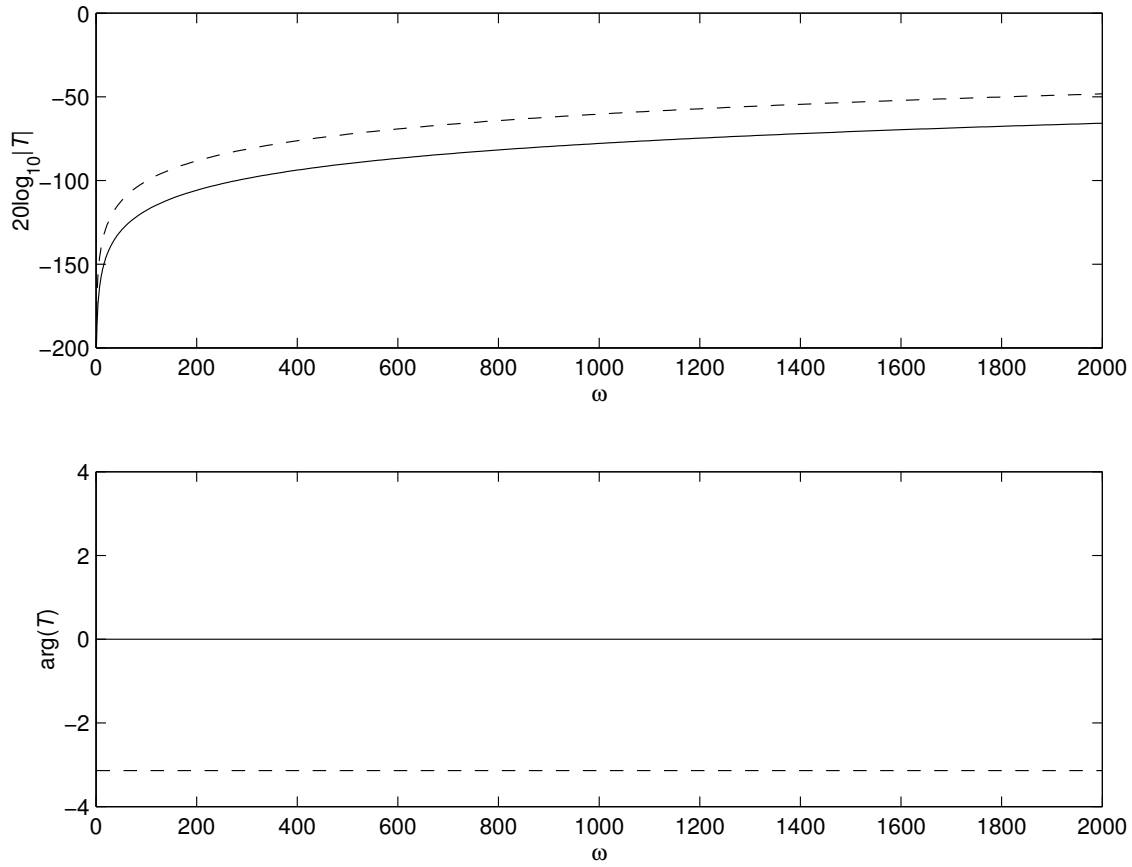


Figure B.7: Hose transfer function for the uniform (solid line) and layered (dashed) models at $r = 0$ for $n = 0$, $k = 50$, $N = 900$, $\phi = 0$, $P_f = 1$.

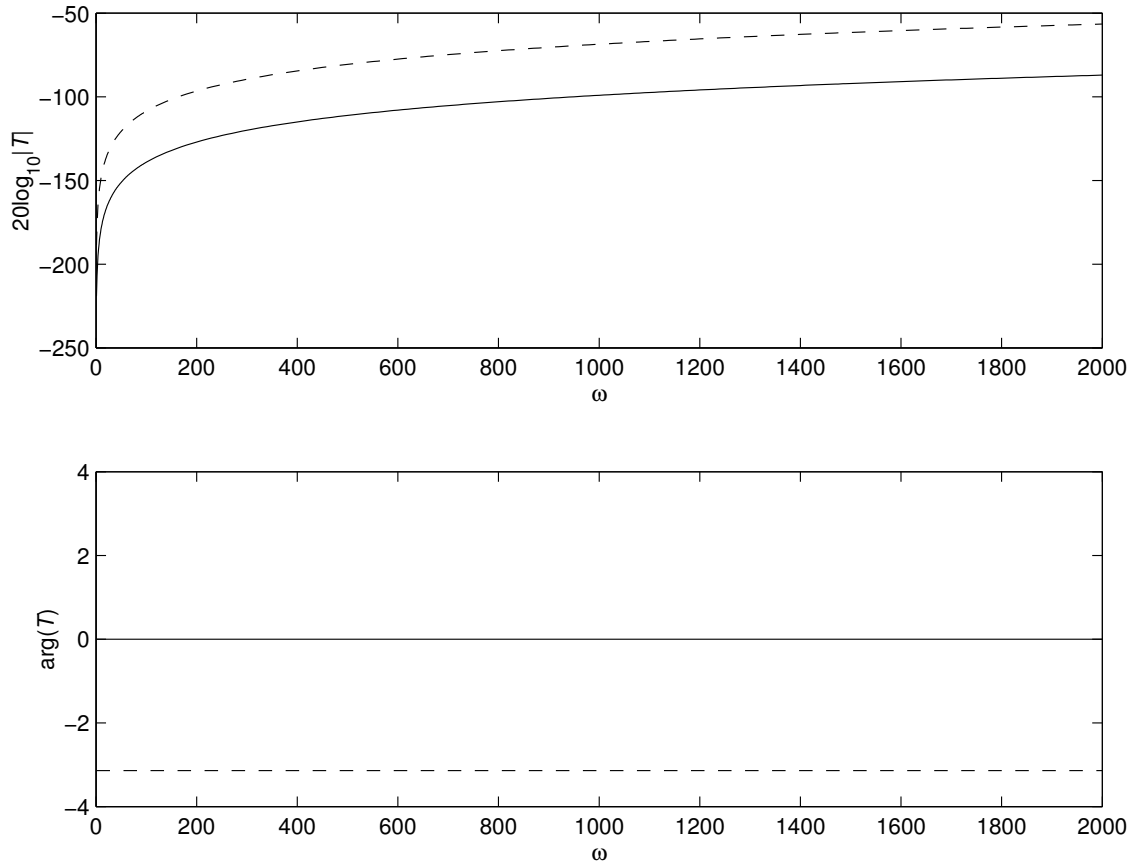


Figure B.8: Hose transfer function function for the uniform (solid line) and layered (dashed) models at $r = 0$ for $n = 0$, $k = 100$, $N = 900$, $\phi = 0$, $P_f = 1$.

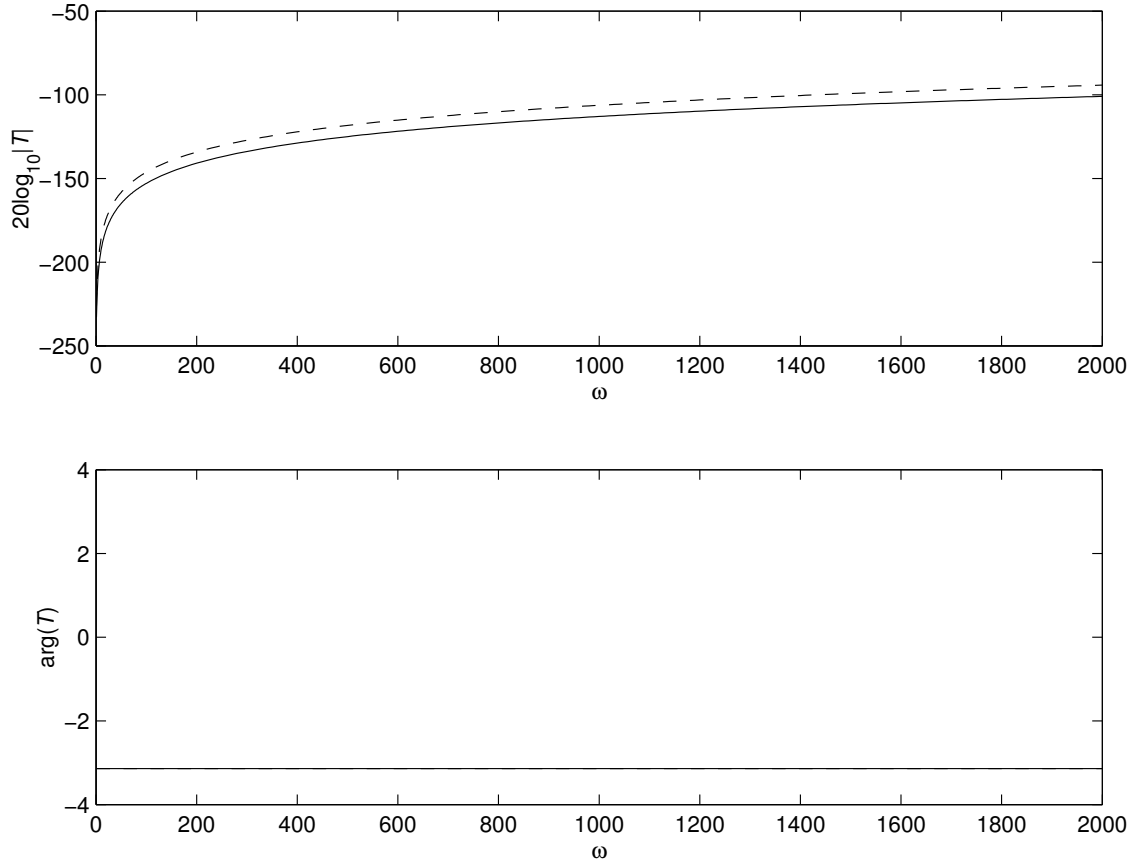


Figure B.9: Hose transfer function function for the uniform (solid line) and layered (dashed) models at $r = 0$ for $n = 0$, $k = 150$, $N = 900$, $\phi = 0$, $P_f = 1$.

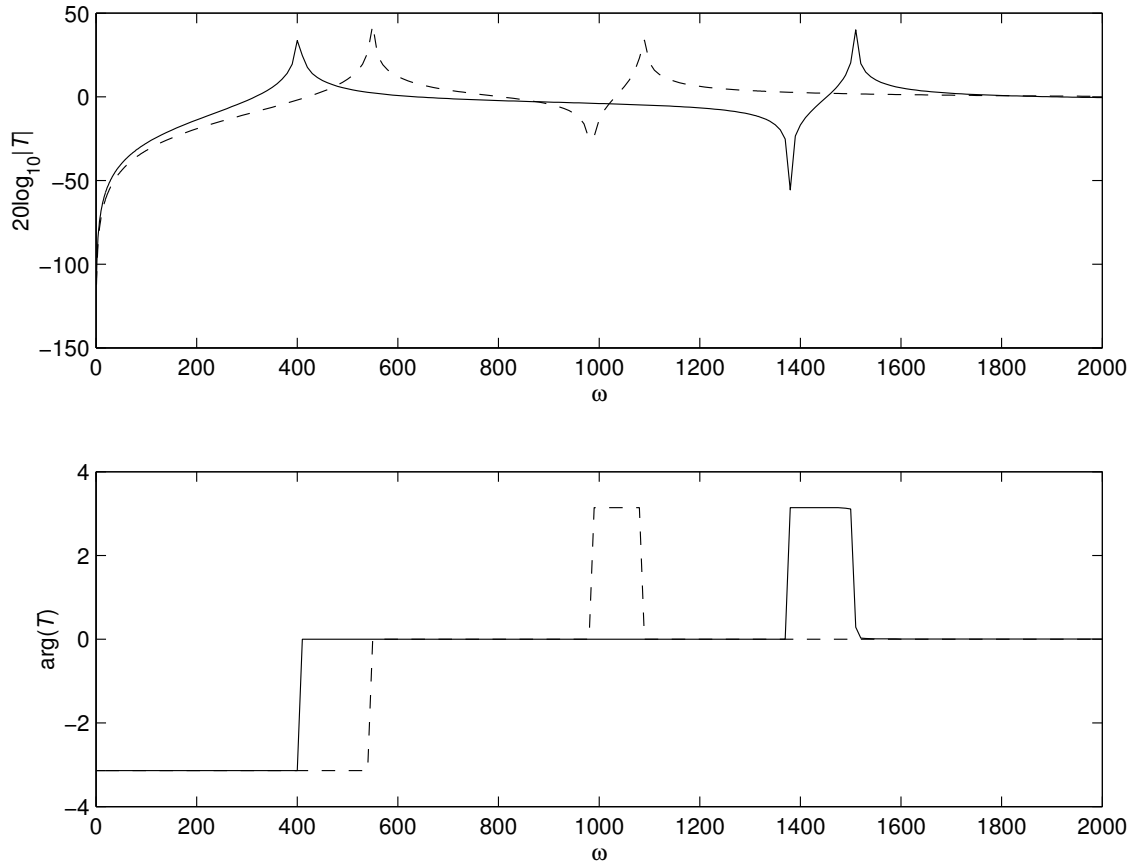


Figure B.10: Hose transfer function for the uniform (solid line) and layered (dashed) models at $r = 0$ for $n = 0$, $k = 1$, $N = 500$, $\phi = 0$, $P_f = 1$.

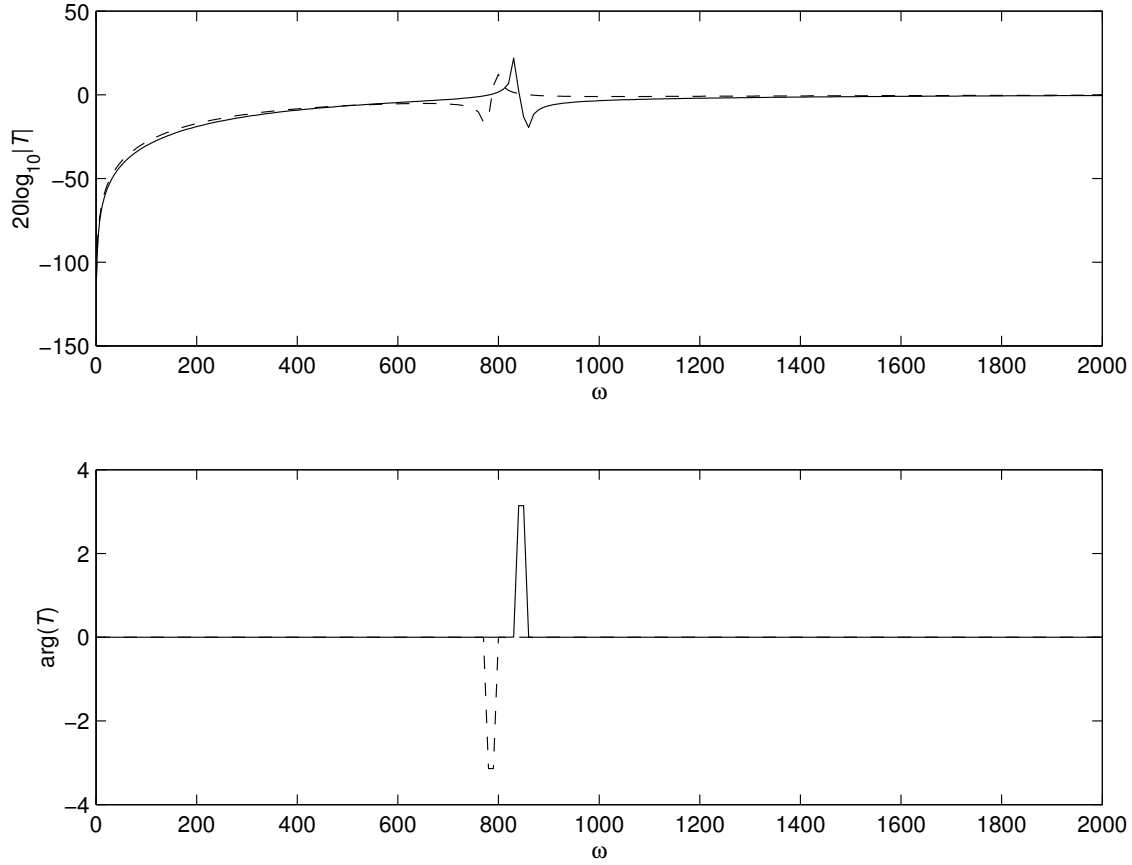


Figure B.11: Hose transfer function function for the uniform (solid line) and layered (dashed) models at $r = 0$ for $n = 0$, $k = 1$, $N = 100$, $\phi = 0$, $P_f = 1$.

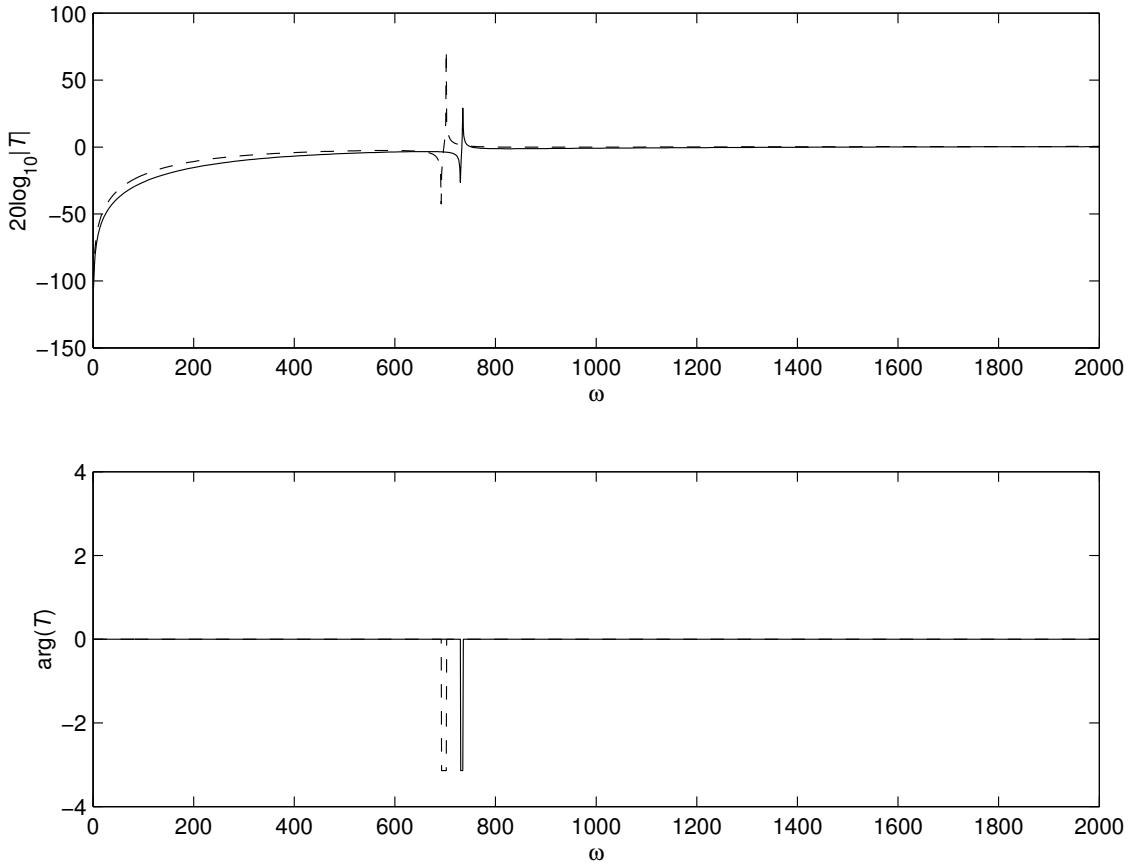


Figure B.12: Hose transfer function function for the uniform (solid line) and layered (dashed) models at $r = 0$ for $n = 0$, $k = 1$, $N = 40$, $\phi = 0$, $P_f = 1$.

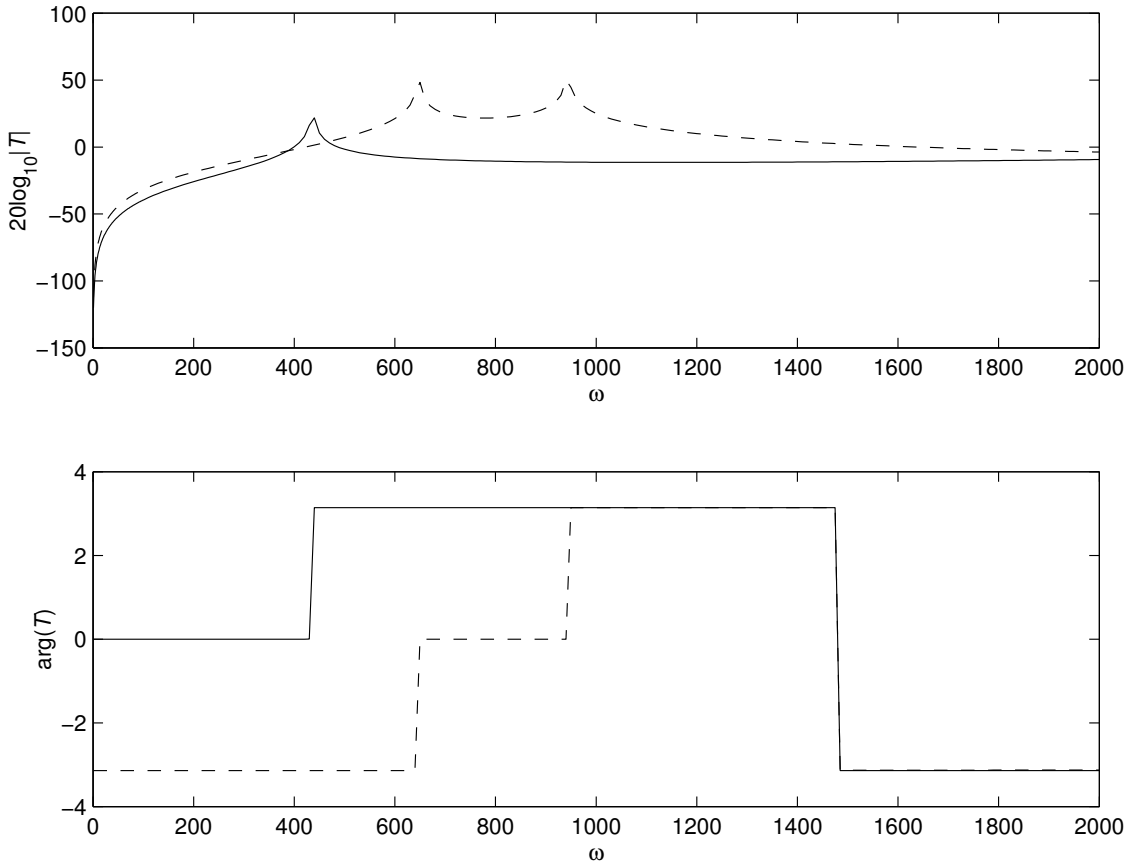


Figure B.13: Hose transfer function function for the uniform (solid line) and layered (dashed) models at $r = 0$ for $n = 0$, $k = 1$, $N = 900$, $\phi = \pi/12$, $P_f = 1$.

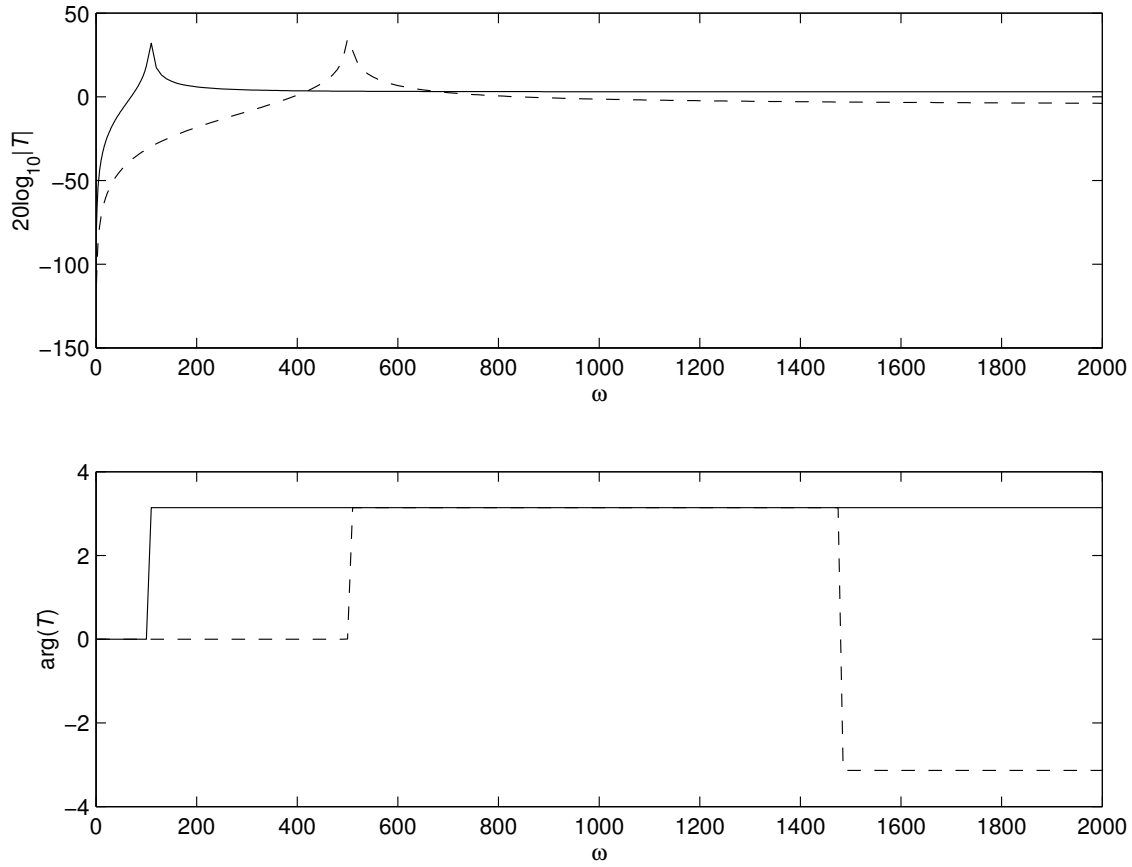


Figure B.14: Hose transfer function function for the uniform (solid line) and layered (dashed) models at $r = 0$ for $n = 0$, $k = 1$, $N = 900$, $\phi = \pi/6$, $P_f = 1$.

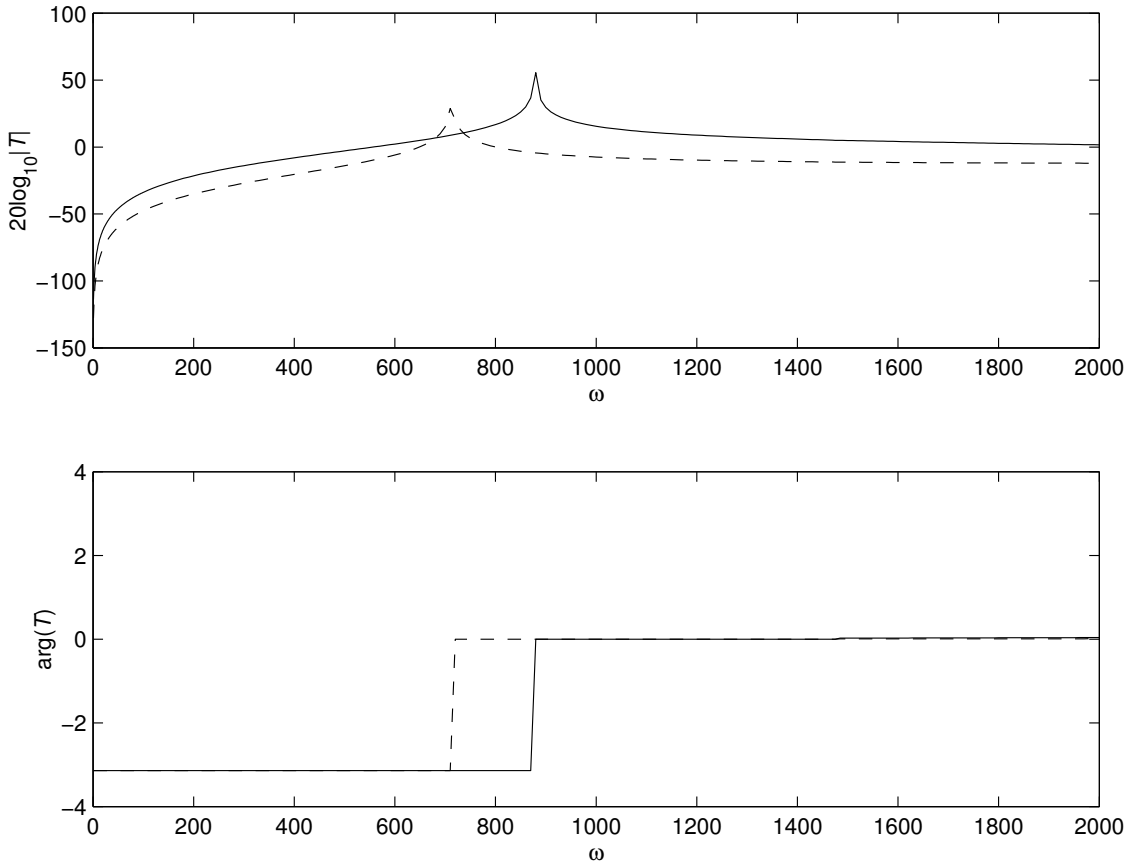


Figure B.15: Hose transfer function function for the uniform (solid line) and layered (dashed) models at $r = 0$ for $n = 0$, $k = 1$, $N = 900$, $\phi = \pi/4$, $P_f = 1$.

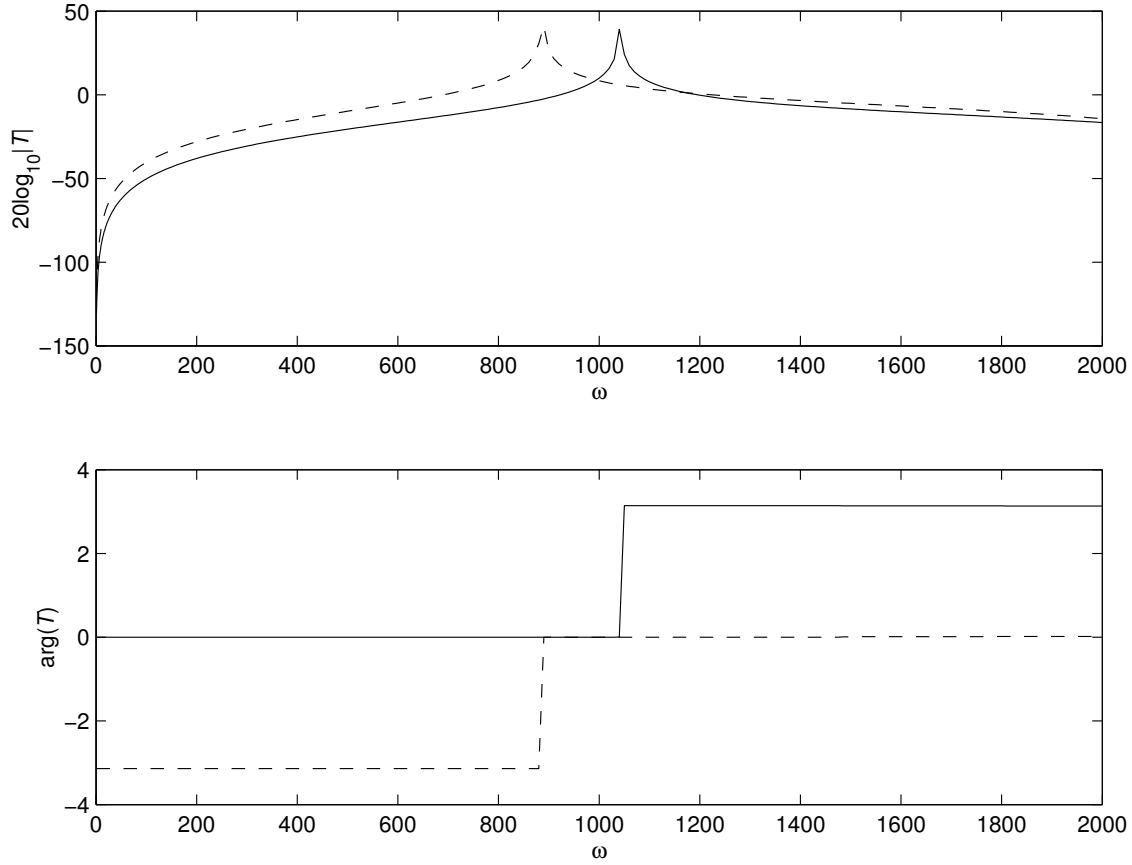


Figure B.16: Hose transfer function function for the uniform (solid line) and layered (dashed) models at $r = 0$ for $n = 0$, $k = 1$, $N = 900$, $\phi = \pi/3$, $P_f = 1$.

Appendix C

MATLAB Routine

C.1 Main Solver

In order to solve our non-dimensional system of ODEs for U, V, W we used the MATLAB routine `hose.m` shown below. The routine outputs plots of U, V and W against r for given values of our parameters.

```
function hose = hose(omega,n1,k,N,phi,Pf)

global A B C D E F G H I alpha beta gamma delta1 delta2 n a C1 kappa1

n = n1;

% hose and fibre dimensions

a = 0.0375;                % outer radius of hose
h = 0.0125;                % thickness of hose
a0 = 0.001;                % radius of fibre

% properties of PVC

rho = 1380;                % density of PVC
E1 = 4.7e8;                % Young's modulus of PVC
nu = 0.33;                 % Poisson's ratio of PVC
G12 = E1/(2*(1+nu));       % shear modulus of PVC
L = 1-nu-2*nu^2;
K = E1/(2*L);              % bulk modulus of PVC

% nylon fibre properties

rhof = 1140;               % density of fibre
E1f = 3.3e9;               % Young's modulus of fibre
nuf = 0.33;                % Poisson's ratio of fibre
G12f = E1f/(2*(1+nuf));    % shear modulus of fibre
Lf = 1-nuf-2*nuf^2;
Kf = E1f/(2*Lf);           % bulk modulus of fibre
```

```
% properties of the composite

delta = (N*a0^2*sec(phi))/(2*a*h-h^2);
                            % volume fraction occupied by fibres
rhobar = (1-delta)*rho + delta*rhof;
                            % composite density
E1bar = (1-delta)*E1 + delta*E1f;
                            % longitudinal Young's modulus
nu12bar = (1-delta)*nu + delta*nuf;
                            % major Poisson's ratio
E2bar = (E1*(2*E1+E1f+2*(E1f-E1)*delta))/(2*E1+E1f-(E1f-E1)*delta);
                            % transverse Young's modulus
nu21bar = nu12bar*E2bar/E1bar;
                            % minor Poisson's ratio
G12bar = (G12*(G12+G12f+(G12f-G12)*delta))/...
             (G12+G12f-(G12f-G12)*delta);
                            % longitudinal shear modulus
G23bar = G12+(G12*(G12f-G12)*(6*K+8*G12)*delta)/...
             (G12*(6*K+8*G12)+(3*K+7*G12)*(G12f-G12));
                            % transverse shear modulus
nu23bar = (E2bar-2*G23bar)/(2*G23bar);
                            % transverse Poisson's ratio


% fluid properties

c1 = 1320;
c2 = 1480;
rho1 = 750;
rho2 = 1000;

kappa1 = sqrt(((omega^2)/(c1^2)) - k^2);
kappa2 = sqrt(((omega^2)/(c2^2)) - k^2);
k0 = sqrt(k^2 - ((omega^2)/(c2^2)));

alpha = 1/(rhobar*(omega*a)^2);
beta = k/(rhobar*omega^2*a);
gamma = (k^2)/(rhobar*omega^2);
delta1 = 1/(rho1*(omega*a)^2);
delta2 = 1/(rho2*(omega*a)^2);
Ubar = (Pf*k)/(rhobar*omega^2);

% determination of the constants

Aprime = ((1-nu23bar)*E1bar)/(1-nu23bar-2*nu12bar*nu21bar);
Bprime = ((1-nu12bar*nu21bar)*E2bar)/...
             ((1+nu23bar)*(1-nu23bar-2*nu12bar*nu21bar));
Dprime = (nu12bar*E2bar)/(1-nu23bar-2*nu12bar*nu21bar);
Fprime = ((nu23bar+nu12bar*nu21bar)*E2bar)/...
             ((1+nu23bar)*(1-nu23bar-2*nu12bar*nu21bar));
Gprime = G12bar;
Iprime = G23bar;
```

```
A = Bprime;
B = Aprime*(sin(phi))^4+Bprime*(cos(phi))^4+...
        2*(Dprime+2*Gprime)*(sin(phi))^2*(cos(phi))^2;
C = Aprime*(cos(phi))^4+Bprime*(sin(phi))^4+...
        2*(Dprime+2*Gprime)*(sin(phi))^2*(cos(phi))^2;
D = Dprime*(sin(phi))^2+Fprime*(cos(phi))^2;
E = Dprime*(cos(phi))^2+Fprime*(sin(phi))^2;
F = Dprime*((sin(phi))^4+(cos(phi))^4)+(Aprime+Bprime-4*Gprime)+...
        (sin(phi))^2*(cos(phi))^2;
G = Gprime*(sin(phi))^2+Iprime*(cos(phi))^2;
H = Gprime*(cos(phi))^2+Iprime*(sin(phi))^2;
I = Gprime*((cos(phi))^2-(sin(phi))^2)+...
        (Aprime+Bprime-2*Dprime)*(sin(phi))^2*(cos(phi))^2;

r1 = 1 - h/a;
r2 = 1;

% solve the equations by a shooting method

Q = zeros(6);
R = zeros(6);
Alpha = zeros(6,1);

Q(1,1) = (D*delta1)/r1 + (2*besselj(n,kappa1*a*r1))/...
           (kappa1*a*(besselj(n-1,kappa1*a*r1)-besselj(n+1,kappa1*a*r1)));
Q(1,2) = (D*n*delta1)/r1;
Q(1,3) = (E*a*k*delta1);
Q(1,4) = (A*delta1);
Q(2,1) = n/r1;
Q(2,2) = 1/r1;
Q(2,5) = -1;
Q(3,1) = a*k;
Q(3,6) = -1;
```

```
if omega^2 >= (c2*k)^2
    R(4,1) = (D*delta2)/r2 + (2*besselh(n,2,kappa2*a*r2))/...
                 (kappa2*a*(besselh(n-1,2,kappa2*a*r2)-...
                  besselh(n+1,2,kappa2*a*r2)));
end

if omega^2 < (c2*k)^2
    R(4,1) = (D*delta2)/r2 - (2*besselk(n,k0*a*r2))/...
                (k0*a*(besselk(n+1,k0*a*r2)+besselk(n-1,k0*a*r2)));
end

R(4,2) = (D*n*delta2)/r2;
R(4,3) = (E*a*k*delta2);
R(4,4) = (A*delta2);
R(5,1) = n/r2;
R(5,2) = 1/r2;
R(5,5) = -1;
R(6,1) = a*k;
R(6,6) = -1;

Alpha(4) = -(a*delta2*Pf)/(Ubar);

% main solver

[r,W1] = ode45(@Uprime,linspace(r1,r2,100),[1; 0; 0; 0; 0; 0]);
[r,W2] = ode45(@Uprime,linspace(r1,r2,100),[0; 1; 0; 0; 0; 0]);
[r,W3] = ode45(@Uprime,linspace(r1,r2,100),[0; 0; 1; 0; 0; 0]);
[r,W4] = ode45(@Uprime,linspace(r1,r2,100),[0; 0; 0; 1; 0; 0]);
[r,W5] = ode45(@Uprime,linspace(r1,r2,100),[0; 0; 0; 0; 1; 0]);
[r,W6] = ode45(@Uprime,linspace(r1,r2,100),[0; 0; 0; 0; 0; 1]);

Wr2 = [W1(end,:)', W2(end,:)', W3(end,:)', W4(end,:)', W5(end,:)', W6(end,:)'];

J = Q + R*Wr2;

s = J\Alpha;

for j =1:100
    W = [W1(j,:)', W2(j,:)', W3(j,:)', W4(j,:)', W5(j,:)', W6(j,:)'];
    U(:,j) = W*s;
    % U is a 6-by-100 matrix U(i,j) is the value if the ith component of U at
      time-step j.
end
```

```
figure
subplot(321)
plot(r,real(U(1,:)),'k')
xlim([r1 r2])
xlabel('\it{r}'), ylabel('Re(\it{U}(\it{r}))')
subplot(322)
plot(r,imag(U(1,:)),'k')
xlim([r1 r2])
xlabel('\it{r}'), ylabel('Im(\it{U}(\it{r}))')
subplot(323)
plot(r,real(U(2,:)),'k')
xlim([r1 r2])
xlabel('\it{r}'), ylabel('Re(\it{V}(\it{r}))')
subplot(324)
plot(r,imag(U(2,:)),'k')
xlim([r1 r2])
xlabel('\it{r}'), ylabel('Im(\it{V}(\it{r}))')
subplot(325)
plot(r,real(U(3,:)),'k')
xlim([r1 r2])
xlabel('\it{r}'), ylabel('Re(\it{W}(\it{r}))')
subplot(326)
plot(r,imag(U(3,:)),'k')
xlim([r1 r2])
xlabel('\it{r}'), ylabel('Im(\it{W}(\it{r}))')

% calculate the interior pressure (for the hose transfer function)

C1 = (2*U(1,1)*Ubar)/(kappa1*a*(besselj(n-1,kappa1*a*r1)-...
         besselj(n+1,kappa1*a*r1)));
                           % P1(r) = C1*besselj(n,kappa1*a*r)
```

```
% subfunctions

function Uprime = Uprime(r,U)

global A B C D E F G H I alpha beta gamma n a

P = zeros(6);

P(1,4) = 1;
P(2,5) = 1;
P(3,6) = 1;
P(4,1) = (((B+G*n^2)*alpha)/(r^2)+H*gamma-1)/(A*alpha);
P(4,2) = (n*(G+B))/(A*r^2);
P(4,3) = (beta*(F-E))/(A*alpha*r);
P(4,4) = -1/r;
P(4,5) = -(n*(G+D))/(A*r);
P(4,6) = -(beta*(E+H))/(A*alpha);
P(5,1) = (n*(G+B))/(G*r^2);
P(5,2) = (((G+B*n^2)*alpha)/(r^2)+I*gamma-1)/(G*alpha);
P(5,3) = (n*beta*(I+F))/(G*alpha*r);
P(5,4) = (n*(G+D))/(G*r);
P(5,5) = -1/r;
P(6,1) = (beta*(H+F))/(H*alpha*r);
P(6,2) = (n*beta*(I+F))/(H*alpha*r);
P(6,3) = ((I*n^2*alpha)/(r^2)+C*gamma-1)/(H*alpha);
P(6,4) = (beta*(E+H))/(H*alpha);
P(6,6) = -1/r;

Uprime = P*[U(1) U(2) U(3) U(4) U(5) U(6)]';
```

C.2 Determination of the Exact Solution

To calculate the exact solution (when $\phi = 0$) for comparison with the numeric solution calculated above we need to determine the constants A_i, B_i for $i = 1, 2, 3$. This was done using the MATLAB routine `exact.m` which also outputs plots of the real and imaginary parts of our exact U, V and W against r.

```
function exact = exact(omega,n1,k,N,Pf)

global n a p1 p2 q lambda1 lambda2

phi = 0;
n = n1;

% hose and fibre dimensions

a = 0.0375;                % outer radius of hose
h = 0.0125;                % thickness of hose
a0 = 0.001;                % radius of fibre
```

```
% properties of PVC

rho = 1380;                 % density of PVC
E1 = 4.7e8;                 % Young's modulus of PVC
nu = 0.33;                  % Poisson's ratio of PVC
G12 = E1/(2*(1+nu));        % shear modulus of PVC
L = 1-nu-2*nu^2;
K = E1/(2*L);               % bulk modulus of PVC

% nylon fibre properties

rhof = 1140;                % density of fibre
E1f = 3.3e9;                % Young's modulus of fibre
nuf = 0.33;                 % Poisson's ratio of fibre
G12f = E1f/(2*(1+nuf));     % shear modulus of fibre
Lf = 1-nuf-2*nuf^2;
Kf = E1f/(2*Lf);            % bulk modulus of fibre

% properties of the composite

delta = (N*a0^2*sec(phi))/(2*a*h-h^2);
                            % volume fraction occupied by fibres
rhobar = (1-delta)*rho + delta*rhof;
                            % composite density
E1bar = (1-delta)*E1 + delta*E1f;
                            % longitudinal Young's modulus
nu12bar = (1-delta)*nu + delta*nuf;
                            % major Poisson's ratio
E2bar = (E1*(2*E1+E1f+2*(E1f-E1)*delta))/(2*E1+E1f-(E1f-E1)*delta);
                            % transverse Young's modulus
nu21bar = nu12bar*E2bar/E1bar;
                            % minor Poisson's ratio
G12bar = (G12*(G12+G12f+(G12f-G12)*delta))/(G12+G12f-(G12f-G12)*delta);
                            % longitudinal shear modulus
G23bar = G12+(G12*(G12f-G12)*(6*K+8*G12)*delta)/...
             (G12*(6*K+8*G12)+(3*K+7*G12)*(G12f-G12));
                            % transverse shear modulus
nu23bar = (E2bar-2*G23bar)/(2*G23bar);
                            % transverse Poisson's ratio


% fluid properties

c1 = 1320;
c2 = 1480;
rho1 = 750;
rho2 = 1000;

kappa1 = sqrt(((omega^2)/(c1^2)) - k^2);
kappa2 = sqrt(((omega^2)/(c2^2)) - k^2);
k0 = sqrt(k^2 - ((omega^2)/(c2^2)));
```

```
alpha = 1/(rhobar*(omega*a)^2);
beta = k/(rhobar*omega^2*a);
gamma = (k^2)/(rhobar*omega^2);
delta1 = 1/(rho1*(omega*a)^2);
delta2 = 1/(rho2*(omega*a)^2);
Ubar = (Pf*k)/(rhobar*omega^2);

% determination of the constants

Aprime = ((1-nu23bar)*E1bar)/(1-nu23bar-2*nu12bar*nu21bar);
Bprime = ((1-nu12bar*nu21bar)*E2bar)/...
             ((1+nu23bar)*(1-nu23bar-2*nu12bar*nu21bar));
Dprime = (nu12bar*E2bar)/(1-nu23bar-2*nu12bar*nu21bar);
Fprime = ((nu23bar+nu12bar*nu21bar)*E2bar)/...
             ((1+nu23bar)*(1-nu23bar-2*nu12bar*nu21bar));
Gprime = G12bar;
Iprime = G23bar;

A = Bprime;
B = Aprime*(sin(phi))^4+Bprime*(cos(phi))^4+...
        2*(Dprime+2*Gprime)*(sin(phi))^2*(cos(phi))^2;
C = Aprime*(cos(phi))^4+Bprime*(sin(phi))^4+
        2*(Dprime+2*Gprime)*(sin(phi))^2*(cos(phi))^2;
D = Dprime*(sin(phi))^2+Fprime*(cos(phi))^2;
E = Dprime*(cos(phi))^2+Fprime*(sin(phi))^2;
F = Dprime*((sin(phi))^4+(cos(phi))^4)+(Aprime+Bprime-4*Gprime)+...
        (sin(phi))^2*(cos(phi))^2;
G = Gprime*(sin(phi))^2+Iprime*(cos(phi))^2;
H = Gprime*(cos(phi))^2+Iprime*(sin(phi))^2;
I = Gprime*((cos(phi))^2-(sin(phi))^2)+...
        (Aprime+Bprime-2*Dprime)*(sin(phi))^2*(cos(phi))^2;

r1 = 1 - h/a;
r2 = 1;

% determine exact solution from boundary conditions

poly = [1, -((A+H)*rhobar*omega^2 + k^2*(E^2+2*H*E-A*C))/(A*H),...
        (rhobar*omega^2 - H*k^2)*(rhobar*omega^2 - C*k^2)/(A*H)];
p = roots(poly);
p1 = sqrt(p(1));
p2 = sqrt(p(2));

lambda1 = (A*p1^2 - rhobar*omega^2 + H*k^2)/(k*(H+E));
lambda2 = (A*p2^2 - rhobar*omega^2 + H*k^2)/(k*(H+E));

q = sqrt((rhobar*omega^2 - H*k^2)/G);

Q = zeros(6);
R = zeros(6);
Alpha = zeros(6,1);
```

```
Q(1,1) = (D*delta1)/r1 + (2*besselj(n,kappa1*a*r1))/...
            (kappa1*a*(besselj(n-1,kappa1*a*r1)-besselj(n+1,kappa1*a*r1)));
Q(1,2) = (D*n*delta1)/r1;
Q(1,3) = (E*a*k*delta1);
Q(1,4) = (A*delta1);
Q(2,1) = n/r1;
Q(2,2) = 1/r1;
Q(2,5) = -1;
Q(3,1) = a*k;
Q(3,6) = -1;

if omega^2 >= (c2*k)^2
    R(4,1) = (D*delta2)/r2 + (2*besselh(n,2,kappa2*a*r2))/...
                (kappa2*a*(besselh(n-1,2,kappa2*a*r2)-...
                 besselh(n+1,2,kappa2*a*r2)));
end

if omega^2 < (c2*k)^2
    R(4,1) = (D*delta2)/r2 - (2*besselk(n,k0*a*r2))/...
                (k0*a*(besselk(n+1,k0*a*r2)+besselk(n-1,k0*a*r2)));
end

R(4,2) = (D*n*delta2)/r2;
R(4,3) = (E*a*k*delta2);
R(4,4) = (A*delta2);
R(5,1) = n/r2;
R(5,2) = 1/r2;
R(5,5) = -1;
R(6,1) = a*k;
R(6,6) = -1;

Alpha(4) = -(a*delta2*Pf)/Ubar;

AB = (Q*Uc(r1) + R*Uc(r2))\Alpha;

for j =1:100
    rj = r1 + (j-1)*(r2-r1)/99;
    r(j) = rj;
    V(:,j) = Uc(rj)*AB;
end

figure
subplot(321)
plot(r,real(V(1,:)),'k:')
xlim([r1 r2])
xlabel('\it{r}'), ylabel('Re(\it{U}(\it{r}))')
subplot(322)
plot(r,imag(V(1,:)),'k:')
xlim([r1 r2])
xlabel('\it{r}'), ylabel('Im(\it{U}(\it{r}))')
subplot(323)
plot(r,real(V(2,:)),'k:')
xlim([r1 r2])
xlabel('\it{r}'), ylabel('Re(\it{V}(\it{r}))')
```

```
subplot(324)
plot(r,imag(V(2,:)),'k:')
xlim([r1 r2])
xlabel('\it{r}'), ylabel('Im(\it{V}(\it{r}))')
subplot(325)
plot(r,real(V(3,:)),'k:')
xlim([r1 r2])
xlabel('\it{r}'), ylabel('Re(\it{W}(\it{r}))')
subplot(326)
plot(r,imag(V(3,:)),'k:')
xlim([r1 r2])
xlabel('\it{r}'), ylabel('Im(\it{W}(\it{r}))')

% calculate the interior pressure (for the hose transfer function)

C1 = (2*V(1,1)*Ubar)/(kappa1*a*(besselj(n-1,kappa1*a*r1)-...
         besselj(n+1,kappa1*a*r1)));
                            % P1(r) = C1*besselj(n,kappa1*a*r)

% subfunction

function Uc = Uc(r)

global n a p1 p2 q lambda1 lambda2

Uc = zeros(6);

Uc(1,1) = p1*(besselj(n-1,p1*a*r)-besselj(n+1,p1*a*r))/2;
Uc(1,2) = p2*(besselj(n-1,p2*a*r)-besselj(n+1,p2*a*r))/2;
Uc(1,3) = n*besselj(n,q*a*r)/(a*r);
Uc(1,4) = p1*(bessely(n-1,p1*a*r)-bessely(n+1,p1*a*r))/2;
Uc(1,5) = p2*(bessely(n-1,p2*a*r)-bessely(n+1,p2*a*r))/2;
Uc(1,6) = n*bessely(n,q*a*r)/(a*r);
Uc(2,1) = -n*besselj(n,p1*a*r)/(a*r);
Uc(2,2) = -n*besselj(n,p2*a*r)/(a*r);
Uc(2,3) = -q*(besselj(n-1,q*a*r)-besselj(n+1,q*a*r))/2;
Uc(2,4) = -n*bessely(n,p1*a*r)/(a*r);
Uc(2,5) = -n*bessely(n,p2*a*r)/(a*r);
Uc(2,6) = -q*(bessely(n-1,q*a*r)-bessely(n+1,q*a*r))/2;
Uc(3,1) = lambda1*besselj(n,p1*a*r);
Uc(3,2) = lambda2*besselj(n,p2*a*r);
Uc(3,4) = lambda1*bessely(n,p1*a*r);
Uc(3,5) = lambda2*bessely(n,p2*a*r);
Uc(4,1) = a*p1^2*(besselj(n-2,p1*a*r)-2*besselj(n,p1*a*r)+...
             besselj(n+2,p1*a*r))/4;
Uc(4,2) = a*p2^2*(besselj(n-2,p2*a*r)-2*besselj(n,p2*a*r)+...
             besselj(n+2,p2*a*r))/4;
Uc(4,3) = (n/r)*((q*(besselj(n-1,q*a*r)-besselj(n+1,q*a*r))/2)-...
             (besselj(n,q*a*r)/(a*r)));
Uc(4,4) = a*p1^2*(bessely(n-2,p1*a*r)-2*bessely(n,p1*a*r)+...
             bessely(n+2,p1*a*r))/4;
Uc(4,5) = a*p2^2*(bessely(n-2,p2*a*r)-2*bessely(n,p2*a*r)+...
             bessely(n+2,p2*a*r))/4;
```

```
Uc(4,6) = (n/r)*((q*(bessely(n-1,q*a*r)-bessely(n+1,q*a*r))/2)-...
              (bessely(n,q*a*r)/(a*r)));
Uc(5,1) = -(n/r)*((p1*(besselj(n-1,p1*a*r)-besselj(n+1,p1*a*r))/2)-...
              (besselj(n,p1*a*r)/(a*r)));
Uc(5,2) = -(n/r)*((p2*(besselj(n-1,p2*a*r)-besselj(n+1,p2*a*r))/2)-...
              (besselj(n,p2*a*r)/(a*r)));
Uc(5,3) = -a*q^2*(besselj(n-2,q*a*r)-2*besselj(n,q*a*r)+besselj(n+2,q*a*r))/4;
Uc(5,4) = -(n/r)*((p1*(bessely(n-1,p1*a*r)-bessely(n+1,p1*a*r))/2)-...
              (bessely(n,p1*a*r)/(a*r)));
Uc(5,5) = -(n/r)*((p2*(bessely(n-1,p2*a*r)-bessely(n+1,p2*a*r))/2)-...
              (bessely(n,p2*a*r)/(a*r)));
Uc(5,6) = -a*q^2*(bessely(n-2,q*a*r)-2*bessely(n,q*a*r)+bessely(n+2,q*a*r))/4;
Uc(6,1) = a*p1*lambda1*(besselj(n-1,p1*a*r)-besselj(n+1,p1*a*r))/2;
Uc(6,2) = a*p2*lambda2*(besselj(n-1,p2*a*r)-besselj(n+1,p2*a*r))/2;
Uc(6,4) = a*p1*lambda1*(bessely(n-1,p1*a*r)-bessely(n+1,p1*a*r))/2;
Uc(6,5) = a*p2*lambda2*(bessely(n-1,p2*a*r)-bessely(n+1,p2*a*r))/2;

% (U,V,W,X,Y,Z)' = (Uc*(A1,A2,A3,B1,B2,B3)')
```

C.3 Calculating the Solution for a Layered Hose

The below routine `layered.m` was used to calculate the displacement field of a layered hose. It is based on `hose.m` but extra code has been added to deal with the boundary conditions at the interfaces between layers. As with the two above routines it outputs plots of U, V and W against r.

```
function layered = layered(omega,n1,k,N,phi,Pf)

global A B C D E F G H I alpha beta gamma delta1 delta2 n a C1 kappa1 Ahat...
       Dhat Ghat

n = n1;

% hose and fibre dimensions

a = 0.0375;                % outer radius of hose
h = 0.0125;                % thickness of hose
a0 = 0.001;                % radius of fibre

% properties of PVC

rho = 1380;                % density of PVC
E1 = 4.7e8;                % Young's modulus of PVC
nu = 0.33;                 % Poisson's ratio of PVC
G12 = E1/(2*(1+nu));       % shear modulus of PVC
L = 1-nu-2*nu^2;
K = E1/(2*L);              % bulk modulus of PVC
```

```
% nylon fibre properties

rhof = 1140;                % density of fibre
E1f = 3.3e9;                % Young's modulus of fibre
nuf = 0.33;                 % Poisson's ratio of fibre
G12f = E1f/(2*(1+nuf));     % shear modulus of fibre
Lf = 1-nuf-2*nuf^2;
Kf = E1f/(2*Lf);            % bulk modulus of fibre
% properties of the composite

delta = (N*a0^2*sec(phi))/(2*(a-0.00175)*(h-0.00350)-(h-0.00350)^2);
                            % volume fraction occupied by fibres
rhobar = (1-delta)*rho + delta*rhof;
                            % composite density
E1bar = (1-delta)*E1 + delta*E1f;
                            % longitudinal Young's modulus
nu12bar = (1-delta)*nu + delta*nuf;
                            % major Poisson's ratio
E2bar = (E1*(2*E1+E1f+2*(E1f-E1)*delta))/(2*E1+E1f-(E1f-E1)*delta);
                            % transverse Young's modulus
nu21bar = nu12bar*E2bar/E1bar;
                            % minor Poisson's ratio
G12bar = (G12*(G12+G12f+(G12f-G12)*delta))/...
             (G12+G12f-(G12f-G12)*delta);
                            % longitudinal shear modulus
G23bar = G12+(G12*(G12f-G12)*(6*K+8*G12)*delta)/...
            (G12*(6*K+8*G12)+(3*K+7*G12)*(G12f-G12));
                            % transverse shear modulus
nu23bar = (E2bar-2*G23bar)/(2*G23bar);
                            % transverse Poisson's ratio


% fluid properties

c1 = 1320;
c2 = 1480;
rho1 = 750;
rho2 = 1000;

kappa1 = sqrt(((omega^2)/(c1^2)) - k^2);
kappa2 = sqrt(((omega^2)/(c2^2)) - k^2);
k0 = sqrt(k^2 - ((omega^2)/(c2^2)));

alpha = 1/(rhobar*(omega*a)^2);
beta = k/(rhobar*omega^2*a);
gamma = (k^2)/(rhobar*omega^2);
delta1 = 1/(rho1*(omega*a)^2);
delta2 = 1/(rho2*(omega*a)^2);
Ubar = (Pf*k)/(rhobar*omega^2);
```

```
% determination of the constants

Aprime = ((1-nu23bar)*E1bar)/(1-nu23bar-2*nu12bar*nu21bar);
Bprime = ((1-nu12bar*nu21bar)*E2bar)/...
             ((1+nu23bar)*(1-nu23bar-2*nu12bar*nu21bar));
Dprime = (nu12bar*E2bar)/(1-nu23bar-2*nu12bar*nu21bar);
Fprime = ((nu23bar+nu12bar*nu21bar)*E2bar)/...
             ((1+nu23bar)*(1-nu23bar-2*nu12bar*nu21bar));
Gprime = G12bar;
Iprime = G23bar;

A = Bprime;
B = Aprime*(sin(phi))^4+Bprime*(cos(phi))^4+...
        2*(Dprime+2*Gprime)*(sin(phi))^2*(cos(phi))^2;
C = Aprime*(cos(phi))^4+Bprime*(sin(phi))^4+...
        2*(Dprime+2*Gprime)*(sin(phi))^2*(cos(phi))^2;
D = Dprime*(sin(phi))^2+Fprime*(cos(phi))^2;
E = Dprime*(cos(phi))^2+Fprime*(sin(phi))^2;
F = Dprime*((sin(phi))^4+(cos(phi))^4)+(Aprime+Bprime-4*Gprime)+...
        (sin(phi))^2*(cos(phi))^2;
G = Gprime*(sin(phi))^2+Iprime*(cos(phi))^2;
H = Gprime*(cos(phi))^2+Iprime*(sin(phi))^2;
I = Gprime*((cos(phi))^2-(sin(phi))^2)+...
        (Aprime+Bprime-2*Dprime)*(sin(phi))^2*(cos(phi))^2;

Ahat = (E1*nu)/((1+nu)*(1-2*nu)) + 2*G12;
Dhat = (E1*nu)/((1+nu)*(1-2*nu));
Ghat = G12;

r1 = 1 - h/a;
r2 = 1;
r3 = r1 + 0.00175/a;
r4 = r2 - 0.00175/a;

% solve the equations by a shooting method

Q = zeros(18);
R = zeros(18);
S = zeros(18);
T = zeros(18);
Alpha = zeros(18,1);

Q(1,1) = (Dhat*delta1)/r1 + (2*besselj(n,kappa1*a*r1))/...
           (kappa1*a*(besselj(n-1,kappa1*a*r1)-besselj(n+1,kappa1*a*r1)));
Q(1,2) = (Dhat*n*delta1)/r1;
Q(1,3) = (Dhat*a*k*delta1);
Q(1,4) = (Ahat*delta1);
Q(2,1) = n/r1;
Q(2,2) = 1/r1;
Q(2,5) = -1;
Q(3,1) = a*k;
Q(3,6) = -1;
```

```
if omega^2 >= (c2*k)^2
    R(16,13) = (Dhat*delta2)/r2 + (2*besselh(n,2,kappa2*a*r2))/...
                   (kappa2*a*(besselh(n-1,2,kappa2*a*r2)-...
                    besselh(n+1,2,kappa2*a*r2)));
end

if omega^2 < (c2*k)^2
    R(16,13) = (Dhat*delta2)/r2 - (2*besselk(n,k0*a*r2))/...
                  (k0*a*(besselk(n+1,k0*a*r2)+besselk(n-1,k0*a*r2)));
end

R(16,14) = (Dhat*n*delta2)/r2;
R(16,15) = (Dhat*a*k*delta2);
R(16,16) = (Ahat*delta2);
R(17,13) = n/r2;
R(17,14) = 1/r2;
R(17,17) = -1;
R(18,13) = a*k;
R(18,18) = -1;

S(4,1) = 1;
S(4,7) = -1;
S(5,2) = 1;
S(5,8) = -1;
S(6,3) = 1;
S(6,9) = -1;
S(7,1) = Dhat/(Ahat*r3);
S(7,2) = (Dhat*n)/(Ahat*r3);
S(7,3) = (Dhat*a*k)/Ahat;
S(7,4) = 1;
S(7,7) = -D/(Ahat*r3);
S(7,8) = -(D*n)/(Ahat*r3);
S(7,9) = -(E*a*k)/Ahat;
S(7,10) = -A/Ahat;
S(8,1) = -n/r3;
S(8,2) = -1/r3;
S(8,5) = 1;
S(8,7) = n/r3;
S(8,8) = 1/r3;
S(8,11) = -1;
S(9,1) = -a*k;
S(9,6) = 1;
S(9,7) = a*k;
S(9,12) = -1;
```

```
T(10,7) = 1;
T(10,13) = -1;
T(11,8) = 1;
T(11,14) = -1;
T(12,9) = 1;
T(12,15) = -1;
T(13,7) = D/(Ahat*r4);
T(13,8) = (D*n)/(Ahat*r4);
T(13,9) = (E*a*k)/Ahat;
T(13,10) = A/Ahat;
T(13,13) = -Dhat/(Ahat*r4);
T(13,14) = -(Dhat*n)/(Ahat*r4);
T(13,15) = -(Dhat*a*k)/Ahat;
T(13,16) = -1;
T(14,7) = -n/r4;
T(14,8) = -1/r4;
T(14,11) = 1;
T(14,13) = n/r4;
T(14,14) = 1/r4;
T(14,17) = -1;
T(15,7) = -a*k;
T(15,12) = 1;
T(15,13) = a*k;
T(15,18) = -1;

Alpha(16) = -(a*delta2*Pf)/(Ubar);

% main solver

[r,W1]  = ode45(@Uprime,linspace(r1,r2,101),[1; 0; 0; 0; 0; 0; 0; 0; 0; 0; 0;...
                                              0; 0; 0; 0; 0; 0; 0;]);
[r,W2]  = ode45(@Uprime,linspace(r1,r2,101),[0; 1; 0; 0; 0; 0; 0; 0; 0; 0; 0;...
                                              0; 0; 0; 0; 0; 0; 0;]);
[r,W3]  = ode45(@Uprime,linspace(r1,r2,101),[0; 0; 1; 0; 0; 0; 0; 0; 0; 0; 0;...
                                              0; 0; 0; 0; 0; 0; 0;]);
[r,W4]  = ode45(@Uprime,linspace(r1,r2,101),[0; 0; 0; 1; 0; 0; 0; 0; 0; 0; 0;...
                                              0; 0; 0; 0; 0; 0; 0;]);
[r,W5]  = ode45(@Uprime,linspace(r1,r2,101),[0; 0; 0; 0; 1; 0; 0; 0; 0; 0; 0;...
                                              0; 0; 0; 0; 0; 0; 0;]);
[r,W6]  = ode45(@Uprime,linspace(r1,r2,101),[0; 0; 0; 0; 0; 1; 0; 0; 0; 0; 0;...
                                              0; 0; 0; 0; 0; 0; 0;]);
[r,W7]  = ode45(@Uprime,linspace(r1,r2,101),[0; 0; 0; 0; 0; 0; 1; 0; 0; 0; 0;...
                                              0; 0; 0; 0; 0; 0; 0;]);
[r,W8]  = ode45(@Uprime,linspace(r1,r2,101),[0; 0; 0; 0; 0; 0; 0; 1; 0; 0; 0;...
                                              0; 0; 0; 0; 0; 0; 0;]);
[r,W9]  = ode45(@Uprime,linspace(r1,r2,101),[0; 0; 0; 0; 0; 0; 0; 0; 1; 0; 0;...
                                              0; 0; 0; 0; 0; 0; 0;]);
[r,W10] = ode45(@Uprime,linspace(r1,r2,101),[0; 0; 0; 0; 0; 0; 0; 0; 0; 1; 0;...
                                              0; 0; 0; 0; 0; 0; 0;]);
[r,W11] = ode45(@Uprime,linspace(r1,r2,101),[0; 0; 0; 0; 0; 0; 0; 0; 0; 0; 1;...
                                              0; 0; 0; 0; 0; 0; 0;]);
[r,W12] = ode45(@Uprime,linspace(r1,r2,101),[0; 0; 0; 0; 0; 0; 0; 0; 0; 0; 0;...
                                              1; 0; 0; 0; 0; 0; 0;]);
```

```
[r,W13] = ode45(@Uprime,linspace(r1,r2,101),[0; 0; 0; 0; 0; 0; 0; 0; 0; 0; 0;...
                                                0; 1; 0; 0; 0; 0; 0;]);
[r,W14] = ode45(@Uprime,linspace(r1,r2,101),[0; 0; 0; 0; 0; 0; 0; 0; 0; 0; 0;...
                                                0; 0; 1; 0; 0; 0; 0;]);
[r,W15] = ode45(@Uprime,linspace(r1,r2,101),[0; 0; 0; 0; 0; 0; 0; 0; 0; 0; 0;...
                                                0; 0; 0; 1; 0; 0; 0;]);
[r,W16] = ode45(@Uprime,linspace(r1,r2,101),[0; 0; 0; 0; 0; 0; 0; 0; 0; 0; 0;...
                                                0; 0; 0; 0; 1; 0; 0;]);
[r,W17] = ode45(@Uprime,linspace(r1,r2,101),[0; 0; 0; 0; 0; 0; 0; 0; 0; 0; 0;...
                                                0; 0; 0; 0; 0; 1; 0;]);
[r,W18] = ode45(@Uprime,linspace(r1,r2,101),[0; 0; 0; 0; 0; 0; 0; 0; 0; 0; 0;...
                                                0; 0; 0; 0; 0; 0; 1;]);

Wr3 = [W1(15,:)', W2(15,:)', W3(15,:)', W4(15,:)', W5(15,:)', W6(15,:)',...
           W7(15,:)', W8(15,:)', W9(15,:)', W10(15,:)', W11(15,:)',...
           W12(15,:)', W13(15,:)', W14(15,:)', W15(15,:)', W16(15,:)',...
           W17(15,:)', W18(15,:)'];

Wr4 = [W1(87,:)', W2(87,:)', W3(87,:)', W4(87,:)', W5(87,:)', W6(87,:)',...
           W7(87,:)', W8(87,:)', W9(87,:)', W10(87,:)', W11(87,:)',...
           W12(87,:)', W13(87,:)', W14(87,:)', W15(87,:)', W16(87,:)',...
           W17(87,:)', W18(87,:)'];

Wr2 = [W1(101,:)', W2(101,:)', W3(101,:)', W4(101,:)', W5(101,:)',...
           W6(101,:)', W7(101,:)', W8(101,:)', W9(101,:)', W10(101,:)',...
           W11(101,:)', W12(101,:)', W13(101,:)', W14(101,:)',...
           W15(101,:)', W16(101,:)', W17(101,:)', W18(101,:)'];

J = Q + R*Wr2 + S*Wr3 + T*Wr4;

s = J\Alpha;

for j =1:101
    W = [W1(j,:)', W2(j,:)', W3(j,:)', W4(j,:)', W5(j,:)', W6(j,:)',...
             W7(j,:)', W8(j,:)', W9(j,:)', W10(j,:)', W11(j,:)',...
             W12(j,:)', W13(j,:)', W14(j,:)', W15(j,:)', W16(j,:)',...
             W17(j,:)', W18(j,:)'];
    U(:,j) = W*s;
    % U is a 18-by-100 matrix U(i,j) is the value if the ith component of U at
      time-step j.
end
```

```
for l = 1:6

    for j = 1:15
        Uhat(l,j) = U(l,j);
    end

    for j = 16:87
        Uhat(l,j) = U(l+6,j);
    end

    for j = 88:101
        Uhat(l,j) = U(l+12,j);
    end

end

% Uhat is a 6-by-100 matrix

figure
subplot(321)
plot(r,real(Uhat(1,:)),'k-.')
xlim([r1 r2])
xlabel('\it{r}'), ylabel('Re(\it{U}(\it{r}))')
subplot(322)
plot(r,imag(Uhat(1,:)),'k-.')
xlim([r1 r2])
xlabel('\it{r}'), ylabel('Im(\it{U}(\it{r}))')
subplot(323)
plot(r,real(Uhat(2,:)),'k-.')
xlim([r1 r2])
xlabel('\it{r}'), ylabel('Re(\it{V}(\it{r}))')
subplot(324)
plot(r,imag(Uhat(2,:)),'k-.')
xlim([r1 r2])
xlabel('\it{r}'), ylabel('Im(\it{V}(\it{r}))')
subplot(325)
plot(r,real(Uhat(3,:)),'k-.')
xlim([r1 r2])
xlabel('\it{r}'), ylabel('Re(\it{W}(\it{r}))')
subplot(326)
plot(r,imag(Uhat(3,:)),'k-.')
xlim([r1 r2])
xlabel('\it{r}'), ylabel('Im(\it{W}(\it{r}))')

% calculate the interior pressure (for the hose transfer function)

C1 = (2*U(1,1)*Ubar)/(kappa1*a*(besselj(n-1,kappa1*a*r1)-...
         besselj(n+1,kappa1*a*r1)));
                            % P1(r) = C1*besselj(n,kappa1*a*r)
```

```
% subfunctions

function Uprime = Uprime(r,U)

global A B C D E F G H I alpha beta gamma n a Ahat Dhat Ghat

P = zeros(6);
P1 = zeros(6);

P(1,4) = 1;
P(2,5) = 1;
P(3,6) = 1;
P(4,1) = (((B+G*n^2)*alpha)/(r^2)+H*gamma-1)/(A*alpha);
P(4,2) = (n*(G+B))/(A*r^2);
P(4,3) = (beta*(F-E))/(A*alpha*r);
P(4,4) = -1/r;
P(4,5) = -(n*(G+D))/(A*r);
P(4,6) = -(beta*(E+H))/(A*alpha);
P(5,1) = (n*(G+B))/(G*r^2);
P(5,2) = (((G+B*n^2)*alpha)/(r^2)+I*gamma-1)/(G*alpha);
P(5,3) = (n*beta*(I+F))/(G*alpha*r);
P(5,4) = (n*(G+D))/(G*r);
P(5,5) = -1/r;
P(6,1) = (beta*(H+F))/(H*alpha*r);
P(6,2) = (n*beta*(I+F))/(H*alpha*r);
P(6,3) = ((I*n^2*alpha)/(r^2)+C*gamma-1)/(H*alpha);
P(6,4) = (beta*(E+H))/(H*alpha);
P(6,6) = -1/r;

P1(1,4) = 1;
P1(2,5) = 1;
P1(3,6) = 1;
P1(4,1) = (((Ahat+Ghat*n^2)*alpha)/(r^2)+Ghat*gamma-1)/(Ahat*alpha);
P1(4,2) = (n*(Ghat+Ahat))/(Ahat*r^2);
P1(4,4) = -1/r;
P1(4,5) = -(n*(Ghat+Dhat))/(Ahat*r);
P1(4,6) = -(beta*(Dhat+Ghat))/(Ahat*alpha);
P1(5,1) = (n*(Ghat+Ahat))/(Ghat*r^2);
P1(5,2) = (((Ghat+Ahat*n^2)*alpha)/(r^2)+Ghat*gamma-1)/(Ghat*alpha);
P1(5,3) = (n*beta*(Ghat+Dhat))/(Ghat*alpha*r);
P1(5,4) = (n*(Ghat+Dhat))/(Ghat*r);
P1(5,5) = -1/r;
P1(6,1) = (beta*(Ghat+Dhat))/(Ghat*alpha*r);
P1(6,2) = (n*beta*(Ghat+Dhat))/(Ghat*alpha*r);
P1(6,3) = ((Ghat*n^2*alpha)/(r^2)+Ahat*gamma-1)/(Ghat*alpha);
P1(6,4) = (beta*(Dhat+Ghat))/(Ghat*alpha);
P1(6,6) = -1/r;
```

```
Phat = [P1 zeros(6,12); zeros(6) P zeros(6); zeros(6,12) P1];

Uprime = Phat*[U(1) U(2) U(3) U(4) U(5) U(6) U(7) U(8) U(9) U(10) U(11)...
                  U(12) U(13) U(14) U(15) U(16) U(17) U(18)]';

% U(1)--U(6) are the components of U1, the solution in [r1,r3]
% U(7)--U(12) are the components of U, the solution in [r3,r4]
% U(12)--U(18) are the components of U2, the solution in [r4,r2]
```

C.4 Plotting the Hose Transfer Function

The plot of the hose transfer function in decibels was produced using the MATLAB routine `transfer.m` shown below. In our loop `hose` can be replaced by `exact` or `layered` to produce the transfer functions corresponding to the exact or layered solutions.

```
function transfer = transfer(r0,n1,k,N,phi,Pf)

global n kappa1 C1 delta1

for j = 1:2e3
    hose(j,n1,k,N,phi,Pf);
    T(j) = (C1*besselj(n,kappa1*a*r0))/(Pf*delta1);
end

omega = 1:2e3;

figure
subplot(211)
plot(omega,20*log(abs(T)),'k')
subplot(212)
plot(omega,angle(T),'k')
```

Bibliography

[1] Acheson, D. J. (1990), *Elementary Fluid Dynamics*, Oxford University Press.

[2] Batchelor, G. K. (1967), *An Introduction to Fluid Dynamics*, Cambridge University Press.

[3] Bourne, D. E. & P. C. Kendall (1992), *Vector Analysis and Cartesian Tensors*, Chapman & Hall, London.

[4] Chen, D. & S. Cheng (1995), *J. Reinf. Plast. Comp.*, **14**(4), 333-348, 'A Micromechanical Analysis of the Elastic Behaviour of Aligned Short-Fiber Reinforced Composites'.

[5] Christensen, R. M. (1979), *Mechanics of Composite Materials*, Wiley, New York.

[6] Davis, J. L. (2000), *Mathematics of Wave Propagation*, Princeton University Press.

[7] Engineer, J. C. (2000), *Thomson Marconi Sonar, Stockport*, CH/RDPROJ/358, 'The Hose Transfer Function Using Thick Shell Theory'.

[8] Engineer, J. C. (2000), *Thomson Marconi Sonar, Stockport*, CH/RDPROJ/370, 'The Hose Transfer Function Using Exact Elastic Theory With Fibre Reinforcing'.

[9] Fu, S. Y., X. Hu & C. Y. Yue (1998), *J. Mater. Sci.*, **33**(20), 4953-4960, 'A New Model for the Transverse Modulus of Unidirectional Fibre Composites'.

[10] Green, A. E. & D. Nicol (1978), *J. Inst. Maths Applics.*, **21**, 227-235, 'A Note on Reinforced Cylindrical Tubes'.

[11] Green, A. E. & M. Troth (1974), *J. Inst. Maths Applics.*, **13**, 39-46, 'Reinforced Hosepipes'.

[12] Gottlieb, H. P. W. (1986), *J. Acoust. Soc. Am.*, **81**(5), 1628-1629, 'On the General Solution of the Vector Helmholtz Equation in Cylindrical Polar Coordinates'.

[13] Halpin, J. C. & J. L. Kordos (1976), *Polym. Eng. Sci.*, **16**(5), 344-352, 'The Halpin-Tsai Equations: A Review'.

[14] Harriman, K. (1997), *M.Sc. Dissertation*, University of Oxford, 'Sonar Acoustics'.

[15] Higham, D. J. & N. J. Higham, *MATLAB Guide*, S.I.A.M., Philadelphia.

[16] Hill, R. (1964), *J. Mech. Phys. Solids*, **12**(4), 199-212, 'Theory of Mechanical Properties of Fibre-Strengthened Materials: I Elastic Behaviour'.

[17] Hill, R. (1965), *J. Mech. Phys. Solids*, **13**(4), 189-198, 'Theory of Mechanical Properties of Fibre-Strengthened Materials: III Self-Consistent Model'.

[18] Hill, R. (1965), *J. Mech. Phys. Solids*, **13**(4), 213-222, 'A Self-Consistent Mechanics of Composite Materials'.

[19] Hudson, J. A. (1980), *The Excitation and Propagation of Elastic Waves*, Cambridge University Press.

[20] Jones, D. S. (1986), *Acoustic and Electromagnetic Waves*, Oxford University Press.

[21] Junger, M. C. & D. Feit (1986), *Sound, Structures and Their Interaction*, M.I.T. Press, Cambridge, Massachusetts.

[22] Keller, H. B. (1992), *Numerical Mehods for Two-Point Boundary-Value Problems*, Dover, New York.

[23] Lighthill, M. J. (1978), *Waves in Fluids*, Cambridge University Press.

[24] Love, A. E. H. (1944), *A Treatise on the Mathematical Theory of Elasticity*, Dover, New York.

[25] Lunn, M. (1991), *A First Course in Mechanics*, Oxford University Press.

[26] Mirsky, I. (1965), *J. Acoust. Soc. Am.*, **37**(6), 1016-1026, 'Wave Propagation in Transversely Isotropic Cylinders Part I: Theory'.

[27] Morse, P. M. & H. Feshbach (1953), *Methods of Theoretical Physics (Part I)*, McGraw-Hill, New York

[28] Ockendon, J. R. (2002), *Applied Solid Mechanics Lecture Notes*, Mathematical Institute, Oxford.

[29] Paul, B. (1960), *Trans. AIME*, **219**, 36-41, 'Prediction of Elastic Constants of Multi-Phase Materials'.

[30] Pipkin, A. C. (1972), *Lectures on Viscoelaticity Theory*, Springer-Verlag, New York.

[31] Riley, K. F., M. P. Hobson & S. J. Bence (1998), *Mathematical Methods for Physics and Engineering*, Cambridge University Press.

[32] Scott, J. F. (1988), *J. Sound Vib.*, **125**(2), 241-280, 'The Free Modes of Propagation of an Infinite Fluid-Loaded Thin Cylindrical Shell'.

[33] Sechler, E. E. (1952), *Elasticity in Engineering*, Wiley, New York.

[34] Shaffer, B. W. (1964), *AIAA J.*, **2**(2), 348-352, 'Stress-Strain Relations of Reinforced Plastics Parallel and Normal to Their Internal Filaments'.

[35] Skelton, E. A. & J. H. James (1993), *J. Sound Vib.*, **161**(2), 251-264, 'Acoustics of an Anisotropic Layered Cylinder'.

[36] Smith, C. S. (1972), *Proc. Symp. on GRP Ship Construction*, RINA, London, 69-80, 'Calculation of Elastic Properties of GRP Laminates for Use in Ship Design'.

[37] Smith, C. S. (1990), *Design of Marine Structures in Composite Materials*, Elsevier Applied Science, London.

[38] Sonneborn, R. H. (1966), *Fiberglas Reinforced Plastics*, van Norstrand Reinhold, New York.

[39] Temme, N. M. (1996), *Special Functions: An Introduction to the Classical Functions of Mathematical Physics*, Wiley, New York.

[40] Tew, R. H. (1987), *D.Phil. Thesis*, University of Oxford, 'Imaging Theory of Surface-Breaking Discontinuities'.

[41] Timoshenko, S. P. & J. N. Goodier (1970), *Theory of Elasticity*, McGraw-Hill Kogakusha, Tokyo.

[42] Überall, H. (1973), *Surface Waves in Acoustics*, extract from *Physical Acoustics: Principles & Methods, Volume X*, edited by W. P. Mason & R. N. Thurston, Academic Press.

[43] Whitney, J. M. (1995), *J. Reinf. Plast. Comp.*, **16**(8), 714-730, 'A Modified Three-Phase Model for Determining the Elastic Constants of a Short Fiber Composite'.

[44] Whitney, J. M. & M. B. Riley (1966), *AIAA J.*, **4**(9), 1537-1542, 'Elastic Properties of Fiber Reinforced Composite Materials'.